
This is the **accepted version** of the article:

Matamales Andreu, Rafel; Mujal, Eudald; Dinarès Turell, Jaume; [et al.]. «Early-middle Permian ecosystems of equatorial Pangaea : Integrated multi-stratigraphic and palaeontological review of the Permian of Mallorca (Balearic Islands, western Mediterranean)». *Earth-Science Reviews*, (January 2022), art. 103948. DOI 10.1016/j.earscirev.2022.103948

This version is available at <https://ddd.uab.cat/record/251863>

under the terms of the  license

Early–middle Permian ecosystems of equatorial Pangaea: integrated multi-stratigraphic and palaeontological review of the Permian of Mallorca (Balearic Islands, western Mediterranean)

Rafel Matamales-Andreu^{a,b,*}, Eudald Muija^{a,c}, Jaume Dinarès-Turell^d, Evelyn Kustatscher^{e,f}, Guido Roghi^g, Oriol Oms^h, Àngel Galobart^{a,i} & Josep Fortuny^a

^a Institut Català de Paleontologia Miquel Crusafont, Universitat Autònoma de Barcelona, Edifici ICTA-ICP, c/ Columnes s/n, Campus de la UAB, 08193 Cerdanyola del Vallès, Barcelona, Spain.

^b Museu Balear de Ciències Naturals, carretera Palma–Port de Sóller Km. 30, 07100 Sóller, Mallorca, Spain.

^c Staatliches Museum für Naturkunde Stuttgart, Rosenstein 1, 70191 Stuttgart, Germany.

^d Istituto Nazionale di Geofisica e Vulcanologia, Via di Vigna Murata 605, 00143 Roma, Italy.

^e Department für Geo- und Umweltwissenschaften, Paläontologie und Geobiologie, Ludwig-Maximilians-Universität, Richard-Wagner-Straße 10, 80333 München, Germany.

^f Bayerische Staatssammlung für Paläontologie und Geobiologie, Richard-Wagner-Straße 10, 80333 München, Germany.

^g Istituto di Geoscienze e Georisorse - CNR, Via Gradenigo 6, 35131 Padova, Italy.

^h Departament de Geologia, Universitat Autònoma de Barcelona, av. de l'eix Central s/n, Campus de la UAB, 08193 Cerdanyola del Vallès, Barcelona, Spain.

ⁱ Museu de la Conca Dellà, c/ del Museu 4, 25650 Isona i Conca Dellà, Lleida, Spain.

*Corresponding author: rafel.matamales@icp.cat

Abstract

The Cisuralian–Guadalupian (early–middle Permian) was a period of climate transition between the Carboniferous icehouse conditions to the latest Permian–Early Triassic hothouse. The landmasses had coalesced in the supercontinent Pangaea and the climate was progressively becoming more arid, especially in a belt over the palaeoequator. The deposits of present-day Mallorca (Balearic Islands, western Mediterranean) were located in those low palaeolatitudes, in the western margin of the Tethys Sea, and correspond to alluvial systems with meandering rivers. The present study divides the stratigraphic succession into three main units, formally described herein as the Bec de s'Àguila Formation, Port des Canonge Formation and Pedra de s'Ase Formation. Based on an exhaustive review of the literature and new magneto- and biostratigraphic data, the sequence has been dated between the early and middle Permian (Artinskian–Wordian). Moreover, the detailed study of the fossils has provided a complete account of the denizens of those ecosystems. Tetrapod tracks occur abundantly in the Port des Canonge Formation, with morphotypes attributed to moradisaurine captorhinid eureptiles, araeoscelidian diapsids/non-varanodontine varanopids, possible pareiasauromorph parareptiles, “pelycosaur”-grade synapsids and indeterminate synapsids. Spores and pollen grains from the Pedra de s'Ase Formation indicate an overall dominance of conifers, accompanied by sphenophytes, ferns and seed ferns. Overall, apart from providing the first detailed interpretation of the ecosystems of the Permian of Mallorca, these new data have made it possible to improve the characterisation of the Permian–Triassic tectonosedimentary cycle in the Balearic Islands, which contribute to the understanding of the evolution of the western peri-Tethys ecosystems.

Key-words: Cisuralian, Guadalupian, magnetostratigraphy, palynology, tetrapod tracks, central Pangaea

1. Introduction

The Permian was a period of great climatic, environmental and biotic changes. The assembly of the supercontinent Pangaea during the Pennsylvanian (late Carboniferous) and throughout the Permian, together with the uplift of the Variscan mountains in the equatorial region, resulted in a profound alteration of the climates of the planet (*e.g.*, Tabor & Poulsen, 2008; Stampfli *et al.*, 2013). There was a sustained aridification trend, from the Carboniferous icehouse conditions to the Triassic hothouse (Montañez *et al.*, 2007; Sun *et al.*, 2012; Montañez & Poulsen, 2013; MacLeod *et al.*, 2017), which contributed to the settling of a megamonsoonal regime that affected the low latitudes of Pangaea, alternating arid seasons with episodes of heavy rainfalls (*e.g.*,

Parrish, 1993). As a result, the ecosystems underwent extensive remodelling, which translated into several important events of biological turnover. The Cisuralian continental tetrapod faunas were reminiscent of those of the Carboniferous, with an abundance of amphibians and “pelycosaur”-grade synapsids (Ruta & Benton, 2008; Brocklehurst *et al.*, 2013). However, a remarkable faunal turnover occurred by the Guadalupian when, in the aftermath of the so-called Olson’s Extinction (Brocklehurst *et al.*, 2017; Olroyd & Sidor, 2017; Brocklehurst, 2020; but see Lucas, 2017), several groups of parareptiles and therapsids first appeared and readily outnumbered the residual representatives of the once-dominant amphibian groups (Sahney & Benton, 2008; Benson & Upchurch, 2013). Another extinction event struck the tetrapod faunas just before the Lopingian (Retallack *et al.*, 2006; Lucas, 2009; Day *et al.*, 2015), which was dominated by a diverse array of derived therapsid groups (Bernardi *et al.*, 2017; Lucas, 2017). The Permian period ended with the most dramatic extinction event in the Phanerozoic, which wiped out almost all life on earth (Erwin, 1994; Benton & Twitchett, 2003; Benton, 2008), leaving empty ecological niches for the succeeding Mesozoic communities to fill (Romano *et al.*, 2020).

During the Permian, sedimentation in the western margins of the Tethys sea (including the present-day Balearic Islands, western Mediterranean) took place in many small, relatively isolated basins (*e.g.*, McCann *et al.*, 2006), making lithostratigraphic comparison among basins, even close ones, difficult. Asselian–Sakmarian (‘Autunian’) deposits of the Iberian Peninsula, Massif Central, Provence and Sardinia usually correspond to a continuation of the organic matter-rich facies of the underlying Carboniferous deposits, representing sedimentation of lakes and floodplains under humid conditions (Sopeña *et al.*, 1977; Cassinis & Ronchi, 2002; Cassinis *et al.*, 2003; Schneider *et al.*, 2006; Durand, 2008; Lopez *et al.*, 2008; Michel *et al.*, 2015; Mugal *et al.*, 2018; López-Gómez *et al.*, 2019a, 2019b, 2021). Sakmarian–Kungurian (‘Saxonian’) deposits also appear in most of the basins mentioned above and in the Alps (Cassinis *et al.*, 2012). They represent semi-arid settings, with playa lake and fluvial channel deposits, sometimes with lacustrine deposits near the top of the sequences (see references cited above). In the cases when both groups are present, they are usually, but not always, bound by an unconformity corresponding to a sedimentary hiatus. Roadian–Wuchiapingian (‘Thuringian’) deposits are usually thicker and more widespread, and appear in Menorca, Iberian Peninsula, Massif Central, Provence and Sardinia, representing semi-arid floodplains traversed by braided or meandering river systems (Cassinis *et al.*, 2003; Gand & Durand, 2006; Schneider *et al.*, 2006; Durand, 2008; Bercovici *et al.*, 2009; Linol *et al.*, 2009; De la Horra *et al.*, 2012; Michel *et al.*, 2015; Mugal *et al.*, 2017a). In the Alps, the ‘Thuringian’ sequences, as defined originally, span from the Wuchiapingian to the Changshingian, and exhibit a marine influence towards the East (Cassinis *et al.*, 2012; Bernardi *et al.*, 2017). In most of the aforementioned sections, the sedimentary palaeoenvironments and even some palaeoclimatic signals seem to reflect local conditions (with a superimposed global

aridification trend), which further complicates correlations. The majority of those units have absolute age attributions from volcanic rocks, which are altogether absent in the sequences of Mallorca studied here, and therefore the datings of the latter rely on constraints imposed by palaeomagnetism and fossils (magneto- and biostratigraphy).

The present work exhaustively reviews and integrates all the previous stratigraphic and palaeontological data on the Permian of Mallorca (Balearic Islands, western Mediterranean) with new pieces of evidence, including palaeomagnetic, palynological, palaeobotanical and ichnological data. The lithostratigraphic framework is revised, providing new stratigraphic sections, clearing previous misconceptions and describing three formal units with rank of formation. The palaeodepositional environments and their evolution through time are interpreted from the sedimentological study, and biotic communities are described by study of spores, pollen and macroplant remains, together with trace fossils produced by both invertebrates and vertebrates. These fossil remains provide relatively precise age attributions for the two upper formations, and the performed magnetostratigraphic analysis further constrains these datings. Finally, these data are considered in the context of equatorial Pangaea in order to identify patterns regarding climate and biogeography.

2. Geographical and geological context

The Balearic Islands are an archipelago located in the western Mediterranean (Figure 1A), as a northeastern extension of the Betic fold and thrust belt, uplifted during the Alpine orogeny (Vera *et al.*, 2004). Rocks of Permian age crop out only on the two largest islands, Mallorca and Menorca (Pomar-Gomà, 1979; Obrador, 1983; Rodríguez-Perea *et al.*, 1987; Calafat, 1988; Rosell *et al.*, 1988; Gómez-Gras, 1993), but their successions were probably deposited in separate basins along the eastern margin of the Iberian plate (Gómez-Gras, 1993; López-Gómez *et al.*, 2019a). In fact, the upper Palaeozoic–lower Mesozoic basins of the Balearic Islands form part of the same structural system as the basins from the Iberian Peninsula, as a whole known as the Iberian area. The Permian basins of the Balearic Islands, similarly to those of the rest of the Iberian Peninsula, were opened during the latest Carboniferous–earliest Permian, when the Variscan orogen started to collapse (McCann *et al.*, 2006; López-Gómez *et al.*, 2019a). This resulted in a dominant transtensional and extensional tectonic regime acting on the region, which favoured the development of semi-grabens where the sediments accumulated (López-Gómez *et al.*, 2019a). Those basins were palaeogeographically located in the western peri-Tethys (see Roscher & Schneider, 2006), drifting from a latitude of about 7 °S in the earliest Permian to about 4 °N during the latest Permian (Scotese, 2014a, 2014b). The climate is thought to have been tropical

throughout (Roscher *et al.*, 2008), under semi-arid, seasonal conditions (Gómez-Gras & Alonso-Zarza, 2003; Bercovici *et al.*, 2009).

On Mallorca, rocks of Permian age intermittently crop out along the coastal cliffs of the northwestern side of the Serra de Tramuntana, between Racó de s'Algar (Banyalbufar) and Platja de sa font Figuera (Valldemossa) (Figure 1). They extend inland only in the valley behind Port des Canonge, but there they are mostly covered by forests. The base of the Permian group of units remains unknown, as the boundary with the underlying Carboniferous *Culm* facies is on a geological fault (Rodríguez-Perea & Ramos, 1984; Ramos & Rodríguez-Perea, 1985; Calafat, 1988). The boundary with the overlying Lower Triassic *Buntsandstein* facies has tentatively been recognised as an unconformity in the Pedrera de sa Cova section for the first time in the present study. Previous authors divided the Permian series into two (Ramos *et al.*, 1985; Ramos, 1995), three (Calafat, 1988) or four (Gómez-Gras, 1993) informal lithostratigraphic units (see Supplementary Text 1; Supplementary Table 1; Matamales-Andreu *et al.*, 2021a), which were never properly collated. The present work provides a detailed study of all the relevant sections of the island (Figure 1B–D) and formal definitions for each of the lithostratigraphic units to avoid ambiguity in future studies.

3. Material and methods

3.1. Stratigraphy and sedimentology

For the stratigraphic and sedimentological study, 12 stratigraphic sections have been logged at 1:25 scale (here presented in 1:40 scale in Supplementary Logs) by means of a Jacob's staff and a measuring tape, down to minimum resolution of 1 cm of bed thickness. Texture, thickness, sedimentary structures, colour, palaeontological content and lithofacies (Table 1) have been also considered. Part of some of the logs corresponds to flooded or vertical passes, which have been logged either from within the water or using climbing gear, respectively. The logs are named, from South-West to North-East (Figure 1): 'Racó de s'Algar' (RA, 149.3 m), 'Torrent de na Nadala' (NA, 192.5 m), 'Es Tamarell' (TA, 27.8 m), 'Punta d'en Pere Mir' (PM, 30.0 m), 'Pedra de s'Ase' (PA, 167.3 m), 'Pedra de s'Ase - Summit' (PS, 11.0 m), 'Volta des General' (VG, 5.9 m), 'Platja de sa Pedrera' (PP, 13.3 m), 'Port des Canonge–Hort de sa Cova' (PC, 604.4 m), 'Pedrera de sa Cova' (CO, 190.0 m), 'Sa Gratallosa' (GR, 8.6 m) and 'Marina de Valldemossa' (MV, 70.0 m). These logs have been synthesised (1:1160 scale) and correlated for each of the four main areas, in order to overcome the local distortion produced by faulting: 'Racó de s'Algar–

Pedra de s'Ase section', 'Port des Canonge–Sa Gratallosa section', 'Pedrera de sa Cova section' and 'Marina de Valldemossa section' (see Supplementary Correlations). Finally, the synthetic logs of each of those sections have been correlated (see '4. Stratigraphy and sedimentology' below). The *datum* to correlate the two main synthetic sections, 'Racó de s'Algar–Pedra de s'Ase section' and 'Port des Canonge–Sa Gratallosa section', is the boundary between the Port des Canonge Formation and the Pedra de s'Ase Formation, that is, the change from dominant red lutites and fine-grained sandstones to pink/white/blue medium-grained sandstones (Figure 2). The position of the 'Marina de Valldemossa section' within the Pedra de s'Ase Formation can only be tentatively assigned to its middle part based on the similarity of the sequences (Figure 3). The boundary between Permian and Triassic units seems to be present at the 'Pedrera de sa Cova section' and thus it has been broadly assigned to the upper part of the Pedra de s'Ase Formation (Figure 3). The sedimentary lithofacies and architectural elements were classified according to the nomenclature of Miall (1977, 1985, 2006) and Postma (1990), with modifications introduced by Linol *et al.* (2009) for the Permian sequence of the neighbouring island of Menorca (Table 1). The architectural elements have been classified according to Miall (1985, 2006) (Table 2).

3.2. Magnetostratigraphy

In order to characterise the geomagnetic polarity of rocks along the studied successions and erect a magnetostratigraphy, 234 oriented hand samples were taken from their corresponding stratigraphic levels, spanning about 835 m of strata. Sampling was focused on lithologies that were potentially most suitable for palaeomagnetism (*i.e.*, the red-coloured, finest-grained lithologies). A regular spacing between samples was usually maintained, although this was not possible in the intervals of medium-/coarse-grained sandstones and those that were not cropping out. Collected samples are distributed along several stratigraphic sections named, from southwest to northeast (Figure 1): 'Racó de s'Algar' (RA1–RA4 sampling levels), 'Torrent de na Nadala' (NA1–NA46), 'Volta des General' (VG1–VG5), 'Platja de sa Pedrera' (PP1–PP3), 'Port des Canonge–Hort de sa Cova' (PC1–PC152), 'Pedrera de sa Cova' (CO1–CO24) (see Supplementary Logs for the precise location of all the collected samples). Disregarding major non-outcropped intervals, the overall sampling resolution is 2–4 m. The aforementioned sections have been correlated and integrated into three main synthesised stratigraphic logs, 'Racó de s'Algar–Pedra de s'Ase section', 'Port des Canonge–Hort de sa Cova section' and 'Pedrera de sa Cova section' (see section '3.1. Stratigraphy and sedimentology' for details). Strata dip along those three sections is similar and moderate (strike/dip angles at about 090/30, 085/28, and 066/26 respectively, see Supplementary Table 2). The similar bedding attitude of the studied sections prevents a meaningful palaeomagnetic fold test.

Collected samples were subsequently cut in standard palaeomagnetic regular specimens for laboratory analysis. A total of 144 samples were fully demagnetised for the present study (about 62% of the collected samples, see Supplementary Table 2). Natural remanent magnetisation (NRM) and remanence through demagnetisation were measured on a 2G Enterprises DC SQUID high-resolution pass-through cryogenic magnetometer (manufacturer noise level of 10^{-12} Am²) operated in a shielded room at the Istituto Nazionale di Geofisica e Vulcanologia in Rome, Italy. A Pyrox oven in the shielded room was used for thermal demagnetisations and alternating field (AF) demagnetisation was performed with three orthogonal coils installed inline with the cryogenic magnetometer. Progressive stepwise AF demagnetisation was routinely used and applied after a single heating step to 150 °C. AF demagnetisation included usually 14 steps (4, 8, 13, 17, 21, 25, 30, 35, 40, 45, 50, 60, 80, 100 mT). Subsequently, thermal demagnetisation resumed through variable temperature increments (20–100 °C) up to 690 °C. In the context of the studied redbeds, applying a first heating step followed by AF demagnetisation prior to full thermal demagnetisation makes it possible to both unblock eventual magnetisation carried by goethite (usually unblocking below 120 °C) and also magnetite-like low coercivity ferromagnetic phases. Consequently, magnetic phases even unblocking at relatively low temperatures during the final thermal protocol must be assigned to high coercivity phases (*i.e.*, hematite). Characteristic remanent magnetisations (ChRM) were calculated by Principal Component Analysis (Kirschvink, 1980) and by the great circle technique (MacFadden & McElhinny, 1988) from orthogonal vector endpoint demagnetisation diagrams (Zijderveld, 2013) using the online open-source software Paleomagnetism.org (Koymans *et al.*, 2016, 2020). The magnetic stratigraphy is based on virtual geomagnetic pole (VGP) latitudes.

In order to characterise ferromagnetic mineralogy, some rockmagnetic experiments were performed in selected samples. Thermomagnetic heating and cooling cycles were measured with an AGICO MFK1 susceptibility bridge with a CS3 furnace attachment with nominal sensitivity (5×10^{-7} SI) and open air into the tube. Hysteresis loops, isothermal remanent magnetization (IRM) acquisition and back-field IRM were measured at room temperature with a Princeton Measurements Corp. Model 3900 MicroMagTM Vibrating Sample Magnetometer (VSM) (noise level 5×10^{-9} Am²). IRM curve unmixing was performed with IRM MaxUnmix package (Maxbauer *et al.*, 2016).

3.3. Palaeopalynology and palaeobotany

For the present study, 35 rock samples were collected from the studied stratigraphic sections in order to search fossil sporomorphs and palynomorphs (Supplementary Table 4). The beds chosen

to be sampled were generally greyish-bluish lutites or very fine-grained sandstones. Specifically, there are three samples in the Port des Canonge Formation of log RA; one sample in the Port des Canonge Formation and three samples in the Pedra de s'Ase Formation of NA; thirteen samples in the Pedra de s'Ase Formation of log PA; two samples in the Pedra de s'Ase Formation of log PS; one sample in the Port des Canonge Formation and three samples in the Pedra de s'Ase Formation of log PC; four samples in the Pedra de s'Ase Formation and one sample in the Punta Roja Formation(?) of log CO; and three samples in the Pedra de s'Ase Formation of log MV (see exact position of all the samples in Supplementary Logs).

To extract the sporomorphs and palynomorphs, rock samples were crushed and treated with HCl (37%) and HF (47%) to dissolve the non-organic material. After washing and sieving (15 μ m nylon mesh), the residue was stored in water and then strew mounted onto microscope slides using Entellan glue as the mounting medium. The microscope slides were studied under a Leica DM750 light microscope, and the index species were photographed using a Leica ICC50 W digital camera. Slides are permanently housed in the Museu de Mallorca (Palma, Mallorca, Balearic Islands, Spain; see '3.5. Institutional abbreviations' below).

Among the different observed macroplant remains, some were not collected because of their very large size (*i.e.*, tree logs) or being included in very large and hard rock surfaces. Those were identified according to the following code: [stratigraphic log label]-[level]-[correlative number for each macroplant remain in that level]. Macroplant remains that were collected are permanently housed in the Museu de Mallorca (Palma, Mallorca, Balearic Islands, Spain; see '3.5. Institutional abbreviations' below).

3.4. Tetrapod ichnites

Digital 3D models of the surfaces with ichnites were made following the procedure explained by Mujal *et al.* (2020). Agisoft Photoscan standard v.1.1.4. (<http://www.agisoft.com>) was used to align the photographs and to create the dense point clouds, meshes and textures. MeshLab v.2016.12 (<http://meshlab.sourceforge.net/>) was used to scale, orient and crop the models. The false colour-coded height maps with contours were built using ParaView v.5.5.0-RC4 64-bit (<http://www.paraview.org>). ImageJ v.1.52d (<https://imagej.nih.gov/ij/>) was used to measure, whenever possible, the standard parameters of the ichnites recommended by Leonardi (1987) and Hasiotis *et al.* (2007). All measurements of the ichnites studied herein are listed in Supplementary Table 5.

The specific nature of the ichnological material, where one ‘specimen’ (=rock slab with footprints) may have several unrelated tracks, or some footprints forming a trackway, calls for a particular set of rules to accurately reference each ichnite. In the present work, the slabs are identified according to following code: [stratigraphic log label]-[level, “exs” if found *ex situ*]-[correlative number for each slab in that level]-[correlative number indicating the trackway][correlative letter indicating the ichnite] (see Supplementary Table 5). All the ichnites considered herein (both left in the field and collected) were consistently numbered using that code. Correspondence of that nomenclature with institutional catalogue numbers of the slabs that were collected from the field are in Supplementary Table 5. Slabs with ichnites that were collected are permanently housed in the Museu de Mallorca (Palma, Mallorca, Balearic Islands, Spain; see ‘3.5. Institutional abbreviations’ below).

The tetrapod tracks studied herein show different states of preservation, depending on the layer and on the size of the ichnites. More than half of the ichnites have a type 3 preservation value (optimal) according to the scale of Marchetti *et al.* (2019a), and the rest are of types 2 (good), 1 (intermediate) and, very rarely, 0 (poor). To count the relative proportions of each ichnotaxon (see ‘8.1. Age attributions’ below), the methodology of Marchetti *et al.* (2017a) was not used because most of the surfaces with ichnites were large (often 0.5–2 m²) and profusely trampled. In this specific case, the “track/slab” method (Marchetti *et al.*, 2017a) would severely underestimate the ichnotaxa with two or more trackways on the same surface, and their “weighting size” method (Marchetti *et al.*, 2017a) would overestimate ichnotaxa with trackways (*i.e.*, *Hyloidichnus*, *Dimetropus*) over those that appear as isolated ichnites (*i.e.*, *Dromopus*). Therefore, in the present work each trackway, regardless of the number of ichnites imprinted, was counted as a single occurrence for that ichnotaxon in that layer. Isolated ichnites (or isolated manus-pes sets) that were not part of a trackway were also counted as a single occurrence. All ichnites have been revised and studied except for one morphotype, attributable to a synapsid trackmaker, which appears to be different from other coeval ichnogenera and is the object of a separate study. Regardless, it has been included in the counts of ‘8.1.3. Tetrapod track biostratigraphy’ as “indeterminate synapsid tracks”.

3.5. Institutional abbreviations

D/21: Museu de Mallorca, Palma, Mallorca, Balearic Islands, Spain.

MBCN: Museu Balear de Ciències Naturals, Sóller, Mallorca, Balearic Islands, Spain.

UIB: Universitat de les Illes Balears, Palma, Mallorca, Balearic Islands, Spain.

4. Stratigraphy and sedimentology

Formal lithostratigraphic units have hitherto never been defined for the Permian red-beds of Mallorca. Previous authors (Cuevas-López, 1958a, 1958b; Pomar-Gomà, 1979; Martí *et al.*, 1985; Ramos *et al.*, 1985; Calafat, 1986, 1987, 1988; Rodríguez-Perea *et al.*, 1987; Barnolas, 1991a, 1991b; Gómez-Gras, 1992, 1993; Ramos, 1995) divided the Permian–Triassic continental sequence into several informal lithostratigraphic units (see Supplementary Text 1 and Supplementary Table 1). Subsequent reviews (Arche *et al.*, 2002; López-Gómez *et al.*, 2002, 2019a; Vera *et al.*, 2004; Bourquin *et al.*, 2007, 2011; Cassinis *et al.*, 2012) upgraded some of those to the rank of formation, without proper description or characterisation. An additional complication is that most of the recent work is based on the stratigraphic framework proposed by Ramos *et al.* (1985) and Ramos (1995), which incorrectly correlated Permian and Triassic units from different outcrops (see Supplementary Text 1; Matamales-Andreu *et al.*, 2021b). This section provides formal descriptions of all the Permian units of Mallorca, preserving the first name used for each of them. Descriptions and interpretations of all the lithofacies and architectural elements are here presented in Table 1 and Table 2.

4.1. Bec de s'Àguila Formation

This formation (Figure 2) is identified by the presence of conglomerates with clasts of quartz or rocks from the Devonian/Carboniferous basement (in the other formations, the clasts are always soft pebbles and carbonate nodules). The clasts can also appear as isolated grains in the sandstone beds. Moreover, the red sandstone deposits are usually medium- or coarse-grained, in contrast to the overlying formations, in which red sandstones are very fine- or fine-grained. Beds of lutites are rare in this formation.

4.1.1. Location and boundaries

The only three outcrops of the Bec de s'Àguila Formation are small, mostly covered and heavily affected by tectonics. There are limited exposures at Volta des General and at Sa Gratallosa, and the thickest section has been measured at Platja de sa Pedrera (Supplementary Logs). With 13.3 m of thickness, the section of Platja de sa Pedrera is hereby formally designed as the stratotype of this formation (Figures 1D, 2; Supplementary Logs). Its lower boundary is always determined by faults, with Carboniferous *Culm* facies in the case of Sa Gratallosa (Rodríguez-Perea & Ramos, 1984; Ramos & Rodríguez-Perea, 1985) (Figure 2A) and Platja de sa Pedrera (Calafat, 1988)

(Figure 2B), and with the Port des Canonge Formation (by means of an inverse fault) in the case of Volta des General. Its upper boundary is a geological fault causing it to contact the Port des Canonge Formation in the case of the sections of Sa Gratallosa (Figure 2A) and Volta des General. At Platja de sa Pedrera, this contact is covered (Figure 2B).

4.1.2. Lithological features and palaeontological content

The lithofacies (Figure 4, Table 1) and architectural elements (Table 2) present in this formation show a very particular arrangement, with abundance of conglomerate, that makes it possible to distinguish it from all other Permian formations of Mallorca. The conglomerate beds (lithofacies type *GmP*, Figure 4B) are especially frequent in the lower part, and comprise a red or yellow matrix of medium- to very coarse-grained sandstones and clasts (of variable size) of quartz and lithic fragments of Carboniferous (or older) rocks, that are sub-rounded to very angular. No clear lamination can be seen in those beds, which are mostly horizontal with irregular tops and slightly erosive bases. The clasts are never imbricated and are usually unsorted, although some beds do present either positive or negative grain sorting. Traces of large roots similar to those described in the Permian P1 unit of Menorca (Gómez-Gras & Alonso-Zarza, 2003) can sometimes be observed. Medium to coarse-grained red sandstone beds are also frequent, and are mostly massive (lithofacies type *Sm*) or show crude trough cross-bedding (lithofacies type *St*). Sandstone deposits with basal scours (lithofacies type *Ss*), beds with planar cross-bedding (lithofacies type *Sp*), horizons with abundant rhizcretions (lithofacies type *Sb*) and even palaeosols (Calcisols, vertic Calcisols or Vertisols; lithofacies type *P*) may also appear. Finally, red lutite beds are very rare, being either massive (lithofacies type *Fm*) or affected by root bioturbation (lithofacies type *Fr*). The dominant architectural elements in this formation are *GB/SG*. Secondly, element *LA* appears in the upper part of the unit, with rare intercalations of element *FF*. The only fossils found so far in Bec de s'Àguila Formation are rhizcretions of diverse sizes.

4.1.3. Interpretation

In this formation, lithofacies type *GmP* represents the deposits of gravity and debris flows in a colluvial/alluvial-fan environment. Lithofacies type *Sm* also corresponds to deposition by dense flows. Other sandstone lithofacies, such as those of types *St* and *Sp*, have been interpreted to be deposited by fluvial currents during intervals of relatively lower flow regime, whereas type *Ss* corresponds to higher energy events with erosive capacity. Lithofacies of types *Sb* and *P* represent the alteration of other lithofacies types by biogenic activity. The presence of calcic Vertisols, vertic Calcisols and Calcisols point to a semi-arid climate with variations of the water table, possibly due to seasonality (Mack *et al.*, 1993; Alonso-Zarza, 2003; Tabor & Poulsen, 2008). Lutite lithofacies of types *Fm* and *Fr* correspond to the fine sediments deposited in the floodplain,

which can be bioturbated by plant roots. The architectural elements *GB/SG* record gravity flows in a colluvial/alluvial fan setting, the element *LA* corresponds to point bars of meandering channels, rarely interbedded with element *FF*, the floodplain fine deposits.

This formation represents colluvial and alluvial-fan debris-flow deposits and the transition towards the fine-grained meandering rivers of the Port des Canonge Formation (see ‘4.2. Port des Canonge Formation’ below). Similar to the P1 unit of Menorca (Gómez-Gras & Alonso-Zarza, 2003; Matamales-Andreu *et al.*, 2021c), the debris-flow conglomerates contain mostly extraformational clasts and may develop palaeosols (Calcisols) with large rhizocretions. The medium to coarse-grained sandstones that appear towards the upper part of the formation are usually massive and somewhat tabular but in some cases, such as at the Platja de sa Pedrera section, they present clear lateral accretion (Figure 2), thus representing medium- to coarse-grained sinuous channels with almost no floodplain deposits. The few palaeocurrents measured in this formation ($n = 2$) point to a possible South–East direction (mean of 137.5°; see ‘8. Discussion’ below).

4.2. Port des Canonge Formation

This formation (Figure 2) can be identified in the field because of the great abundance of very fine-grained rocks compared to the other two Permian formations of Mallorca. Specifically, the typical sequence consists of intervals of very fine- to fine-grained red sandstones of about 2–4 metres-thick, with lateral accretion surfaces, overlain by about 2–5 metres of red lutites and very fine-grained red sandstones forming tabular beds.

4.2.1. Location and boundaries

The Port des Canonge Formation crops out extensively at the Racó de s’Algar–Pedra de s’Ase section (about 222.5 m thick, including covered intervals, Figures 1B, 2C, 2D) and at the Port des Canonge–Hort de sa Cova section (about 368.8 m thick, including covered intervals, Figure 1D). Smaller exposures also occur in the surroundings of Sa Gratallosa (Figures 1D, 2A) and possibly at Nedador de ses Dones (Figure 1C). The thickest and most easily accessible section is that of Port des Canonge–Hort de sa Cova, which is here formally designed as the stratotype for this formation (Figure 2; Supplementary Logs). Its lower boundary is faulted in all cases, whereas its transitional upper boundary with the Pedra de s’Ase Formation is visible in both of the logged sections and is defined by a shift from very fine- to fine-grained red sandstone beds to medium- to coarse-grained pink/blue/white beds with blue lutites at their base (Figures 3A, 3C; Supplementary Logs; Supplementary Correlations). There are large covered stretches in all the

outcrops representing the lower half of this formation, probably concealing faults; for this reason, the thickness of this unit has been given in ranges. The minimum corresponds to the thickness of the part of the sequence that is certainly continuous and not faulted, whereas the maximum includes all the covered parts and faulted zones.

4.2.2. Lithological features and palaeontological content

The lithofacies (Figure 4, Table 1) and architectural elements (Table 2) of this formation show a notable diversity accounting for different depositional palaeoenvironments. Breccia lithofacies of types *Gm* and *Gt* (Figure 4A) constitute the base of sandstone packages or as isolated beds among lutites, may be massive or have crude bedding, and their clasts are always soft pebbles of lutite and sandstone, sometimes with carbonate nodules and fragments of rhizocretions. Sandstones account for about the 60% of all the rocks of the studied sections, and the most abundant lithofacies are those of types *St* and *Sl* (Figure 4E). In some cases, lithofacies of types *Sp*, *Sm* and, rarely, *Sh* also appear. Lithofacies of types *Sr* and *Sl* become abundant towards the upper part of the sandstone intervals, and occur in tabular beds intercalated between lutites. Lithofacies type *Ss* (Figure 4I) appears rarely, in the form of sandstone beds with erosive bases, with crude bedding and usually soft pebbles. Lithofacies type *Sb* (Figure 4C) corresponds to sandstones with abundant invertebrate bioturbation. Regarding lutite lithofacies, the most abundant type is certainly *Fm*, massive, followed by type *Fl*, with horizontal or ripple lamination. Lithofacies of types *Fr* and *Fb* (Figure 4N) show bioturbation produced by plant roots and invertebrate burrows, respectively. Lithofacies type *P* (Figure 4O), in the form of calcic Vertisols, vertic Calcisols and Calcisols, shows rhizocretions, carbonate nodules of about 1–3 cm of diameter (rarely, calcrete hardpans are present in the lower part of the unit) and/or gleyed patches. In terms of architectural elements, this formation is clearly dominated by the elements *LA*, with lateral accretion surfaces, *LV+CR+CS*, sandstones and lutites with tabular or locally erosive geometries, and *FF*, fine sediments. The element *SS* is also present very rarely. It is also interesting to note that at the type section (Port des Canonge–Hort de sa Cova), the element *LA* is overall more frequent than *LV+CR+CS* and *FF*, whereas at the Racó de s’Algar–Pedra de s’Ase section the three elements appear in a more balanced proportion. The Port des Canonge Formation is locally very rich in fossils, which include rhizocretions, macrofloral remains, invertebrate trace fossils, tetrapod tracks and tetrapod bones (including complete skeletons).

4.2.3. Interpretation

In this formation, breccia lithofacies of types *Gm* and *Gt* constitute the basal lag of lateral accretion bars and major channel deposits, or as isolated events interbedded between floodplain lutites. They can be interpreted as the reworking of the underlying sediments (usually floodplain

lutites, sandstones or palaeosols) by meandering channels or unconfined flows of crevasse splays, respectively, exactly as in the Permian of Menorca as described in great detail by Gómez-Gras & Alonso-Zarza (2003). Sandstone lithofacies of types *St* and *Sl*, often *Sp* and *Sm* and, rarely, *Sh*, are the main constituents of the lateral accretion bars of major channels. Towards the top of the channel deposit sequences, lithofacies of types *Sr* and *Sl* become abundant, representing the waning of the flow and overbank deposits over the floodplains. Lithofacies type *Ss* appears rarely in the floodplains, corresponding to confined flows, possibly from sporadic events of increased energy, forming scour deposits. Lithofacies type *Sb* can appear in any combination with the ones above, representing a halt of the sedimentation and the colonisation of those beds by burrowing invertebrates and/or plants. Lutite lithofacies type *Fm* corresponds to settled sediments in the floodplains, although in some parts the slightly more energetic lithofacies type *Fl* can also appear. Lithofacies of types *Fr* and *Fb* represent the reworking of floodplain lutites by plant roots and invertebrate burrows, respectively, indicating periods of very little sedimentation or subaerial exposure. Finally, lithofacies type *P* culminates this biogenic occupation of the soils, with very abundant carbonate nodules and even calcretes, with occasional gleyed patches, indicative of palaeosols formed under climatic conditions with low precipitation regimes (see Mack *et al.*, 1993; Alonso-Zarza, 2003). Calcrete hardpans and large calcareous nodules appear only in the lower and middle parts of the Port des Canonge Formation, and in the upper part nodules are generally smaller. Architectural element *LA* represents point bar deposits, *LV+CR+CS* correspond to levée, crevasse channel and crevasse splay deposits, *SS* has been interpreted as sheetflood deposits, and *FF* as floodplain fine sediments (playas and playa lakes).

The fining-upwards sequences with thick lutitic packs corresponding to floodplain deposits, the abundance of lateral accretion surfaces in the vast majority of the sandstone channel deposits (Figures 2D, 2E, 2F), and the fact that those surfaces dip mostly perpendicular to the main palaeocurrent trend (NE/SW vs. SE: Calafat, 1988), point to fine-grained sandy meandering river systems (Miall, 2006) as the main palaeoenvironment recorded in the Port des Canonge Formation. During the dry season, the swales and chute channels were ponded or even completely desiccated, as evidenced by the development of large mud cracks and palaeosols in the bar top lutites. Those ponds probably functioned as waterholes, and in some occasions they were intensely trampled by tetrapods (Matamalas-Andreu *et al.*, 2021d). The palaeocurrents measured in this formation (n = 50) show a wide dispersion but with a general trend towards the South–East (mean of 149.2°; see ‘8. Discussion’ below).

4.3. Pedra de s’Ase Formation

This formation (Figure 3) can be identified in the field because the sandstones form thick packages, they are usually medium-grained and their colour is usually yellowish, white, blue or pink (contrary to the red sandstones of the two other Permian formations of Mallorca). Lutites are comparatively less frequent, and they can either be red or blue in colour.

4.3.1. Location and boundaries

The two largest outcrops of the Pedra de s'Ase Formation are at the Racó de s'Algar–Pedra de s'Ase section (190.8–202.8 m, Figures 1B, 3B) and at the Port des Canonge–Hort de sa Cova section (167.5–225.2 m, Figures 1D, 3D). Other important sites are those including Pedrera de sa Cova (100.4 m, Figures 1D, 3E) and Marina de Valldemossa (70 m, Figure 1C) sections. There are smaller outcrops at Na Vermella (Figure 1C), at Platja de sa font Figuera (Figure 1C) and at Platja des Mabres (Figure 1D), although they are heavily affected by tectonics and are in some cases mostly covered. The Racó de s'Algar–Pedra de s'Ase section is the thickest and the one least affected by tectonics and, although it is at some points quite inaccessible (flooded and vertical passes), it is here formally defined as the stratotype for this formation (Figure 3). Its lower boundary has been described in '4.2. Port des Canonge Formation'. Its upper boundary probably crops out at Pedrera de sa Cova (Figure 3E) in the form of an unconformable contact that gives way to the pink–white sandstones of the Triassic Punta Roja Formation (Matamales-Andreu *et al.*, 2021b). Its minimum thickness is about 200 m and its total thickness is difficult to precisely establish because the section, including the top of the formation, cannot be reliably correlated with the rest.

4.3.2. Lithological features and palaeontological content

In this formation, all the lithofacies (Figure 4, Table 1) broadly represent the same depositional processes and environments as those of the Port des Canonge Formation (see '4.2. Port des Canonge Formation' above), although their grain size is almost always coarser and the floodplain-related deposits are scarcer (Figure 4D, 4F, 4G, 4J, 4K, 4M). Apart from that, the most remarkable difference is the appearance of blue or, very rarely, greenish lutites, horizontally laminated and rich in organic matter (lithofacies type *Fl*, Figure 4L), that represent sedimentation in oxbow lakes. Lithofacies type *P* contains abundant invertebrate burrows, rhizocretions, carbonate nodules (diameter of 1–3 cm) and, occasionally, gleyed patches. The dominant architectural elements (Table 2) are *SS*, representing sheetflood deposits, and *LA*, corresponding to point bar deposits. Secondly, elements *LV+CR+CS* and *FF* also appear as overbank deposits. In the Pedra de s'Ase Formation, sheetflood/channel sandstone deposits are dominant at the type section (Racó de s'Algar–Pedra de s'Ase), whereas at the Port des Canonge–Hort de sa Cova section the overbank deposits are almost as frequent as the sheetflood/channel deposits, contrary to the

underlying formation. Plant fossils, usually in the form of unidentifiable debris, are very common in the Pedra de s'Ase Formation. Towards the middle part of the unit, some blue lutite beds have yielded palynomorphs. Rhizocretions and invertebrate trace fossils are abundant in the beds representing floodplain and crevasse splay deposits, which can also sporadically contain plant impressions and tetrapod tracks. Complete and fragmentary tetrapod bones rarely appear in the breccia beds.

4.3.3. Interpretation

The palaeoenvironments represented by this formation are also river systems with meandering channels, although their grain size is distinctly coarser than in the underlying Port des Canonge Formation. The common stacking of the channels, and the fact that floodplain deposits (red lutites and very fine to fine-grained sandstones) appear less frequently, point to a general prograding trend. This is perhaps related to a combined increase of both the subsidence rate of the basin and the sediment input (*e.g.*, Miall, 2006). The palaeocurrents measured in this formation ($n = 50$) show a rough trend towards the South (mean of 171.2° ; see '8. Discussion' below). Floodplain settings had a rich biota, as indicated by the relative high abundance of rhizocretions and invertebrate traces, and sporadic occurrences of plant impressions, tetrapod tracks and bones. Fluvial channels probably transported large logs and other plant fragments, and oxbow lakes preserved a relatively rich record of microflora.

5. Magnetostratigraphy

The NRM intensity of the demagnetised specimens generally ranged from 10×10^{-4} to 88×10^{-4} A/m. Upon demagnetisation, NRM intensity decreases somewhat after the first heating step at 150°C in most demagnetised specimens (Figure 5A, C, D) but is noticeable in other samples (Figure 5B) and may account for 30% NRM intensity loss. This may be an indication of goethite carrying a spurious secondary magnetisation. Then, stepwise AF demagnetisation up to 100 mT does not remove any remanence in some specimens (Figure 5A, C), whereas in other specimens there is a slight decrease removing a relatively steep and downward component (Figure 5B, D) denoting the presence of a minor magnetite-like phase. Finally, thermal demagnetisation defines a straight line toward the origin of the demagnetisation diagram, which is always southerly directed and shallowly upward in the $640\text{--}690^\circ\text{C}$ range that is ascribed to hematite, likely of detrital origin (Figure 5A, C). This high temperature component conforms the ChRM direction. However, in many samples (74 out of the 144 demagnetised samples), remanence removal in the

300–640 °C range delineates a trajectory that does not trend towards the origin of the demagnetisation diagram and describes a great circle in stereographic projection. In such cases, further demagnetisation at higher temperature does not clearly define the ChRM (Figure 5B, D), and thus the ChRM directions have been calculated using the McFadden & McElhinny (1988) great circle technique, implemented in the Paleomagnetism.org software. It is argued that the carrier of this medium temperature component, which has to be of high coercivity attending the demagnetisation protocol as discussed above, may be hematite of chemical origin that would carry an undefined secondary magnetisation.

Figure 6 shows all ChRM computed directional data and derived VGP latitude plotted along corresponding lithological logs and in stereographic projections (see also Supplementary Table 2). The lack of sufficient bedding differences among the three sections precludes a fold test, and statistical parameters at specimen-level in geographic and tectonic coordinates are similar (Figure 6B). Yet, the high temperature of the unblocked ChRM that suggests detrital hematite as the main magnetic carrier and its shallow inclination, which would be incompatible with an age older than Triassic, indicates that the ChRM directions are primary. All ChRM directions are reverse and conform to the Kiaman reverse polarity Superchron (see ‘8. Discussion’ below). Note that the boundary of the Port des Canonge Formation and the Pedra de s’Ase Formation is included in both the Racó de s’Algar–Pedra de s’Ase and in the Port des Canonge–Hort de sa Cova sections. Consequently, the magnetostratigraphy from the first should overlap that from the latter section. In this scenario, the interval with no data due to lack of outcrops at the Port des Canonge–Hort de sa Cova section (290–235 m) is completed by the other section, assuming thickness of formations and intervals are comparable. Stereograms of ChRM directional data and VGPs from all analysed specimens divided for the three main sections are here presented in Supplementary Figure 1. For full ChRM data and statistics see Supplementary Table 2 and Supplementary Table 3.

Some rockmagnetic experiments have been performed and are illustrated in Supplementary Figure 2. Thermomagnetic heating curves (Supplementary Figure 2A–B) appear blurred due to the low measured values close to the sensitivity of the instrument, and only a clear decrease below about 120 °C is seen. A subtle decrease above 640 °C as indication of hematite is doubtful. Heating curves are irreversible as cooling curves show increased values denoting the formation of new ferromagnetic phases upon heating. Two clear differentiated phases with Curie temperatures of about 580 °C and 420–450 °C are observed particularly for sample PC75A (Supplementary Figure 2B). The presence of high coercivity phases is clearly illustrated by the acquisition of isothermal remanent magnetisation (IRM) curves and corresponding backfield IRMs (Supplementary Figure 2B–C). IRM acquisition curves do not saturate at the maximum fields applied (1.2 T) and coercive force H_c values around 400–450 mT fall in the range of

hematite (Özdemir & Dunlop, 2014). Unmixing of the magnetic coercivity distributions of the backfield IRM is best modelled by three components (Supplementary Figure 2D–E). The predominant component (component_1) has coercivity $\log(B)$ values around 2.69 mT ($B = 494$ mT). Another two components have slightly higher and lower coercivity respectively (component_2, $\log(B)/(B)$ of 2.92 mT/870 mT, and component_3 $\log(B)/(B)$ of 2.23 mT/176 mT). These three relatively high coercivity components could correspond to different types of hematite or grain sizes.

6. Palaeobotany

6.1. Palynology

For the present work, only five out of 35 collected samples yielded palynomorphs (Figure 7), as most of the sampled lithologies are too coarse-grained and oxidised to preserve any organic remains. In general, the sporomorphs are severely damaged and altered, and the palynomorphs are heavily oxidised. The samples yielding palynomorphs from the Pedra de s'Ase log, P-PA-05, P-PA-09 and P-PA-12, are relatively well preserved, with up to 20 different taxa (Supplementary Table 4). The samples P-CO-03 and P-CO-04 from the Pedrera de sa Cova log are poorly preserved, but it has been possible to recognise at least some sporomorphs and identify them at genus and/or species level (Supplementary Table 4).

The palynological assemblages, with almost 30 genera and almost 40 taxa (Table 3), show how diverse the local and regional flora was, despite poor preservation of the macroremains (see '6.2. Macroplant remains' below). The palynological assemblages are dominated, both quantitatively and qualitatively, by pollen grains (see Supplementary Table 4), as was previously pointed out by Ramos & Doubinger (1989). Most of them are non-taeniate bisaccate pollen grains such as *Alisporites*, *Klausipollenites*, *Jugasporites*, *Gigantospores* and *Minutosaccus*. Taeniate pollen grains are less abundant (but certainly more abundant than spores) and include, among others, the genera *Lueckisporites*, *Strotersporites* and *Protohaploxypinus*. Other bisaccate pollen grains such as *Limitisporites* and specimens assigned doubtfully to *Triadisporea* are rare. Asaccate, costate pollen grains such as *Vittatina* or other genera such as *Marsupipollenites* are very rare. The spores are rare and poorly diverse; the only genera that could be identified are *Endosporites*, *Granulatisporites*, *Osmundacidites* and *Reticulatisporites*.

Among the samples from the Pedra de s'Ase log, P-PA-05 and P-PA-09 are the two with the most diverse palynological assemblages (20 and 19 taxa, respectively), whereas the sample P-PA-12 is

less well preserved, with only 14 different identified taxa (Supplementary Table 4). The two samples from the Pedrera de sa Cova log (P-CO-03 and P-CO-04) are less diverse and yielded eight and four different taxa, respectively (Supplementary Table 4). Only *Lueckisporites virkkiae* is present in all samples yielding sporomorphs, and *Klausipollenites schaubergeri* and *Limitisporites* sp. are present at least in four of the five samples. Other taxa are present in only one of the samples, suggesting that they are rare in the palynological assemblages: among the spores, *Endosporites* sp., *Osmundacidites* sp. and *Reticulatisporites* sp., and among the pollen, *Falcisporites zapfei*, *Gardenasporites leonardii*, *Jugasporites delasaucei*, *Jugasporites* sp., *Limitisporites rectus*, *Lueckisporites globosus*, *Marsupipollenites* sp., *Minutosaccus* sp. 1, *Paravesicaspora* sp., *Platysaccus leschikii*, *Playfordiaspora cancellosa*, *Protohaploxypinus limpidus*, *Protohaploxypinus* sp., *Striatoabieites richteri*, *Strotersporites* sp., *Vitreisporites* sp., *Vittatina* sp., and doubtful assignments to the taxa *Cordaitina* sp. and *Triadispora* spp.

A comparison with previous papers of Permian rocks of Mallorca (Ramos & Doubinger, 1989; Diez, 2000; Juncal, 2019) (see Supplementary Table 4) shows that several taxa had already been mentioned before, such as the lycophyte genus *Endosporites*, whereas several fern genera such as *Granulatisporites* and *Osmundacidites* and putative bryophytes (*Reticulatisporites*) are reported here for the first time. On the other hand, some sphenophyte (*Calamospora*), lycophyte (*Kraeuselisporites*, *Lundbladispota*) and fern (*Deltoidospora*) spores, which were already known from the area, could not be identified in the samples studied for the present work. There is a close resemblance among the previous and the new assemblages, at least at a genus level. The genera *?Bascanisporites*, *Crucisaccites*, *Crustaesporites*, *Maculatasporites*, *Platysaccus*, *Potonieisporites*, *Sahnisporites*, *Striatoabieites*, *Striatopodocarpites*, *Taeniaesporites* and *Tiwariasporis* were previously listed from the area (Diez, 2000; Juncal, 2019), whereas *Gigantosporites*, *Limitisporites*, *Marsupipollenites*, *Minutosaccus* and *?Triadispora* have been identified here for the first time (Supplementary Table 4). With the exception of *Marsupipollenites* (Glossopteridales), these palynomorphs were all produced by primitive conifers (Table 3).

6.2. Macroplant remains

Well-preserved plant remains are very scarce in both the Port des Canonge and Pedra de s'Ase formations. In the former, Calafat (1988) mentioned unidentifiable carbonaceous debris, and from the latter, previous authors (Freeman & Obrador, 1979; Calafat, 1988; Ramos, 1995; Diez, 2000) mentioned and illustrated large carbonised tree logs from a specific bed near Cova des Carbó, which has been found again in the present work (Figure 8A). This work is the first to report plant shoots preserved as impressions in very fine-grained sandstones, which are described below.

Sphenophyta indet.

Figure 8B

Studied material: Several internal casts with surrounding organic material, preserved with random orientation in the sedimentary strata, left in the field. From the Pedra de s'Ase log (metre 81.0), middle part of the Pedra de s'Ase Formation, Roadian–Wordian.

Description: The stems are tens of decimetres long and few decimetres wide, the internal cast comprises yellowish to grey sandstone, surrounded by a few millimetres-thick organic film. No ornamentation is evident on the surface.

Remarks: Several of the stems probably belong to sphenophytes, although the surface is too badly preserved to show the casts of the vascular bundles. Although no clear distinction in nodes and internodes can be distinguished, this could be due to the broken surface that could also partly conceal them.

Genus *Hermitia* Kerp *et* Clement-Westerhof *in* Visscher *et al.*, 1986

Hermitia sp.

Figure 8C–D

Studied material: DA/21-15-05-01. From the Torrent de na Nadala log (metre 25.6), upper part of the Port des Canonge Formation, Artinskian–Kungurian. DA/21-15-05-03, DA/21-15-05-04 and DA/21-15-05-05. From the Torrent de na Nadala log (*ex situ* rock probably corresponding to metre 34.0), upper part of the Port des Canonge Formation, Artinskian–Kungurian.

Description: Three foliated penultimate shoot fragments of *Hermitia* sp. are preserved as coarse impressions in a reddish very fine-grained sandstone. The pinnately branched shoot fragments are up to 70 mm long with alternatively inserted two series of ultimate shoots up to 45 mm long, which arise at an angle of 45–60° from the axes. Leaves of ultimate shoots are needle-like, S-shaped and spirally arranged, 2–5 mm long and about 1 mm wide.

Remarks: The material is very fragmentary and badly preserved, with no organic material preserved. Nonetheless, the plant fossils show the typical pinnate architecture of the shoots and the narrow, needle-like leaves. The general morphological features mostly resemble *Ernestiodendron filiciformes* (Sternberg) Florin, 1934 emend. Clement-Westerhof, 1984. The fact that no epidermal features or reproductive structures are preserved, supports the assignment to the genus *Hermitia*, erected by Kerp & Clement-Westerhof (*in* Visscher *et al.*, 1986) to accommodate

remains previously assigned to the genus *Walchia*, which preserve no epidermal features and therefore can only be diagnosed in terms of leaf morphology (Visscher *et al.*, 1986).

Genus *Feysia* Kerp *et* Clement-Westerhof *in* Visscher *et al.*, 1986

?*Feysia* sp.

Figure 8E–I

Studied material: DA21/15-03-01, DA21/15-03-02, DA21/15-03-03, DA21/15-03-04, DA21/15-03-05, DA21/15-03-06, DA21/15-03-07 and DA21/15-03-09. From the Racó de s'Algar log (metre 68.9), middle part of the Port des Canonge Formation, Artinskian–Kungurian. DA21/15-04-02. From the Racó de s'Algar area (*ex situ* rock), middle–upper part of the Port des Canonge Formation, Artinskian–Kungurian. DA21/15-05-06. From the Torrent de na Nadala log (*ex situ* rock probably corresponding to metre 34.0), upper part of the Port des Canonge Formation, Artinskian–Kungurian. DA21/15-08-05, DA21/15-08-06 and DA21/15-08-07. From the Platjola des munt de Pedres area (*ex situ* rock), upper part of the Port des Canonge Formation, Artinskian–Kungurian. DA21/15-15-01 and three other specimens left in the field. From Es Tamarell log (*ex situ* rock probably corresponding to metre 18.0), lower part of the Pedra de s'Ase Formation, Roadian–Wordian?

Description: Shoot fragments preserved as coarse impressions. The ultimate shoot fragments are 30–180 mm long with spirally arranged bifacial leaves, which arise with an angle of 40–65° and can turn, in the upper part, slightly toward the apex. Leaves are linear with a slightly smooth apex, 5–20 mm long and 0.5–1.5 mm wide. One specimen that is 72 mm long and 11 mm wide has spirally arranged lanceolate to triangular leaves with a slightly pointed apex, up to 6.5 mm long and 2 mm wide.

Remarks: The plant remains are very fragmentary and preserved only as impressions with no organic material. The shoot fragments show characteristic linear, long leaves that are spirally inserted. The most similar specimens were figured as *Pseudovoltzia* sp. by Bercovici *et al.* (2009) from the upper Permian of Menorca (Balearic Islands, western Mediterranean). However, the specimens of Bercovici *et al.* (2009) not only show the typical gross morphology of *Pseudovoltzia*, but are coalified and preserve a coal film suggesting the presence of a cuticle, even if the latter is not figured nor described. The specimens of Mallorca studied here, on the other hand, do not permit the extraction of cuticle. *Pseudovoltzia liebeana* (Geinitz) Florin, 1927, from the upper Permian of Germany, closely resembles the impressions of Mallorca in the general shape of the leaves (slightly lanceolate to linear with a slightly pointed apex) and in the loose

spiral of attachment of the leaves (see Schweitzer, 1962, for a detailed description). The specimens studied here, however, have much smaller and triangular leaves in the original conifer shoots (Broutin & Kerp, 1994). This rather supports an assignment to the genus *Feysia*, since the latter was created for conifers with bifacial leaves that are spirally arranged and are broad triangular, oblong to obovate in shape with a constricted base. Most importantly, this genus includes those broad-leaved conifer shoots for which no cuticle is known. Macromorphologically very similar are the fragments of ultimate conifer shoots figured by Forte *et al.* (2018: fig. 10D) as *Quadrocladus* sp. from the Kungurian of the Southern Alps. Within the genus *Quadrocladus* Mädlar, 1964, the most similar species is *Quadrocladus orobiformis* (Schlotheim) Schweitzer, 1962, typical of the upper Permian of the Central European Basin. Our specimens resemble *Quadrocladus orobiformis* in the loose spiral manner in which the leaves are attached and in the bifacial, linear shape of the leaves. The specimens from Mallorca and the Central European Basin differ, however, in the looser spiral with a wider angle (almost 90°), as well as in the more linear shape with a more rounded leaf apex of the latter. Unfortunately, similar to *Pseudovoltzia*, the genus *Quadrocladus* is a conifer with well-known cuticles and a general morphological similarity is not sufficient for a genus-level identification in Permian conifers.

7. Trace fossils

7.1. Invertebrate traces

In the sequences of the Port des Canonge Formation studied here, invertebrate bioturbation is abundant in most of the beds representing crevasse splay deposits and floodplain fine deposits, and even in the upper part of some channel sequences. In the Pedra de s'Ase Formation, on the other hand, invertebrate burrows are less common and appear restricted to the red sandstone and lutite intervals between medium-grained whitish sandstone channel deposits. Ramos & García-Ramos (1992) reported the presence of the ichnogenera *Ancorichnus* Heinberg, 1974, *Palaeophycus* Hall, 1847, and *Planolites* Nicholson, 1873. Of these, only the latter two have been observed in the course of the present work, together with the four other ichnotaxa described here.

Ichnogenus *Arenicolites* Salter, 1857

Arenicolites isp.

Figure 9A

1 Studied material: Numerous specimens, left in the field. From the Port des Canonge–Hort de sa
2 Cova log (metre 494.2), among others, middle part of the Pedra de s’Ase Formation, Radian–
3 Wordian.

4 Description: Vertical, straight, unbranched, cylindrical burrows (diameter between 10–30 mm)
5 filled with a sediment with a texture slightly different to that of the surrounding matrix (both very
6 fine-grained sandstones), and almost always evident as paired circular openings on the bedding
7 surface (similar to those illustrated by Díez-Canseco *et al.*, 2016).

8 Remarks: The lack of complete specimens in lateral section has precluded ichnospecies-level
9 identification. The tracemakers of this ichnogenus are considered to be suspension-feeding and
10 deposit-feeding worms and crustaceans (Díez-Canseco *et al.*, 2016 and references therein).

11
12 Ichnogenus *Cochlichnus* Hitchcock, 1858

13 *Cochlichnus anguineus* Hitchcock, 1858

14 *Cochlichnus anguineus*

15 Figure 9B

16 Studied material: Six specimens, left in the field. From the Torrent de na Nadala log (metre 26.5),
17 upper part of the Port des Canonge Formation, Artinskian–Kungurian.

18 Description: Convex hyporelief (natural cast) in the base of a medium-grained sandstone bed,
19 corresponding to thin (about 1.2 mm wide), sinuous (wavelength 6.2–7.5 mm) grooves made on
20 the sediment.

21 Remarks: This ichnotaxon occurs rarely and has only been observed on the base of one sandstone
22 bed with climbing ripples corresponding to a point bar deposit, filling the surface of the
23 underlying lutites. Laterally in the same bed, there are abundant tetrapod tracks and large mud-
24 cracks. Nematodes and/or dipteran insect larvae are considered to be the most probable
25 tracemakers of this trace (Uchman *et al.*, 2004 and references therein).

26
27 Ichnogenus *Cruziana* d’Orbigny, 1842

28 *Cruziana* isp.

29 Figure 9C

1 Studied material: One specimen, left in the field. From a recently fallen, *ex situ* block
2 corresponding to the metres 95.0–97.0 of the Port des Canonge–Hort de sa Cova section, and thus
3 in a channel deposit of the lower part of the Port des Canonge Formation, Sakmarian–Kungurian?

4 Description: Traceway preserved as a convex hyporelief on the base of a medium-grained
5 sandstone bed. The observed morphotype corresponds to a bilobate trace about 20 mm wide,
6 displaying a central longitudinal ridge with a furrow on each side. On each of the furrows, there
7 are two rows of small impressions, anterolaterally elongated, probably made by the tips of the
8 appendices of the tracemaker.

9 Remarks: The only specimen studied here has not been identified to ichnospecies level because
10 of its poor preservation. Given its size, this trace may have been produced by notostracan
11 crustaceans, similar to those described from the Massif Central (Gand *et al.*, 2008).

12
13 Ichnogenus *Palaeophycus* Hall, 1847

14 *Palaeophycus tubularis* Hall, 1847

15 *Palaeophycus tubularis*

16 Figure 9D

17 Studied material: Numerous specimens, left in the field. From the Port des Canonge–Hort de sa
18 Cova log (metre 570.0), among others, upper part of the Pedra de s’Ase Formation, Roadian–
19 Wordian.

20 Description: Relatively small (diameter of 5–10 mm), cylindrical, linear to slightly sinuous
21 burrows, which are sometimes branched, have smooth thin walls, are oblique or horizontal to
22 stratification, and their filling is the same as the surrounding matrix (very fine- to medium-grained
23 sandstone).

24 Remarks: The specimens observed in Mallorca correspond to the ichnospecies *Palaeophycus*
25 *tubularis* because their walls are smooth and thin (see Pemberton & Frey, 1982). It has been
26 observed sporadically in the sandstone deposits of the upper part of channel sequences, both in
27 the Port des Canonge Formation and in the Pedra de s’Ase Formation. In continental settings,
28 these traces have been interpreted as a dwelling structure, possibly made by orthopteran,
29 hemipteran or coleopteran insects (Krapovickas *et al.*, 2008 and references therein).

30
31 Ichnogenus *Planolites* Nicholson, 1873

1 *Planolites beverleyensis* (Billings, 1862)

2 *Planolites beverleyensis*

3 Figure 9E

4 Studied material: Numerous specimens, left in the field. From the Pedra de s'Ase log (metre 3.0),
5 among others, lower part of the Pedra de s'Ase Formation, Roadian–Wordian.

6 Description: Cylindrical, large (diameter between 5–15 mm), linear to slightly sinuous, usually
7 unbranched, smooth, horizontal or oblique, unwallled burrows with a filling that is slightly
8 different to that of the surrounding matrix (lutites, very fine- or fine-grained sandstones).

9 Remarks: Overall, this ichnospecies is dominant in the floodplain deposits of all studied sections,
10 both in the Port des Canonge Formation and in the Pedra de s'Ase Formation. It corresponds to
11 this ichnospecies because they are relatively large, straight to gently curved burrows (see
12 Pemberton & Frey, 1982). This ichnogenus is thought to have been produced by deposit-feeder
13 vermiform organisms (Díez-Canseco *et al.*, 2016 and references therein).

14
15 Ichnogenus *Taenidium* Heer, 1877

16 *Taenidium barretti* (Bradshaw, 1981)

17 *Taenidium barretti*

18 Figure 9F

19 Studied material: Several specimens, left in the field. From the Pedra de s'Ase log (metre 61.5),
20 middle part of the Pedra de s'Ase Formation, Roadian–Wordian.

21 Description: Slightly sinuous to winding, unbranched, unwallled, horizontal burrows (width of
22 about 10 mm) with a meniscate backfill (with short, arcuate and densely-packed menisci) filled
23 with similar sediment to that of the surrounding matrix (medium-grained sandstones).

24 Remarks: This ichnospecies has been identified in a crevasse splay sandstone deposit in a
25 floodplain interval of the middle part of the Pedra de s'Ase Formation. The specimens are similar
26 to what Ramos (1995) figured as *Ancorichnus*, which is characterised by a thick wall (*e.g.*, Boyd
27 & McIlroy, 2017) that is not observed in the ones studied here. In continental environments,
28 *Taenidium* is thought to have been produced by coleopterans (Baucon *et al.*, 2014) aestivating in
29 moist sediment during dry periods (Minter *et al.*, 2007).

7.2. Ichnofacies

The ichnofossils recognised in the present study can be attributed to different kinds of ichnofacies (Buatois & Mángano, 1998), making it possible to infer the palaeoenvironment in which they were formed. Among the recognised invertebrate trace fossils, *Arenicolites* isp. is a representative of the *Skolithos* ichnofacies, typical of high-energy environments (Buatois & Mángano, 1998), in this case crevasse splay lobes. *Cruziana* isp., *Taenidium barretti* and the tetrapod tracks (see ‘7.3. Tetrapod tracks’ below) are indicative of the *Scoyenia* ichnofacies, representing areas with periodic flooding and desiccation (Buatois & Mángano, 1998). Finally, *Cochlichnus anguineus*, *Palaeophycus tubularis* and *Planolites beverleyensis* are indicative of the *Mermia* ichnofacies, typically developed in deposits with more persistent water bodies (Buatois & Mángano, 1998). Therefore, in the studied sequences, the *Skolithos* ichnofacies was probably established on freshly deposited crevasse splays, the *Scoyenia* ichnofacies corresponded to the margins of channels and playa lakes, and the *Mermia* ichnofacies developed in the deepest parts of the relatively shallow playa lakes and swales.

7.3. Tetrapod tracks

In the Permian deposits of Mallorca, ichnogenus-level identifiable tetrapod ichnites have so far only been found at the Racó de s’Algar–Pedra de s’Ase section. There, 15 beds with tracks have been located in the upper part of the Port des Canonge Formation, and two other beds have been observed in the lower part of the Pedra de s’Ase Formation. In almost all cases, they are preserved in convex hyporelief (natural casts) on the base of very fine- to fine-grained sandstone beds corresponding to crevasse splay deposits, which record the surface of underlying lutite beds where the tracks were originally imprinted. In only two cases the ichnites are preserved as concave epireliefs on the surface of very fine-grained sandstones. Calafat *et al.* (1986, 1986–1987) and Calafat (1988) were the first to report some of the tracksites here studied, but they provided only preliminary identifications. In Supplementary Figure 3 we present pictures taken by those authors in the 1980s. Most of these ichnites no longer exist.

Ichnogenus *Hyloidichnus* Gilmore, 1927

Hyloidichnus bifurcatus Gilmore, 1927

Hyloidichnus bifurcatus, large morphotype

Figure 10A–C; Supplementary Table 5

Studied material: NA-25.6-01a, NA-25.6-01b, NA-25.6-01c, NA-25.6-01d, NA-25.6-01e, NA-25.6-01f (natural cast of a trackway with two left manus-pes sets, a right manus track and a right pes track). From the Torrent de na Nadala section (metre 25.6), upper part of the Port des Canonge Formation, Artinskian–Kungurian. NA-26.0-02c, NA-26.0-02d, NA-26.0-02e (natural cast of a partial trackway with a left manus-pes set and a right pes track). From the Torrent de na Nadala section (metre 26.0), upper part of the Port des Canonge Formation, Artinskian–Kungurian. NA-77.5-01a, NA-77.5-01b, NA-77.5-01c, NA-77.5-01d (natural cast of a partial trackway with two left manus-pes sets) and NA-77.5-01e (natural cast of a right pes track). From the Torrent de na Nadala section (metre 77.5), upper part of the Port des Canonge Formation, Artinskian–Kungurian. PM-15.7-01a, PM-15.7-01b (natural cast of a right manus-pes set). From the Punta d'en Pere Mir section (metre 15.7), lower part of the Pedra de s'Ase Formation, Roadian–Wordian?

Description: Pes imprint semiplantigrade, pentadactyl, ectaxonic and slightly wider (ca. 10–12 cm) than long (ca. 7–10 cm). The digit imprints are relatively stout, straight and long, especially in the case of digits III and IV. The imprints of digits I and II are usually only preserved proximally, and that of digit V is either not present or preserved only as the tip. Their relative lengths are ordered as follows: $I < V \approx II < III < IV$. There is a general decrease in depth from digit I to digit V, giving a more slender appearance to the imprints of digits III and, especially, IV. Moreover, those two often show expanded, “T”-shaped tip imprints. Digit imprints radiate from the sole with no superimposition, forming a wide digit I–V angle (ca. 135°). The oval sole imprint is anteroposteriorly short, much wider than it is long, and may be slightly concave posteriorly. The most deeply imprinted area is digit II, followed by the medial part of the sole and digits I and III, and then the tips of digits IV and V (medial functional prevalence of the autopodia).

Manus imprint semiplantigrade, pentadactyl, ectaxonic and wider (ca. 9–10 cm) than long (ca. 6.5–8.5 cm). The digit imprints are of variable stoutness (probably depending on the substrate), ranging from thin, straight, long digits with “T”-shaped expanded tip imprints to thick, straight, long digits with round tip imprints. Their relative lengths are ordered as follows: $I < V < II < III < IV$. All digits are equally well-imprinted except for the proximal part of digit V, which may be missing. Digit imprints radiate from the palm with no superimposition, forming a digit I–V angle of about 95°. The palm imprint is oval and very short anteroposteriorly, with a posterior margin than can be straight or slightly concave. The most deeply imprinted area is usually located around digit III, becoming shallower laterally (medial-median functional prevalence of the autopodia).

Trackway quadrupedal with semi-alternating manus-pes sets, and with pes imprints slightly larger than manus imprints. Pace angulations for both the pes and the manus imprints are around 90°. Pes impressions are essentially parallel to the midline (can be very slightly rotated laterally or

medially), whereas manus impressions are rotated ca. 30° medially and located anteromedially from the pes impressions. Pes and manus imprints are often well separated; however, in rare cases they are almost in contact, but never overstepping. No tail traces have been observed either.

Remarks: The specimens studied here agree with the ichnogenus *Hyloidichnus* based on the following combination of characters: (1) semiplantigrade ichnites, wider than long, ectaxonic, with relatively long, straight and radial digit imprints ended in expanded tips, (2) pes digit V impression short, (3) acute angle between manus digit IV–V imprints, (4) manus imprints slightly smaller than those of the pes, and (5) manus imprint rotated inwards and pes imprints parallel to the midline (Gand, 1988; Voigt, 2005; Marchetti, 2016, Marchetti *et al.*, 2020). The Mallorcan material agrees with the only considered valid ichnospecies (see discussion in Marchetti *et al.*, 2013), *Hyloidichnus bifurcatus*.

The ichnogenus *Hyloidichnus* is known from the Sakmarian (lower Permian) to the Wuchiapingian (upper Permian) of southern North America, South America, Lodève and Provence, the Iberian Peninsula, the island of Menorca, the Alps, northern Africa, central Africa, and the Anatolian Peninsula (Schneider *et al.*, 2020; Logghe *et al.*, 2021; Matamales-Andreu *et al.*, 2021c and references therein). It is generally agreed that the trackmakers of *Hyloidichnus* were captorhinomorph eureptiles (*e.g.*, Gand, 1988; Haubold, 2000; Gand & Durand, 2006; Voigt *et al.*, 2010; Logghe *et al.*, 2021). Interestingly, a fragment of maxilla with parts of the palate of an indeterminate moradisaurine captorhinid eureptile was recently reported from the Port des Canonge Formation at Platja de son Bunyola (Liebrecht *et al.*, 2017; see also Matamales-Andreu *et al.*, 2021c; Supplementary Text 2; Supplementary Logs: metre 69 of the Port des Canonge–Hort de sa Cova log presented herein). Although the scarcity of osteological remains makes it impossible to confirm it, these large *Hyloidichnus* tracks from the Racó de s’Algar site could correspond to footprints of a large moradisaurine such as the one recovered from the Platja de son Bunyola site.

Hyloidichnus bifurcatus, small morphotype

Figure 10D–F; Supplementary Table 5

Studied material: NA-26.0-09r, NA-26.0-09s (natural cast of a right manus-pes set). From the Torrent de na Nadala section (metre 26.0), upper part of the Port des Canonge Formation, Artinskian–Kungurian. NA-66.4-02a, NA-66.4-02b (natural cast of a left manus-pes set) and NA-66.4-04a, NA-66.4-04b (natural cast of a left manus-pes set). From the Torrent de na Nadala section (metre 66.4), upper part of the Port des Canonge Formation, Artinskian–Kungurian.

Description: Pes imprint semiplantigrade, pentadactyl, ectaxonic and slightly wider (ca. 5–6 cm) than it is long (ca. 4–5.5 cm). The digit imprints are thin, straight and relatively long, often with expanded (“T”-shaped) tip imprints. Their relative lengths are ordered as follows: $I < V \approx II < III < IV$. Digit imprints radiate from the sole with no superimposition, forming a wide digit I–V angle (ca. 122°). The oval sole is usually poorly imprinted, and it has been observed that it is anteroposteriorly very short, much wider than it is long, and may be slightly concave posteriorly. The most deeply imprinted area is the tip of digit III, followed by the rest of the digit, digits II and IV and the sole (medial-median functional prevalence of the autopodia). Digits I and V are usually poorly imprinted, often only as the tip.

Manus imprint semiplantigrade, pentadactyl, ectaxonic and slightly wider (ca. 4.5–5 cm) than it is long (ca. 3–4.5 cm). The digit imprints are thin, straight and relatively long, with slightly expanded tips. Their relative lengths are ordered as follows: $I < V < II < III < IV$. There is a general decrease in depth from digit I to digit V, with digits IV and V being more weakly imprinted, especially their proximal parts. Digit imprints radiate from the palm with no superimposition, forming a digit I–V angle of about 113° . The palm imprint is very short anteroposteriorly, with a posterior margin that is somewhat concave. Metatarsophalangeal pads have been observed at the bases of digit I–V imprints. They are round and they diminish in size from digit I to V, but this is probably because the imprint is deepest in the medial part. The most deeply imprinted areas are the tips of digits II and III, followed by the rest of digits II, III, digits I and IV and the medial half of the palm (medial functional prevalence of the autopodia).

Trackway not clearly observed but certainly quadrupedal, with pes-manus sets showing that the manus imprints are slightly smaller than those of the pedes. The imprints of the manus are rotated medially and are located slightly medially (inwards) with respect to the pes imprints. No overstepping of pes and manus imprints has been observed.

Remarks: These ichnites are very similar to the larger *Hyloidichnus* described above, and can be attributed to the same ichnogenus and ichnospecies based on the features mentioned above. However, they have been individualised here because (1) the consistent separation in two size classes, which roughly correspond to the two different-sized moradisaurines of which bone fossils appear in the same formation (Liebrecht *et al.*, 2017; Matamales-Andreu *et al.*, 2021e), and (2) the slightly different relative depth pattern of both the pes and manus impressions. The functional prevalence of the autopodia of the large morphotype has been inferred to be medial for the pes and medial-median for the manus, whereas in the small morphotype it is medial-median and medial, respectively.

Ichnogenus *Dromopus* Marsh, 1894

Dromopus isp.

Figure 10G–H; Supplementary Table 5

Studied material: NA-77.5-01f (natural cast of a right pes track) and NA-77.5-01g (natural cast of a right ichnite, possibly a pes track, partially overlapped with another ichnite, perhaps a manus track). From the Torrent de na Nadala section (metre 77.5), upper part of the Port des Canonge Formation, Artinskian–Kungurian.

Description: Pes imprint semiplantigrade–digitigrade, pentadactyl, ectaxonic and as long as it is wide (ca. 1×1 cm) (NA-77.5-01f), or clearly longer (2.6 cm) than it is wide (2 cm) (NA-77.5-01g). The digit imprints are long and slender, and have pointed tips. In NA-77.5-01f, they are very thin and knobby. Imprints of digits II, III and IV are distally curved medially (inwards) and have slightly expanded tips, corresponding to pointed to rounded claw traces. In NA-77.5-01f, digit I imprint is straight and digit V is only recorded by a triangular, pointed tip imprint. In NA-77.5-01g, only the proximal part and tip imprints of digits III and IV are preserved, and the imprint of digit V is present only as the tip. Their relative lengths are ordered as follows: $I < V < II < III < IV$. In the case of NA-77.5-01f, digit imprints radiate from the sole with no superimposition, whereas in NA-77.5-01g the imprints of digits I–IV are strongly directed anteriorly and their bases are slightly overlapped. Only the most anterior part of the sole is imprinted, in the form of the basal region of the digits I–IV. In the two studied ichnites, the angle between the imprint of digits II–IV ranges between $51\text{--}59^\circ$. In NA-77.5-01f, the most deeply imprinted area are the proximal parts of digits I–III, followed by its distal parts and the proximal part of digit IV (medial functional prevalence of the autopodia). In NA-77.5-01g, the most deeply imprinted area is the distal half of digit II, followed by digit I and the tips of digits III and IV (medial functional prevalence of the autopodia).

A possible manus imprint is overstepped by that of the pes in NA-77.5-01h. It is digitigrade, with three preserved digit imprints, which are much shorter than those of the pes. It has not been possible to measure most of the parameters, and it can only be said that it is located slightly medial–posterior with respect to the imprint of the pes.

Remarks: Ichnites of this morphotype are usually preserved in the form of a few isolated digits, hindering its description. The ichnites studied herein can be attributed to the ichnogenus *Dromopus* based on the following combination of characters: (1) long, slender digit imprints (especially those of III–IV), slightly curved medially and with pointed tips, (2) digit I imprint not curved posteriorly, and (3) pes imprint more deeply impressed than the manus imprint (see Gand,

1988; Voigt, 2005; Marchetti *et al.*, 2017b). However, it has been left in open nomenclature given the lack of complete manus imprint and trackway information.

Dromopus is a widespread ichnogenus of Europe, North America and North Africa, ranging from the Moscovian (upper Carboniferous) to the Changhsingian (upper Permian) (Voigt & Lucas, 2015; Meade *et al.*, 2016 and references therein). Araeoscelidian diapsid reptiles and non-varanodontine varanopids are considered to be their most probable trackmakers (Gand, 1988; Haubold, 2000; Voigt, 2005; Gand & Durand, 2006; Marchetti *et al.*, 2021a, 2022).

Ichnogenus *Pachypes* Leonardi, Conti, Leonardi, Mariotti *et* Nicosia, 1975

Pachypes olliery (Ellenberger, 1983)

cf. *Pachypes olliery*

Figure 10I; Supplementary Table 5

Studied material: NA-66.6-01a (natural cast of a right pes track). From the Torrent de na Nadala section (metre 66.6), upper part of the Port des Canonge Formation, Artinskian–Kungurian.

Description: Pes imprint semiplantigrade–plantigrade, pentadactyl, ectaxonic and essentially as wide (9.49 cm) as it is long (9.52 cm). The digit imprints are stout, thick and relatively short, have round tips, and their relative lengths are ordered as follows: V<I<II<III<IV. The imprints of digits I and II are straight, whereas the tip imprints of digits III and IV are slightly curved medially, ending in sliding traces towards the medial part. There is a notable decrease in depth from digit I to digit IV, especially considering the proximal and middle parts of each of them. This gives a slenderer appearance to digit III and IV imprints, which are clearly shallower in their proximal and middle portions. Digit V imprint is the shortest, and is wide but faintly impressed. The imprints of digits II–IV are slightly convergent at their bases, whereas those of digits I and V are more separated. Possible skin impressions can be observed in the bases of the imprints of digits II–IV in the form of conspicuous creases. The sole imprint is wider than it is long, and its posterior margin is convex. There are two main depressed areas: the first one occupies the anterolateral region, from the base of the imprint of digit II to the base of the imprint of digit V (metatarsophalangeal pads of digits III–V); the second one, medial–posterior, goes from the base of the imprint of digit I (metatarsophalangeal pad of digit I) to the posterior margin of the sole impression. The most deeply imprinted areas are the tips of digits II–IV, followed by the medial part of the sole and the tip of digit I (medial functional prevalence of the autopodia).

Remarks: The ichnite studied here may be assigned to the ichnogenus *Pachypes* based on the following combination of characters: pes imprint indicating a medial functional prevalence, almost as wide as long, with short and thick digit imprints that converge proximally and have round tips, and well-impressed sole, slightly wider than it is long. Relatively similar, coeval ichnogenera with which it could be confused are *Limnopus* Marsh, 1894, *Amphisauropus* Haubold, 1970, *Ichniotherium* Pohlig, 1892 and *Hyloidichnus* Gilmore, 1927. It differs from *Limnopus* and *Amphisauropus* because the digit imprints of the Mallorcan track are relatively short, thick, stout, slightly curved medially (digits III and IV) and proximally superimposed (digits II–IV) (see Gand, 1988; Lucas *et al.*, 2001; Voigt, 2005; Marchetti, 2016; Marchetti *et al.*, 2017c). It differs from *Ichniotherium* because of the anteroposteriorly longer sole imprint lacking the distinct, mediolaterally extended ovate pad, in the lack of proximal superimposition of the digit imprints, and in the significantly shorter digit V imprint, well-separated from that of digit IV (see Voigt, 2005; Voigt *et al.*, 2007; Romano *et al.*, 2016; Buchwitz & Voigt, 2018; Marchetti *et al.*, 2018; Mujal & Marchetti, 2020). It differs from *Hyloidichnus* in the anteroposteriorly long sole and in the digit imprints being very thick, stout, short, slightly curved medially and, in the case of imprints of digits II–IV, converging at their bases (see Gand, 1988; Voigt, 2005; Marchetti, 2016; Logghe *et al.*, 2021). Nevertheless, the use of open nomenclature at ichnogenus level is here preferred, given that only one isolated ichnite is available for study.

The ichnogenus *Pachypes* currently includes three valid ichnospecies that differ essentially in their digit imprint thickness, superimposition and in the maximum size of the tracks (Marchetti *et al.*, 2021b). Of those three, the only coeval ichnospecies is *Pachypes ollieryi* (Ellenberger, 1983), which ranges from the Cisuralian to the Guadalupian of southern North America and southern Europe (Marchetti *et al.*, 2021b and references therein). The Mallorcan specimen is quite large for that ichnospecies but falls in its range of sizes, being slightly smaller than the largest known specimen (see Marchetti *et al.*, 2021b). Small specimens of *Pachypes dolomiticus* Leonardi, Conti, Leonardi, Mariotti *et* Nicosia, 1975, illustrated by Valentini *et al.* (2009: fig. 3A–B, G–H), are also similar to the track studied herein in terms of general proportions, but have thicker digit III–IV impressions and show a higher degree of proximal digit superimposition (see discussion in Marchetti *et al.*, 2021b). Specimens of *Pachypes loxodactylus* (Dudgeon, 1878) have pes imprints with digits proportionally longer than the sole and less proximally superimposed (see Marchetti *et al.*, 2019b, 2021b; Mujal *et al.*, 2020). Taking all of the above into account, if the specimen on the slab NA-66.6-01 belonged to the ichnogenus *Pachypes*, it would agree with *P. ollieryi* in both age and general shape.

Ichnites of the ichnogenus *Pachypes* have been attributed to pareiasauromorph parareptiles (Valentini *et al.*, 2009). Specifically, *P. ollieryi* was assigned to small nycteroletid non-pareiasaur pareiasauromorphs (Marchetti *et al.*, 2021b).

Ichnogenus *Dimetropus* Romer & Price, 1940

Dimetropus leisnerianus (Geinitz, 1863)

Dimetropus leisnerianus

Figure 11A–G; Supplementary Table 5

Studied material: NA-25.6-01g (natural cast of a left pes track), NA-25.6-01h (natural cast of a right pes track). From the Torrent de na Nadala section (metre 25.6), upper part of the Port des Canonge Formation, Artinskian–Kungurian. NA-26.0-02f, NA-26.0-02g (natural cast of a right manus-pes set), NA-26.0-03b, NA-26.0-03c, NA-26.0-03d, NA-26.0-03e, NA-26.0-03f, NA-26.0-03g, NA-26.0-03h, NA-26.0-03i, NA-26.0-03j, NA-26.0-03k (natural cast of a trackway with two right manus-pes sets and three left manus-pes sets) and NA-26.0-09g, NA-26.0-09h, NA-26.0-09i, NA-26.0-09j, NA-26.0-09k, NA-26.0-09l, NA-26.0-09m, NA-26.0-09n, NA-26.0-09o, NA-26.0-09p, NA-26.0-09q (natural cast of a trackway with three right manus-pes sets, two left manus-pes sets and a left manus track). From the Torrent de na Nadala section (metre 26.0), upper part of the Port des Canonge Formation, Artinskian–Kungurian.

Description: Pes imprint plantigrade, pentadactyl, ectaxonic and longer (ca. 4.0–6.2 cm) than wide (ca. 3.7–4.9 cm). The digit imprints are long, straight and thin; they are thinner proximally, because they are more weakly imprinted, whereas distally they are deeper and end in expanded, pointed claw traces with rounded to anteriorly elongated shape. The imprint of digit V is usually very shallow or only preserved as the tip. The relative lengths of the digit imprints are ordered as follows: V<I<II<III<IV. Digit imprints radiate from the sole with no superimposition, forming a variably wide digit I–V angle (ca. 54–118°). The imprints of the metatarsophalangeal pads in the bases of digits II–V are deep and round, and are especially conspicuous in digits II–IV. The sole imprint, slightly wider than it is long, is usually elongated posterolaterally, acquiring a crescent shape. The most deeply imprinted areas are the metatarsophalangeal pad imprints of digits III–IV and the median–lateral region of the sole, followed by the claw traces of digits I–IV and the rest of the sole (median–lateral functional prevalence of the autopodia).

Manus imprint semiplantigrade–plantigrade, pentadactyl, ectaxonic and slightly longer (ca. 4.0–4.9 cm) than wide (ca. 3.8–4.8 cm). The digit imprints are relatively long, thin and, in the case of digits II–IV, with their distal part slightly curved medially (inwards). They end in

1 pointed claw traces that may be slightly curved medially. The relative lengths of the digit imprints
2 are ordered as follows: $I < V < II < III < IV$. Digit imprints radiate from the palm with no
3 superimposition, forming a wide I–V angle (ca. 83–144°). The imprints of the
4 metacarpophalangeal pads are not always visible, but they are deep and round, and are especially
5 conspicuous in the bases of the imprints of digits III–V. The palm imprint is wider than long, and
6 is oval in shape, with a convex, curved posterior margin. The most deeply imprinted areas are the
7 metacarpophalangeal pad imprints of digits III–V and the median–lateral region of the palm,
8 followed by the claw traces of digits II–V and the rest of the palm (lateral functional prevalence
9 of the autopodia).

10 Trackway quadrupedal with alternating manus–pes sets. Pes imprints slightly larger than
11 manus imprints (weak heteropody). Pace angulations for manus imprints (99–113°) are slightly
12 wider than those for the pes imprints (ca. 97–101°). Pes imprints usually slightly rotated medially
13 (inwards), about 9–11°, whereas manus imprints are more strongly rotated medially, about 20–
14 39°, and are located anteromedially from the pedes. Pes and manus imprints are usually close to
15 each other (manus–pes distance = 4.6–7.8 cm), but they are usually not overstepping. The
16 glenoacetabular distance ranges between 18.1 and 20.4 cm.

17 Remarks: The specimens studied here are attributed to the ichnogenus *Dimetropus* and,
18 specifically, to the ichnospecies *Dimetropus leisnerianus*, based on the following combination of
19 characters (see Gand, 1988; Voigt, 2005; Sacchi *et al.*, 2014; Marchetti *et al.*, 2019c; Matamales-
20 Andreu *et al.*, 2021d): (1) ectaxonic manus and pes imprints, (2) depth of the ichnites increasing
21 towards the median–lateral part, (3) plantigrade pes imprint with posterolaterally elongated sole
22 (somewhat “crescent-shaped”), and (4) digits II–IV weakly imprinted proximally, with the clawed
23 tips being notably deeper. Preservation of all the digits is rare in the material studied herein (*e.g.*,
24 Figure 11B), and in most cases only the palm/sole imprint is preserved. When only the most
25 proximal parts of the digit imprints are preserved, these ichnites are reminiscent of the ichnogenus
26 *Gilmoreichnus* Haubold, 1971 (see Gand, 1988; Van Allen *et al.*, 2005), which may in fact be a
27 junior synonym of *D. leisnerianus*, but exploring this aspect is beyond the scope of the present
28 work. Quite commonly, tracks of this ichnospecies can also have a “pseudo-tridactyl” mode of
29 preservation, only with a well-imprinted digit IV, the proximal parts of digits III and V and the
30 median–lateral part of the palm/sole (Figure 11F).

31 *Dimetropus leisnerianus* has been reported from the upper Carboniferous to the lower
32 Permian of Great Britain (Meade *et al.*, 2016), central Europe (Voigt, 2005, Voigt *et al.*, 2012),
33 Lodève (Gand, 1988; Gand & Durand, 2006), the Iberian Peninsula (Mujal *et al.*, 2016), and
34 North America (*e.g.*, Lucas *et al.*, 2016). The possible trackmakers for *D. leisnerianus* and other
35 similar forms (*e.g.*, Gand, 1988; Voigt & Ganzewski, 2010; Lagnaoui *et al.*, 2018) are caseid,

ophiacodontid, edaphosaurid and/or sphenacodontid “pelycosaur”-grade synapsids (Voigt & Ganzelewski, 2010 and references therein).

cf. *Dimetropus* isp.

Figure 11H–I

Studied material: NA-26.0-02a, NA-26.0-02b (natural cast of a left manus-pes set), NA-26-031 (natural cast of a right pes imprint), NA-26.0-04a (natural cast of a right manus imprint), NA-26-05a (natural cast of a left manus imprint) and NA-26.0-09a, NA-26.0-09b, NA-26.0-09c, NA-26.0-09d, NA-26.0-09e, NA-26.0-09f (natural cast of a trackway with two left manus-pes sets and a right manus-pes set). From the Torrent de na Nadala section (metre 26.0), upper part of the Port des Canonge Formation, Artinskian–Kungurian.

Description: (adapted from Matamales-Andreu *et al.*, 2021d) Pes track semiplantigrade, pentadactyl, almost as long as wide (*ca.* 7.3–8.3 cm). The digit imprints are slender, strongly curved laterally (outwards) and relatively long. Preservation is quite variable: in some cases, the distal parts of digits are not well imprinted (especially digits II and III), whereas in other cases digit I seems to be imprinted twice. No clear claw traces have been observed on any specimen. The relative length of the digit imprints is ordered as follows: $V < I \approx II \approx IV \approx III$. The total divergence angle between digits I–V of pes tracks ranges from 77° to 95°. The digit imprints usually have sharp posterolateral margins, whereas their anteromedial margins have gentler slopes. The sole imprint is oval, with an almost straight to weakly convex posteromedial margin and a length of about 1/2 of the whole track. Metatarsophalangeal pads are well impressed, especially at the bases of digits I–III. The most deeply imprinted areas of the pes tracks are the metatarsophalangeal pads of digits I–III (medial functional prevalence of the autopodia).

Manus track plantigrade, pentadactyl, usually slightly wider (6.9–7.1 cm) than long (6.7–9.5 cm). Digit I–IV imprints are slender, relatively long and show clawed tips. The proximal parts of the digit imprints are directed medially, whereas the imprints of the tips are curved laterally, giving digit imprints a “hook-shaped” appearance, especially in digit III. They become thinner and gradually decrease in depth distally. Digit V imprint, which is the shortest, is almost as short as digit I, slender and usually straight, although its tip is often not well impressed. Some digit imprints, especially I and II, can have drag traces in front of their tips. The relative lengths of the digit imprints are ordered as follows: $V \approx I < II \approx IV < III$. Digits radiate from the palm, usually without significative overlapping, although the bases of digits I and II can be slightly superimposed. The total divergence angle between the imprints of digit I–V is wide, ranging

1 between 115° and 150°. The palm imprint is posterolaterally elongated, with a concave medial
2 margin (“lunate shape”). Metacarpophalangeal pads are rounded and well-impressed, especially
3 at the bases of digits I–IV with slight overlap in I and II. The most deeply imprinted areas of the
4 manus track are the metacarpophalangeal pads of digits II–III (medial-median functional
5 prevalence of the autopodia), followed by those of digits I and IV.

6 Trackway produced by a quadrupedal animal, with pes tracks slightly larger than manus
7 tracks (weak heteropody). The manus-pes sets are alternately arranged, with the manus tracks
8 positioned at the height of the mid-proximal portion of the pes track of the next couple. The pace
9 angulations of the pes and the manus imprints are of about 80° and 90°, respectively. With respect
10 to the trackway midline, pes imprints are rotated laterally (outwards) by 20–30°, whereas manus
11 imprints are rotated medially (inwards) by 9–26° and are located anteriorly from the pes imprints.
12 Manus tracks can be positioned medially or laterally from the pes tracks. The glenoacetabular
13 distance is of about 32.5 cm.

14 Remarks: Tracks attributable to this morphotype have been recently studied in depth by
15 Matamales-Andreu *et al.* (2021d), and thus only the most relevant points will be addressed here.
16 Tracks herein identified as cf. *Dimetropus* isp. (Figure 11H) are consistently larger and have a
17 different morphology than the *Dimetropus leisnerianus* tracks that appear on the same surface
18 (Figure 11A). Some particular traits of this morphotype are the mesaxonic manus tracks with
19 distally tapering digit imprints, which have claw traces directed laterally. Its pes tracks are
20 strongly rotated laterally, with digit imprints also curved laterally. The relative depth pattern of
21 the tracks is also different to that of *Dimetropus leisnerianus*, as in the latter it becomes deeper
22 laterally, whereas in the cf. *Dimetropus* isp. from Mallorca they are deeper laterally in their
23 posterior part but medial-median in their anterior part. *Ennatosaurus*-like medium-sized caseid
24 synapsids have been considered the possible trackmakers of this morphotype (Matamales-Andreu
25 *et al.*, 2021d).

26
27 Ichnogenus *Characichnos* Whyte & Romano, 2001

28 *Characichnos* isp.

29 Supplementary Figure 4

30 Studied material: RA-exs-02a (natural cast). From the Racó de s’Algar section (*ex situ* rock),
31 middle–upper part of the Port des Canonge Formation, Artinskian–Kungurian. NA-66.1-01
32 (natural casts). From the Torrent de na Nadala section (metre 66.1), upper part of the Port des
33 Canonge Formation, Artinskian–Kungurian. NA-72.4-02a (natural cast). From the Torrent de na

Nadala section (metre 72.4), upper part of the Port des Canonge Formation, Artinskian–Kungurian. PM-14.8-01a (natural cast). From the Punta d'en Pere Mir section (metre 14.8), lower part of the Pedra de s'Ase Formation, Roadian–Wordian.

Description: Elongate, parallel scratches of variable length (each of them generally between 2–11 cm long), which may be straight or slightly curved. The ends of each scratch are usually pointed, but may also be round. Two to four dragged digit imprints are preserved.

Remarks: The ichnogenus *Characichnos* has been interpreted as a swimming trace of tetrapods attributed to a wide range of trackmakers (Whyte & Romano, 2001; Melchor & Sarjeant, 2004; Klein & Niedźwiedzki, 2012; Mujal *et al.*, 2016, 2017b). The fact that *Characichnos* corresponds to a swimming trace does not exclude fully terrestrial forms as their possible trackmakers, as Smith *et al.* (2015) found swimming traces associated to *Hyloidichnus* tracks, and attributed them to the late Permian moradisaurine captorhinid eureptile *Moradisaurus*, which may have been able to swim in shallow ponds. In the case of the specimens from Mallorca, the identity of the producer(s) remains obscure.

8. Discussion

8.1. Age attributions

8.1.1. Magnetostratigraphy

Given that all ChRM directions display reverse polarity, the length of the studied sections and the biostratigraphic constraints (see '8.1.2. Palynostratigraphy' and '8.1.3. Tetrapod track biostratigraphy' below), the sampled succession is placed within the Kiaman Superchron. This long chron of reverse polarity extends from the middle Carboniferous to the middle Permian. It is set to end by the middle Wordian (middle Guadalupian), after which reverse and normal polarity intervals (the so-called Illawarra Series or Superchron) occur during the remainder of the Guadalupian and Lopingian (middle–upper Permian), extending into the Triassic (Steiner, 2006; Hounslow & Balabanov, 2018; Henderson *et al.*, 2020) (Figure 12A).

In a previous study (Banda *et al.*, 1986) reported three paleomagnetic sites sampled in red sandstones from northern Mallorca (MB03, Cala d'Estellencs, and MB01 and MB02, Port des Canonge) and assigned them to purported *Buntsandstein* facies (Triassic). They presented the mean directions plotted on a stereogram without detailed polarity and directional data, or site mean values. Later, Parés *et al.* (1989, 1992a, 1992b) reused the data from the three aforementioned sites and provided an overall mean for them ($N = 3$, Dec/Inc = 10.0/11.0 $a_{95} =$

6.0), still without information on polarity and/or individual site mean nor information at sample level. Nevertheless, the present work shows that the outcrops that Banda *et al.* (1986) sampled at Port des Canonge do not correspond to the *Bundsandstein* facies (Triassic) but rather to the Permian Port des Canonge Formation defined herein (specifically, the borings were found in metres 164–171 and 286–295 of the Port des Canonge log, see Supplementary Logs). It is difficult to compare datasets given the lack of detailed information, but our bedding-corrected mean direction for the Port des Canonge–Hort de sa Cova section ($N = 83$, $Dec/Inc = 179.41/-14.92$, $a_{95} = 3.63$) clearly supersedes the previous data (see Supplementary Figure 3).

It is well known that some sedimentary rocks, and particularly redbeds, are prone to the palaeomagnetic inclination shallowing effect, in which rocks block a magnetic remanence shallower than the expected direction for the site latitude at deposition time. Although there are methods to correct for this effect, the easiest one, which is the elongation/inclination (E–I) approach, requires a great number of directions (more than 100 are recommended) (Li & Kodama, 2016 and references therein). Considering that only 70 directions (out of the 144 computed ChRMs) are linear fits calculated with Principal Component Analysis, we refrain at this stage to attempt any correction for the shallowing effect or to provide a palaeopole from the studied strata.

8.1.2. Palynostratigraphy

Sporomorphs and palynomorphs have been found in the Pedra de s'Ase Formation, indicating a Guadalupian (middle Permian) age for at least its middle part (see Figure 12A). It is peculiar that several species described from Mallorca were reported for the first time in upper Permian deposits of the Southern Alps (*e.g.*, Klaus, 1963) or Central Europe (*e.g.*, Visscher, 1967), but have lately also been identified in Kungurian deposits of Tregiovo (*e.g.*, *Gardenasporites*, *Gigantosporites*, *Limitisporites*) (Marchetti *et al.*, 2015a; Forte *et al.*, 2018). This mixed composition of the palynoflora, with “typical” early and late Permian elements, reflects its ‘Thuringian’ character (*e.g.*, Visscher, 1968; Juncal *et al.*, 2018), corresponding to a “middle–late” Permian age. Originally, Visscher (1968) described those mixed floras as typical ‘Zechstein’ assemblages, which today would correspond to part of the Wuchiapingian and the Changhsingian (*e.g.*, Legler & Schneider, 2013), but later the term was used more and more to describe a “middle Permian” flora (*e.g.*, Juncal *et al.*, 2018). Generally speaking, it is possible to distinguish an ‘Autunian’ flora (early Permian flora), based on the presence of *Potonieisporites novicus* and *Vittatina costabilis*, among others, and a ‘Thuringian’ flora (middle–late Permian) characterised by *Lueckisporites virkkiae*, *Nuskoisporites dulhuntyi* and *Paravesicaspora splendens* (*e.g.*, Arche & López-Gómez, 2006; Juncal *et al.*, 2020). In the deposits of Mallorca, these three typical

1 ‘Thuringian’ taxa are well represented in the samples studied by Ramos & Doubinger (1989),
2 Diez (2000) and Juncal (2019) (see Supplementary Table 4). However, the latter two authors also
3 mentioned *Potonieisporites novicus* from the same bed, which is a typical ‘Autunian’ marker.
4 Regarding the new samples yielding palynomorphs studied in the present work (Figure 7, 12A;
5 Supplementary Table 4), *Lueckisporites virkkiae* is present in all five, *Nuskoisporites dulhuntyi*
6 has only been identified in P-PA-09 (Pedra de s’Ase log) and *Paravesicaspora splendens* has not
7 been found in any of them. Moreover, the association of *Crucisaccites variosulcatus* (also present
8 in all the samples reported by previous authors, see Supplementary Table 4) with pollen of the
9 *Lueckisporites* complex is considered to be characteristic of the Roadian–Wordian in Western
10 Europe (Vázquez & Césari, 2017).

11 Taking all the above into account, the samples studied by Ramos & Doubinger (1989), Diez
12 (2000) and Juncal (2019) could be considered Roadian–Wordian, yet a slightly younger age
13 cannot be completely excluded based on the palynomorphs alone. Indeed, Juncal (2019) proposed
14 a Wordian–Capitanian stage, although all taxa described can also be present during the Roadian
15 (see Supplementary Table 4), and the fact that this formation is still in the Kiaman Superchron
16 excludes a Capitanian or younger stage (Figure 12A, see also ‘8.1.1. Magnetostratigraphy’
17 above). The age attributions for the samples collected in the present work are more uncertain.
18 Only P-PA-12 (Pedra de s’Ase log), from the same bed as the samples studied by Diez (2000)
19 and Juncal (2019), can be attributed to the same age. P-PA-05 and P-PA-09 (Pedra de s’Ase log),
20 which are from below in the series, and P-CO-03 and P-CO-04 (Pedrera de sa Cova log), which
21 are from above, show relatively similar assemblages suggesting a middle Permian age as well,
22 given that they are still in the Kiaman Superchron (Figure 12A).

23 Bercovici *et al.* (2009) assigned the upper part of the Cala del Pilar section (Menorca, Balearic
24 Islands) to the middle–upper Permian (‘Thuringian’). Their palynological samples and the conifer
25 remains described from the stratigraphic succession of Cala del Pilar closely resemble those
26 identified in the present paper, although the material described in Bercovici *et al.* (2009) is much
27 more diverse. Most of the taxa described herein or listed by Ramos & Doubinger (1989), Diez
28 (2000) and Juncal (2019) were also found by Bercovici *et al.* (2009) (see Supplementary Table
29 4). However, there are also some genera that have not been reported in Mallorca so far, such as
30 *Densoisporites*, *Palaeospongisporis* and *Playfordispora* among the spores, and *Platysaccus*,
31 *Striatoabieites*, *Taeniaesporites* and *Tiwariasporis* among the pollen. The presence of
32 *Lueckisporites virkkiae*, and the absence of *Nuskoisporites dulhuntyi* and *Paravesicaspora*
33 *splendens*, in combination with the younger taxa present in the section of Menorca, support a
34 younger age for the upper part of the unit P3 in the Cala del Pilar section. Both the palynoflora

and the macroflora of Menorca are definitively late Permian in age, whereas the samples from Mallorca are somewhat older.

8.1.3. Tetrapod track biostratigraphy

Tetrapod tracks indicate a Cisuralian (lower Permian) age for the Port des Canonge Formation (Figure 12A). The present work has revised the ichnites studied by Matamales-Andreu *et al.* (2019), together with many new finds, which provide a thorough interpretation for the whole ichnoassemblage. The relative numbers of the identified ichnotaxa in each of the studied sites is presented in Figure 12B. At the site located lowest in the stratigraphic section, Racó de s'Algar 1, swimming traces are dominant (50%) over reptile tracks (25%), “pelycosaur”-grade synapsid tracks (25%) and anamniote tracks (0%), although the sample is very small ($n = 4$). In the Racó de s'Algar 2 site, stratigraphically located slightly higher, the trackway sample is the most abundant of all the observed sites ($n = 46$), and there is a clear dominance of tracks attributed to “pelycosaur”-grade synapsid trackmakers (84.8%) over reptile tracks (15.2%) and anamniote tracks (0.0%). In the Platjola des munt de Pedres 1 site ($n = 12$), the proportions are reversed, with numerous reptile tracks (83.3%), few synapsid tracks (8.3%) and swimming traces (8.3%), and no anamniote tracks (0.0%). The site of Platjola des munt de Pedres 2 is not represented in the charts as the sample is very low ($n = 2$) and indeterminate. Stratigraphically higher, at the Platjola des munt de Pedres 3 site ($n = 29$), reptile (51.7%) and synapsid tracks (48.3%) show very similar proportions, whereas those of anamniotes are missing (0.0%). “Pelycosaur”-grade synapsid tracks are again more numerous (60.0%) than reptile tracks (40.0%) in the Platjola des munt de Pedres 4 site, but the small sample size ($n = 5$) could easily account for a skewed proportion. Finally, in the Punta d'en Pere Mir site, which is the only tracksite in the Pedra de s'Ase Formation, the ichnoassemblage comprises reptile tracks (66.7%) and swimming traces (33.3%) but again, the sample size is very low ($n = 3$).

From the foregoing data, it is clear that synapsid tracks are generally dominant in the Port des Canonge Formation, with only one site (Platjola des munt de Pedres 3) in which reptile tracks are slightly more numerous than synapsid tracks. In this sense, although the palaeoenvironment of all the ichnite-bearing beds is essentially the same, there could be slight differences affecting the local proportions of the different ichnotaxa. Because of this, the tetrapod ichnoassemblage has been considered as a whole for the relative proportions of tracks ($n = 96$) to minimise the impact of the local particularities. This way, synapsids account for slightly more than a half of the observations (59.4%), reptile tracks are less represented (37.5%), and swimming traces are the rarest (3.1%). Anamniote tracks are altogether absent.

Based on the stratigraphic range of the ichnotaxa identified in the present work (see ‘7.3. Tetrapod tracks’ above), the Port des Canonge Formation can be dated in the Cisuralian (lower Permian); specifically, as Artinskian and/or Kungurian (Figure 12A). One of the most relevant ichnotaxa to constrain the age of this formation is *Dimetropus leisnerianus*, as it ranges from the upper Carboniferous to the lower Permian (upper Kungurian) (see Schneider *et al.*, 2020). Other ichnotaxa provide additional information: *Hyloidichnus* ranges from the lower to the upper Permian (Sakmarian–Wuchiapingian) (see Schneider *et al.*, 2020; Logghe *et al.*, 2021; Matamales-Andreu *et al.*, 2021c), *Dromopus* ranges from the upper Carboniferous to the middle Permian (middle Capitanian) (see Schneider *et al.*, 2020), and *Pachypes ollieryi* has been found from the lower to the middle Permian (Artinskian–middle Capitanian) (see Marchetti *et al.*, 2021b). cf. *Dimetropus* isp. and *Characichnos* provide no additional information, as the former is so far only known from the Port des Canonge Formation (Matamales-Andreu *et al.*, 2021d), and the latter is a long-ranging trace produced by a wide variety of tetrapods (*e.g.*, Whyte & Romano, 2001).

The relative proportions listed above make it possible to hypothesise a lower–middle Artinskian age for the Port des Canonge Formation (Figure 12A). In the Cisuralian, two successive sauropsid radiation events occurred in the middle part of the Artinskian age, and are recognised by an increase of the proportions of reptile tracks in many sites world-wide (Marchetti *et al.*, 2019d, 2022). Before the radiation, reptile tracks accounted for an average of 27% (0–40%) of the ichnoassemblages. Their numbers increased slightly during the first phase of the radiation, with an average of 37% (25–44%), and in the second phase, with an average of 47% (25–66%). In successions deposited after these two phases, reptile tracks become dominant, with an average of 68% (50–100%) (Marchetti *et al.*, 2019d). Given the relative proportions of tracks in the Port des Canonge Formation, it could correspond to the first phase of the sauropsid radiation. Remarkably, the absence of the widespread ichnogenus *Erpetopus* Moodie, 1929, in the tracksites of Mallorca may point to a pre-*Erpetopus* biochron age (Schneider *et al.*, 2020), and thus tentatively date the ichnite-bearing beds of the Port des Canonge Formation in the lower–middle Artinskian (Figure 12A). However, this age attribution is based on a relatively small sample of tetrapod ichnites, the proportions of which could vary depending on the represented sedimentary setting. Therefore, for the present work, the Port des Canonge Formation is considered Artinskian–Kungurian (Figure 12A), accepting the possibility that the lowermost part could also stretch into the Sakmarian.

8.2. Sedimentary evolution and palaeoclimate

1 Tectonics were the main factor shaping the environments in the Permian of Mallorca, which may
2 secondarily have also been affected by changes in climate. During the Artinskian and the
3 Kungurian, most rift basins of the western peri-Tethys, which had opened during the late
4 Carboniferous, were reactivated (McCann *et al.*, 2006; Cassinis *et al.*, 2012; López-Gómez *et al.*,
5 2019a). Of special interest for the present work are the tetrapod ichnite-bearing successions of the
6 Sagra/Sotres Formation (western Pyrenees; see Gand *et al.*, 1997; López-Gómez *et al.*, 2019b),
7 the Lower Red Unit/Peranera Formation (south-central Pyrenees; see Mujal *et al.*, 2016, 2018)
8 and the Rabejac Formation (Massif Central; see Gand & Durand, 2006; Michel *et al.*, 2015), all
9 dated as Artinskian and located relatively close to the study area. Those units share most of the
10 tetrapod ichnotaxa reported here from the Port des Canonge Formation (see ‘7.2. Tetrapod tracks’
11 above), such as *Hyloidichnus*, *Dromopus*, *Pachypes* and *Dimetropus* (although some are missing
12 in certain sections) and correspond to fluvial palaeoenvironments and playa lake deposits (Gand
13 & Durand, 2006; Mujal *et al.*, 2016; López-Gómez *et al.*, 2019b). Those units show a trend
14 towards semi-arid conditions in the late Cisuralian and Guadalupian, as demonstrated by the study
15 of palaeosols and geochemical proxies (Michel *et al.*, 2015; compare Mujal *et al.*, 2017a, and
16 Mujal *et al.*, 2018; López-Gómez *et al.*, 2021). In fact, by the middle Permian, most basins of
17 central Pangaea have evidence of arid climates (Schneider *et al.*, 2006; Tabor & Poulsen, 2008;
18 De la Horra *et al.*, 2012; Michel *et al.*, 2015). However, even though the succession of Mallorca
19 spans part of the lower and middle Permian (see ‘8.1. Age attributions’ above), no dramatic
20 changes in river style or palaeosol types have been observed in the three described units.

21 The lowermost Permian unit of Mallorca, the Bec de s’Àguila Formation (Figure 2), corresponds
22 to alluvial fans developed near the footwall scarp during the first stages of rifting (Figure 13).
23 Similar conglomeratic units have been reported at the base of the Permian units of other western
24 Tethyan basins (López-Gómez *et al.*, 2019a), interpreted as systems that developed transversally
25 to the main basin axis in response to the great erosion of the scarps in a period with high
26 subsidence rates (*e.g.*, Speksnijder, 1985; Franzel *et al.*, 2021; Matamales-Andreu *et al.*, 2021c;
27 see Miall, 2006 for a review of this kind of deposits). Towards the upper part of this formation,
28 sinuous channels transporting coarse-grained sediments began to develop. The climate of the Bec
29 de s’Àguila Formation was comparable to that interpreted for the Permian P1 unit of the
30 neighbouring island of Menorca (Gómez-Gras & Alonso-Zarza, 2003; Matamales-Andreu *et al.*,
31 2021c), that is, semi-arid conditions, which can be inferred because of the development of
32 carbonate palaeosols and calcretes, typical of environments with low precipitation regimes (Mack
33 *et al.*, 1993; Alonso-Zarza, 2003; Tabor & Poulsen, 2008).

34 With the likely decrease of subsidence rate, the dominant depositional setting of the Port des
35 Canonge Formation (Figure 2) was a meandering river system flowing towards the southeast and

1 following the main axis of the rift basin (Figure 13). Generation of accommodation space was
2 still significant, given the abundance of fine-grained deposits such as mudstones and very fine-
3 grained sandstones. These sequences are typical of rift basins, which have an initial stage of
4 alluvial sedimentation from the nearby scarps that is followed by the settling of a fluvial system
5 longitudinal to the basin (Miall, 2006). The fine-grained meandering channels can readily be
6 identified because of the abundant and conspicuous lateral accretion surfaces dipping roughly
7 perpendicular to the main palaeocurrent trend. One of the main factors prompting the
8 development of rivers of such style is the presence of abundant vegetation on the floodplains,
9 stabilising the riverbanks and hampering the widening of the channel and the formation of bars
10 (*e.g.*, Ebisemiju, 1994; Rowntree & Dollar, 1999; Huisink, 2000; Miall, 2006; Davies & Gibling,
11 2010; Borrueal-Abadía *et al.*, 2015). Evidence of such a plant cover lies in the abundant formation
12 of soils on the floodplains, and the sporadic presence of vegetative plant organs and logs in some
13 beds despite the unfavourable conditions for preservation of such remains in the heavily oxidised
14 red-beds. Moreover, the presence of abundant carbonate palaeosols and calcretes (calcic
15 Vertisols, vertic Calcisols and Calcisols) throughout the Port des Canonge Formation points to a
16 seasonal climate with periods of very low precipitation (Mack *et al.*, 1993; Alonso-Zarza, 2003;
17 Gómez-Gras & Alonso-Zarza, 2003; Tabor & Poulsen, 2008), similar to the underlying formation.
18 However, the presence of purported alfisols (metres 10 to 12.5 of the Torrent de na Nadala log),
19 identical to those described by Bercovici *et al.* (2009) in Menorca, also suggests the presence of
20 seasonally persistent water bodies on the floodplains. Accordingly, the climate for this formation
21 may be inferred as the alternation of sub-humid and semi-arid conditions, probably as the effect
22 of seasons. Since the palaeosols with the largest carbonate nodules and calcrete hardpans are in
23 the lower and middle parts of the Port des Canonge Formation, the climate may have been slightly
24 more arid during the deposition of those parts of the unit.

25 Energy conditions may have increased again during the time of deposition of the Pedra de s'Ase
26 Formation (Figures 3, 13), resulting in the increase of sand grain size and the amalgamation of
27 meandering point bar deposits. The increase in grain size is abrupt, whereas the decrease in the
28 amounts of lutites, very fine- and fine-grained sandstones is progressive (Figure 3). In the upper
29 part, there is again a progressive increase in the amount of lutites, very fine- and fine-grained
30 sandstones (Figure 3). Gómez-Gras (1993) suggested that in this unit, generation of new
31 accommodation space by subsidence of the basin was decreasing, and the meandering channels
32 kept migrating while reworking the floodplain and older channel deposits. This, however, could
33 also be caused by an increase of water or sediment supply, or both. The former would be expected
34 in a climate with a more regular precipitation regime, whereas the latter could be a consequence
35 of higher subsidence rates (Speksnijder, 1985; Miall, 2006). The petrological study of sandstones
36 performed by Gómez-Gras (1993) showed that the composition of the sand grains in the Port des

Canonge and Pedra de s'Ase formations was very similar. This indicates that the source area of the sediments did not change significantly, thus pointing to tectonic stability. Therefore, the most probable cause of the sedimentological change between the two formations is increased water flow. Moreover, intercalated between point bar deposits, there are tabular sandstone deposits with structures of high-flow regime indicative of flashflood episodes, as also pointed out by Ramos (1995).

The accumulation of large woody debris in the margins or in the base of shallow channels of the Pedra de s'Ase Formation (Figure 8A–B) may be either due to their being transported or even wrenched out during flashfloods, or by bank undercutting during lateral migration of the channels (*e.g.*, Braudrick & Grant, 2001; Gulbranson *et al.*, 2020). The abundance of woody debris points to densely vegetated river margins, and the fact that it appears more frequently than in the underlying Port des Canonge Formation is probably because of the increased regularity of high-energy events that could transport more large woody debris and bury it faster. The development of the same dominant types of palaeosols (vertic Calcisols and Calcisols) in both the Port des Canonge Formation and the Pedra de s'Ase Formation (with calcareous nodules of roughly the same size: 1–3 cm) suggests that the climate did not change drastically from one unit to the other, and could conflict with the hypothesis of an increased water supply derived from a more humid climate. Nevertheless, the climate could be relatively more humid in the headwaters and similarly semi-arid in the basins here studied, which would increase the water flow, but the palaeosol types would remain the same (Miall, 2006). Added to this, the increased frequency of floods would also have played a part in the formation of high-energy deposits and the generally coarser grain size of the channel deposits. Therefore, during the deposition of the Pedra de s'Ase Formation, the climate seems to have been semi-arid but with more marked seasonality and a greater water input than in the Port des Canonge Formation. Because of increased flooding, high-energy events were relatively common and the sediments were coarser in an otherwise semi-arid climate.

In line with this hypothesis, the palynological assemblage of the Pedra de s'Ase Formation reflects a complex regional landscape with a variety of different habitats under a generally semi-arid regional climate. This is reflected by the dominance of bisaccate pollen, despite the macroplant fossil assemblage being mostly represented by horsetail and/or putative conifer stems (Figure 8A–B) and conifer shoot fragments (Figure 8I). Spores of hygrophytic plants (*e.g.*, lycophytes, sphenophytes and ferns) are very rare. Those plants were probably restricted along the river banks, since most of the observed sporomorphs are bisaccates, and therefore they are well-adapted to travel over longer distances. Given that most sedimentary deposits are linked to water transport, the composition of the palynoflora is best explained by a semi-arid climate with occasional rainfall. Humid conditions in localised environments were, however, present at least occasionally,

and were covered by vegetation. This is exemplified by spores of hygrophytic plants such as bryophytes (*Reticulatisporites*), lycophytes (*Endosporites*, *Kraeuselisporites*, *Lundbladispota*), sphenophytes (*Calamospora*), and ferns (*Granulatisporites*, *Osmundacidites*), which would have colonised the margins of rivers and ponds and/or the understorey of the humid lowland. The major component of the flora were voltzialean conifers, most of which belonging to the Utrichtiaceae and other primitive families such as the Rufloriaceae and Emporiaceae (e.g., *Jugasporites*, *Limitisporites*, *Lueckisporites*, *Nuskoisporites*). Seed ferns such as Peltaspermales (e.g., *Platysaccus*, *Vittatina*) were also very abundant. The botanical affinities of some palynomorphs would support the presence of Callistophytales (e.g., *Vesicasporites*, *Paravesicaspora*), Zygopteridales (*Leiotriletes*), Corystospermales/Caytoniales (e.g., *Vitreisporites*), and Glossopteridales (*Marsupipollenites*, *Protohaploxypinus*, *Crustaesporites*) (see Table 3). The presence of especially the latter two groups is, however, doubtful, since no macroremains of these groups have so far been found in the Permian of the Central European Basin. Therefore, it is possible that the botanical affinity of these taxa is too poorly known and that these palynomorphs belong to other gymnosperms that have not been identified so far. Nevertheless, it could also be possible that a few pollen grains were transported by the wind over a distance of some thousands of kilometres, from the nearest glossopteris floras in the Southern Hemisphere to the deposits of Mallorca.

8.3. The early Permian tetrapod ichnoassemblages of Mallorca in the context of equatorial Pangaea

The global record of Cisuralian tetrapod tracks is mainly concentrated in the palaeoequatorial latitudes of Pangaea (Figure 14) (Marchetti *et al.*, 2019c, 2022 and references therein). Most of the localities share a fairly constant set of ichnotaxa, although variations through time and space can also be observed. These tracks have been used to create a biostratigraphic framework, establishing biochrons and sub-biochrons of characteristic ichnogenera based on their presence (Lucas, 2019; Schneider *et al.*, 2020). Track variation in time and space has made it possible to infer local (*i.e.*, depending on the sedimentary environment) (Hunt & Lucas, 2006; Marchetti *et al.*, 2015b, 2015c; Mujal *et al.*, 2016) or global (Marchetti *et al.*, 2019b, 2020, 2021b, 2022; Francischini *et al.*, 2020; Mujal & Marchetti, 2020; Matamalas-Andreu *et al.*, 2021d) patterns of distribution of the trackmakers.

8.3.1. Lack of tracks attributed to anamniotes in the Permian of Mallorca

Ichnogenera attributed to anamniote trackmakers, such as lepospondyls and/or temnospondyls (*Matthewichnus*, *Batrachichnus*, *Limnopus*) and “reptiliomorphs” (*Amphisauropus*, *Ichniotherium*) (see Lucas, 2019) appear to be absent in the deposits of Mallorca, which stands in sharp contrast with most other lower Permian localities worldwide (Marchetti *et al.*, 2019d, 2022). Based on the recent reviews of Marchetti *et al.* (2019d, 2022), ichnites attributed to lepospondyl and/or temnospondyl trackmakers are present (decreasing in abundance towards the end of the lower Permian) in most fluvio-lacustrine units, which is consistent with their mode of life as aquatic animals, at least during the larval stage (*e.g.*, Schoch, 2014). In the upper Artinskian–upper Kungurian Coconino and De Chelly formations of southern North America, interpreted as erg palaeoenvironments with little water availability, tracks attributed to lepospondyl and/or temnospondyl trackmakers are missing (Marchetti *et al.*, 2019d). Nevertheless, tracks attributed to seymouriamorph and diadectomorph “reptiliomorphs” have been reported from both formations (Marchetti *et al.*, 2019d), indicating that those anamniotes may have been well adapted to thrive in such arid environments. Regarding the diadectomorphs, Francischini *et al.* (2020) hypothesised that this group may have developed directly without a larval stage, and that their reproduction and early ontogenetic development stages could have been relatively independent of water. In that context, however, the putative presence of co-occurring seymouriamorphs is harder to explain, as they are known to have had aquatic larvae (*e.g.*, Klembara *et al.*, 2007), and their reproduction and early stages of development may have been related to short-lived aquatic environments developed in those erg systems. In any case, the presence of tracks attributed to both seymouriamorphs and diadectomorphs suggests that, at least during their adult stages, those groups were already adapted to environments with very low water availability.

Even though the Port des Canonge Formation of Mallorca was deposited under a semi-arid climate (see ‘8.2. Sedimentary evolution and palaeoclimate’ above), the lack of anamniote tracks and trackways amongst almost 100 occurrences is puzzling. This is especially remarkable in the case of “reptiliomorphs”, because, as discussed above, species of those groups appear to have been able to endure seasonal drying of the water bodies. In the chronostratigraphically similar and palaeogeographically close Lower Red Unit/Peranera Formation of the Pyrenean Basin, Mújal *et al.* (2016) showed that the taxonomical composition of the ichnoassemblages hinged upon their proximity to the main water bodies (*i.e.*, meandering fluvial channels). Tracks and, in some cases, swimming traces (*Characichnos* isp.) attributable to lepospondyl/temnospondyl (*Batrachichnus*, *Limnopus*), diadectomorph (cf. *Ichniotherium*), parareptile (*Pachypes*, see Marchetti *et al.*, 2021b) and araeoscelidian/bolosaurid (*Dromopus*) trackmakers were found in the lutite drapes of meandering river point bar deposits of non-functional channels (ponds or oxbow lakes). There, the swimming traces were located in the deeper parts of the channel (with traces being more abundant when it was still functioning), whereas the walking tracks had been imprinted near its

margins (Mujal *et al.*, 2016). Conversely, water runoff deposits representing palaeoenvironments with much less available water contained tracks attributable to captorhinomorph (*Hyloidichnus*), parareptile (cf. *Varanopus*) and “pelycosaur”-grade synapsid (*Dimetropus*) trackmakers (Mujal *et al.*, 2016).

It is tempting to explain the lack of tracks attributed to anamniotes in Mallorca as a result of a similar bias produced by the local setting. However, both palaeoenvironments yielding tracks in the Pyrenean Basin are also represented in the sequences of the Port des Canonge Formation of Mallorca. Essentially all the tracksites of the latter correspond to waterhole deposits (Figures 15, 16) developed in swales or abandoned chute channels in the near-channel environment, and in playa lakes in the floodplain environment (see description of similar environments by Smith, 1993). In both cases, the trampled mud was later covered by crevasse splay or low-energy channel sands. The sporadic presence of *Characichnos* (swimming traces) indicates that some of those water bodies were relatively deep, at least temporarily. The rest of the tracks were imprinted in the vicinity of those water bodies, without drastic changes in the main faunal components between near-channel environments and the floodplain. It is possible that those seasonal palaeoenvironments were more short-lived than those described in the Pyrenean Basin (Mujal *et al.*, 2016, 2018), posing a challenge for the survival of aquatic taxa. Even though no evidence of their presence has been confirmed so far, it is likely that fish and amphibians did live in the major, active channels, where preservation of biotic traces or fossils was much more difficult given the generally coarser grain size, higher energy conditions and the mode of locomotion of the (aquatic) faunas, which may have not touched the substrate (Mujal & Schoch, 2020).

Therefore, compared to the ichnoassemblages of the lower Permian of the Pyrenean Basin, those from Mallorca show that tetrapods did not have a preferential distribution with respect to the main water bodies, as the ichnoassemblages of near-channel palaeoenvironments are essentially the same as those of the floodplain palaeoenvironments. It is unlikely that the apparent absence of anamniotes was because of the semi-arid climate, as even in the hyper-arid “wet desert” of the upper Permian Moradi Formation of central Africa, Smith *et al.* (2015 and references therein) reported fish coprolites and two endemic temnospondyl species: *Nigerpeton*, interpreted to have been aquatic, and *Saharastega*, possibly more terrestrially adapted (Sidor *et al.*, 2005; Steyer *et al.*, 2006). All these animals probably lived in groundwater-fed perennial lakes. A situation similar to that of Mallorca probably occurs in the Artinskian deposits of northern Africa: in the Koudiat El Hamra - Haiane Basin, Zouicha *et al.* (2021) described an ichnoassemblage in which tracks attributable to anamniote trackmakers (cf. *Batrachichnus*) were scarce (<10%), whereas in the paleogeographically close and probably coeval Tiddas Basin, Voigt *et al.* (2011) reported that tracks produced by anamniote trackmakers were very abundant (80%). This reflects the high

variability in the distribution of these forms, and suggests that the lack of tracks attributed to anamniote trackmakers in Mallorca may be a consequence of the local palaeoenvironment rather than reflecting a true palaeobiogeographic pattern.

8.3.2. Distribution of the tetrapod tracks *Hyloidichnus* and *Dimetropus*

Hyloidichnus, attributed to captorhinomorph trackmakers (Logghe *et al.*, 2021), and *Dimetropus*, attributed to “pelycosaur”-grade synapsids (Matamales-Andreu *et al.*, 2021d), are two ichnogenera that appear in the Permian of Mallorca and that were common in the equatorial latitudes of central Pangaea (Marchetti *et al.*, 2019d, 2022 and references therein; Matamales-Andreu *et al.*, 2021c). However, despite the large number of samples collected from central Europe, *Hyloidichnus* seems to be missing (*e.g.*, Voigt, 2005). In a similar manner, *Dimetropus* appears to be extremely rare in the well-sampled sites of the Southern Alps (*e.g.*, Santi *et al.*, 2020; Marchetti *et al.*, 2022).

In both cases, those “gaps” in their distribution are probably caused by a biostratigraphic bias rather than by a true palaeobiogeographical effect. The oldest occurrence of *Hyloidichnus*, from the Abo Formation of Southern North America, has been dated as ‘Coyotean’, in this case corresponding to the Sakmarian (Lucas *et al.*, 2013; Schneider *et al.*, 2020). *Hyloidichnus* has yet to be reported from any other Sakmarian–lower Artinskian tetrapod-bearing units of the Massif Central and central Europe (Voigt, 2005; Gand & Durand, 2006; Marchetti *et al.*, 2019d), perhaps reflecting low abundance or absence of trackmakers of *Hyloidichnus* there during the Sakmarian. It is only during the middle Artinskian and the Kungurian (after the sauropsid radiation *sensu* Marchetti *et al.*, 2019d), that *Hyloidichnus* becomes abundant and almost ubiquitous (Marchetti *et al.*, 2019d). The reason behind the rarity of *Dimetropus* in outcrops of the Southern Alps (Marchetti, 2016) is probably similar, as it is the youngest (*i.e.*, Kungurian) confirmed record of this ichnogenus worldwide (Marchetti *et al.*, 2019d; Santi *et al.*, 2020; but see Lucas *et al.*, 1999, and Gand & Durand, 2006, for other putative records of this ichnogenus from the middle/upper Permian). Even though the presence of large “pelycosaur”-grade synapsids has been suggested in slightly younger deposits of the western peri-Tethys (Roadian of Sardinia: Romano *et al.*, 2019), it is possible that by the late Kungurian they had become relatively rare (Marchetti *et al.*, 2022). This is in contrast to the pre-Kungurian times, when pelycosaurs seem to have been abundant worldwide, at least based on their purported tracks (Marchetti *et al.*, 2019d, 2022). Therefore, both *Hyloidichnus* and *Dimetropus* seem to have attained widespread distribution in central Pangaea, and their absence or paucity in some regions may reflect a bias caused by the chronology of the different units.

8.4. The Permian–Triassic cycle in the Balearic Islands

In the Balearic Islands, Permian and Lower–Middle Triassic rocks representing continental palaeoenvironments only crop out on Mallorca and Menorca, whereas Middle–Upper Triassic marine and lagoonal facies appear on Mallorca, Menorca, Eivissa and Cabrera. It is currently unknown if all the islands were part of the same basin or if sedimentation took place in separate, small basins, although the latter is currently the most accepted hypothesis (*e.g.*, López-Gómez *et al.*, 2019a). Based on the review and update of all the age attributions known so far, this section proposes a correlation scheme between the three major islands (Figure 17).

The tripartite nature of the Permian series of Mallorca and Menorca could indicate they underwent a similar tectonic history with three main phases of activity, especially given their close geographical location. In Menorca, the Permian sequence consists of three units, named, from base to top, P1, P2 and P3 (Rosell *et al.*, 1988) (Figure 17). The P1 unit corresponds to transversal alluvial-fan conglomerates deposited in the first phases of rifting, the P2 unit comprises floodplain lutites with rare interbedded crevasse splay sandstones, and the P3 unit represents an alluvial plain with abundant sandstones corresponding to flashflood and meandering channel deposits (*e.g.*, Matamales-Andreu *et al.*, 2021c). In Mallorca, the lower unit (Bec de s'Àguila Formation) is essentially equivalent to the P1 unit, although neither units have been precisely dated. Regarding the other units, a similar trend exists in that the upper ones (P3 unit and Pedra de s'Ase Formation) are coarser-grained and show evidence of high-energy episodes, which are very rare in the middle units (P2 unit and Port des Canonge Formation). The P2 unit has not been reliably dated (Matamales-Andreu *et al.*, 2021c), whereas the upper part of the Port des Canonge Formation is here dated to the Artinskian–Kungurian (see ‘8.1.3. Tetrapod track biostratigraphy’ above). The upper part of the P3 unit has been dated to the Wuchiapingian–Changshingian (Bercovici *et al.*, 2009), whereas the middle part of the Pedra de s'Ase Formation is considered Roadian–Wordian (see ‘8.1.2. Palynostratigraphy’ above). Following this scheme, the P2 unit is tentatively considered lower Permian, and deposition of the unit P3 and the Pedra de s'Ase Formation may also have been coeval, at least in their lower parts (Figure 17).

The *Buntsandstein* facies (Lower–Middle Triassic) of Mallorca and Menorca also follow a similar upwards trend. On Menorca, the base of the B1 unit is represented by a conglomerate of rounded quartz pebbles and ventifacts (Rosell *et al.*, 1988; Linol *et al.*, 2009). Such beds were interpreted as the reworking of aeolian-dominated plains by braided rivers, and were tentatively dated as Lower Triassic upon correlation with similar units of the western peri-Tethys (Linol *et al.*, 2009). The rest of the unit has been interpreted as a braided river system, with a marked paucity of fine-

grained sediments (Rosell *et al.*, 1988). This unit can be correlated to the Punta Roja Formation of Mallorca (Matamales-Andreu *et al.*, 2021b), which is lithologically similar, but appears to lack the basal conglomerate (Figure 17). This appears to be similar to the Triassic deposits of Provence, where conglomerates only appeared in sections located near the depocentre of the basin (“Sanary type”), and towards the margins, the deposits are above a disconformity (“Gonfaron type”) or an angular unconformity (“Vidauban type”) (Durand, 2006). As indicated above, it is possible that the sequences of Mallorca and Menorca were deposited in two different basins; regardless, it appears that in the former, sedimentation took place near the margin of the basin (probably a “Vidauban type” boundary), whereas in the latter it occurred in the deepest parts (“Gonfaron type” boundary). The rest of the continental Triassic beds of Menorca are included in the unit B2, representing floodplain and meandering river deposits in its lower part, and coastal deposits transitional to the overlying *Muschelkalk* marine facies in the upper part (Gómez-Gras, 1987; Linol *et al.*, 2009). On Mallorca, its lateral equivalents are the Estellencs Formation (Matamales-Andreu *et al.*, 2021b) for the lower part and, possibly, the M2 unit for its upper part (Figure 17). The braided river interval of the Pedra Alta Formation and the tidal mud-flats of the Son Serralta Formation (Matamales-Andreu *et al.*, 2021b) have not been identified on Menorca (Figure 17). The absence of the latter is because the M1 unit (see below) appears to be also missing on Menorca, and the Son Serralta Formation represents the coastal environments before the initial marine transgression during the Anisian (Matamales-Andreu *et al.*, 2021b) (Figure 17).

The *Muschelkalk* facies (Middle–Upper Triassic) crop out on the three major islands of the Balearic Archipelago, but each of them appears to have unique traits. On Mallorca, three main units have been described: M1, corresponding a first marine transgression, represented by dolostones, probably of middle–upper Anisian stage (Rodríguez-Perea *et al.*, 1987; Matamales-Andreu *et al.*, 2021f), M2, interpreted as mud-flats deposited during a brief regressive pulse (Matamales-Andreu *et al.*, 2021f), and M3, the second marine transgression, with a lower part comprising dolostones and an upper part of limestones (Rodríguez-Perea *et al.*, 1987; Matamales-Andreu *et al.*, 2021f). The ammonoids of the genus *Gevanites* reported by Virgili (1952) and Goy (1995) represent the lower Ladinian (Pérez-Valera *et al.*, 2016), and ammonoids of the genus *Protrachyceras* found in the upper M3 limestones indicate an upper Ladinian stage for those (Matamales-Andreu *et al.*, 2021f). On Eivissa, the Middle Triassic marine sequence has not yet been studied in detail. Rangheard (1971) distinguished two main units, a lower one made up of limestones and calcareous dolostones (not represented in Figure 17 because of lack of more precise information), and an upper unit of limestones containing, among others, the ammonoid genus *Protrachyceras*, indicative of the upper Ladinian (Pérez-Valera, 2015). The lower unit might be correlatable to the lower M3 dolostones of Mallorca and El Toro formation of Menorca (note that the *Muschelkalk* formations of Menorca are not formally described, as stratotypes were

not defined by Escudero-Mozo *et al.*, 2014), and the upper unit is equivalent, at least in part, to the upper M3 limestones of Mallorca and the Arenal d'en Castell formation of Menorca (Figure 17). On Menorca, it seems that the first Middle Triassic transgression event did not reach the area, as there is a single, continuous sequence (Escudero-Mozo *et al.*, 2014). It probably rests upon a lateral equivalent of the M2 unit of Mallorca, which on Menorca is continuous with the underlying red-beds (Figure 17), similar to the most proximal areas of Iberia (Arche *et al.*, 2004; López-Gómez *et al.*, 2019a). As implied above, El Toro formation, made up of dolostones, is probably equivalent to the lower M3 dolostones of Mallorca and Eivissa (Figure 17). The Arenal d'en Castell formation, with its lower part dated to the lower Ladinian because of the presence of the ammonoid *Eoprotrachyceras curionii*, a middle part dated as upper Ladinian based on the presence of the ammonoid *Protrachyceras hispanicum* (Escudero-Mozo *et al.*, 2014), and an upper part dated as lower Carnian based on the presence of the ammonoid *Daxatina canadensis* (Escudero-Mozo *et al.*, 2014), roughly agrees in age and lithology with the M3 of Mallorca and Eivissa (Figure 17). The lower part of the M3 of Mallorca, however, also yielded the ammonoid genus *Gevanites* (e.g., Goy, 1995) and is, therefore, of a different bioprovince than the deposits of Menorca (Sephardic faunas vs. northeastern Iberian Peninsula faunas: Pérez-Valera, 2015). This suggests that the units of Mallorca and Menorca were deposited in two different basins, at least until the lower part of the upper M3 limestones. The Fontanelles formation is dated as lower Carnian based on the presence of the ammonoid species *Daxatina canadensis* in the upper part of the underlying Arenal d'en Castell formation, typical of the lower Carnian (Escudero-Mozo *et al.*, 2014), and a lower Carnian palynoassemblage described from the base of the overlying *Keuper* facies (Rosell *et al.*, 1989). An equivalent to the Fontanelles formation has not yet been found on the other islands, as is probably coeval with the lower part of the *Keuper* facies elsewhere (Figure 17).

Keuper facies (Upper Triassic) have been poorly studied on the three islands, as they are usually strongly deformed and relatively complete sequences have so far been described only on Mallorca (Rodríguez-Perea *et al.*, 1987). On Menorca, the base of the *Keuper* contains a palynoassemblage that was dated to the lower Carnian (Rosell *et al.*, 1989). Correlations among the *Keuper* units of each island are only tentative, given the lack of detailed stratigraphic and palaeontological studies (Figure 17). The uppermost Triassic–lowermost Jurassic dolostones of the Balearic Islands (Felanitx formation on Mallorca, with a base dated to the upper Norian by Boutet *et al.*, 1982) have not been described in detail either (Figure 17).

Using this information, the following is a preliminary reconstruction of the tectonosedimentary evolution of the Permian–Triassic basins of the Balearic Islands. The basin of Mallorca experienced a higher subsidence rate, since in all cases, the sequences are thicker than those of

Menorca. After an initial stage of colluvial/alluvial transverse sedimentation as a consequence of the opening of the basins (Bec de s'Àguila Formation and P1 unit), axial sedimentation took place through meandering river systems (Port des Canonge Formation and P2 unit). Towards the upper part of the sequences, flashflood events appear to have become more common (Pedra de s'Ase Formation and P3 unit). This was followed by a period of no sedimentation and erosion, probably during the uppermost Permian and lowermost Triassic. Deposition began again as a result of shallow braided river systems transporting quartz-rich sands (Punta Roja Formation and B1 unit). On Menorca, this unit is initiated with a basal conglomerate, probably indicating that the sequence corresponds to the deeper part of the basin, whereas in the case of Mallorca, the lack of basal conglomerate suggests that the sequences represent more marginal parts of the basin (see discussion above on unconformity types *sensu* Durand, 2006). Following this, floodplains and meandering rivers developed (Estellencs Formation and lower part of B2 unit). On Mallorca, this unit is overlain by braided river deposits (Pedra Alta Formation), tidal mud-flats (Son Serralta Formation) and the first shallow carbonate platform (M1 unit). This first marine unit is absent on Menorca, indicating that the Anisian Tethys transgression did not reach that basin, suggesting that it was at higher altitude and perhaps further inland. After that, there was a brief regressive event, in which mud-flats developed on Mallorca (M2 unit). This was followed by a more extensive transgression, developing tidal mud-flats on Menorca (upper part of the B2 unit) and completely flooding those basins ("Muschelkalk" unit of Eivissa, M3 unit, El Toro and Arenal d'en Castell formations). At least during the first stages of flooding, the basins of Mallorca and Menorca were not connected, as indicated by the different palaeobiogeographical affinities of the ammonoid faunas. An important regressive event took place at the early Carnian, indicated by a karstified interval on Menorca and probably the onset of sedimentation of the "Keuper" sabkha units on Eivissa and Mallorca. After that, a short-lived transgressive pulse again flooded the basin of Menorca (Fontanelles formation), which was followed by deposition of the "Keuper" unit. This transgression has not been recognised in neither Eivissa nor Mallorca, perhaps indicating a lower subsidence rate for the latter two during that time. Finally, another major transgressive event occurred in the lower Norian (Felanitx formation and "Triassic–Jurassic dolostone" units of Menorca and Eivissa), which gave way to the Jurassic marine platforms.

9. Conclusions

The present work offers a comprehensive and interdisciplinary review of all the previous studies on the Permian deposits of Mallorca (Balearic Islands, western Mediterranean), together with new analyses, integrating data on lithostratigraphy, magnetostratigraphy, palaeobotany, palaeoichnology and biochronology. Three formal lithostratigraphic units have been described, from lower to upper these being: the Bec de s'Àguila Formation (colluvium, alluvial fans and meandering rivers), the Port des Canonge Formation (meandering rivers with abundant floodplain deposits) and the Pedra de s'Ase Formation (meandering rivers with scarce floodplain deposits). A detailed reconstruction of the palaeoecosystem has been provided for each of them, integrating the study of stratigraphy, sedimentology and fossils. The latter, together with the palaeomagnetic data, have also yielded chronostratigraphic information for all the units, dating the sequence between the lower and the middle Permian for the first time.

The floras and faunas are similar to those of other sites of the western peri-Tethys. The tetrapod ichnites of the Port des Canonge Formation reveal an ichnoassemblage with typical components of the palaeoequatorial early Permian, with tracks attributed to captorhinomorph eureptiles, araeoscelidian diapsids/non-varanodontine varanopids, pareiasauromorph parareptiles, “pelycosaur”-grade synapsids and other indeterminate synapsids. The lack of anamniote tracks probably points to a palaeoenvironmental bias, as the tracksites correspond to relatively short-lived waterhole margins in which water-dependent anamniotes may have struggled to survive. The pollen of the overlying Pedra Alta Formation, of ‘Thuringian’ character (middle–late Permian), shows a diverse plant community with abundance of conifers, where the paucity of horsetail/fern spores probably points to semi-arid climate conditions. The age of this formation has been further constrained by magnetostratigraphy, which revealed that the entire Permian sequence falls within the Kiaman reverse Superchron (middle Carboniferous–middle Permian). This detailed characterisation has made it possible to provide the timing of the different phases of the Permian–Triassic tectonosedimentary evolution of the Balearic Islands, which is similar to the situation in the rest of the western peri-Tethys.

The present work shows the diverse palaeoecosystems of the lower–middle Permian of eastern equatorial Pangaea during a period of global sauropsid and synapsid diversification. It also manifests the fossiliferous potential of the deposits of the Iberian area, and the importance of comprehensive interdisciplinary studies to better correlate the sedimentary successions from different basins and understand their evolution through time.

10. Acknowledgements

We thank Sebastià Matamalas and Antoni Pasqual for assistance with fieldwork. To Feliu Calafat, Tomeu Sáez, Antoni Rodríguez Perea (UIB, Palma) and Joan Josep Fornós (UIB, Palma) for providing historical pictures of the outcrops and fossils. To David Gómez Gras (UAB, Cerdanyola del Vallès), Jocelyn Falconnet (MNHN, Paris) and Jean Broutin (UPMC, Paris) for providing literature. To Llorenç Homar (UIB, Palma) and Onofre Rullan (UIB, Palma) for offering an insight into local toponymy. To Judit Marigó (ICP, Cerdanyola del Vallès) for reviewing the English. To the three reviewers, two anonymous and Philip John Hancox (ESI, Johannesburg) for their insightful comments. To the editor, Christopher Fielding, for handling the manuscript. To the Comissió Insular de Patrimoni Històric (Consell Insular de Mallorca) for granting us the excavation permits (file number 75/2021). We acknowledge support from the CERCA program (Generalitat de Catalunya). R.M.A. was supported by the predoctoral grant FPU17/01922 (Ministerio de Ciencia, Innovación y Universidades) and the travel grant Synthesys+ DE-TAF-23 (European Commission). O.O. and À.G. are members of the consolidated research group 2017 SGR 1666 GRC (Generalitat de Catalunya). J.F. is member of the consolidated research group 2017 SGR 086 GRC (Generalitat de Catalunya, Spain). J.F. acknowledges support of the grant PID2020-117118GB-I00 funded by MCIN/AEI/10.13039/501100011033. We acknowledge support from the project “Mallorca abans dels dinosaures: estudi dels ecosistemes continentals del Permià i Triàsic amb especial èmfasi en les restes de vertebrats” (ref. 15 - 619/2020), based at the Institut Català de Paleontologia Miquel Crusafont and funded by the Departament de Cultura, Patrimoni i Política Lingüística (Consell Insular de Mallorca).

11. References

- Alonso-Zarza, A.M. (2003). Palaeoenvironmental significance of palustrine carbonates and calcretes in the geological record. *Earth-Science Reviews*, 60: 261–298.
- Alvin, K.L.; Watson, J. & Spicer, R.A. (1994). A new coniferous male cone from the English Wealden and a discussion of pollination in the Cheirolepidiaecae. *Palaeontology*, 37(1): 173–173.
- Arche, A. & López-Gómez, J. (2006). Late Permian to Early Triassic transition in central and NE Spain: biotic and sedimentary characteristics. *Geological Society, London, Special Publications*, 265: 261–280.

- Arche, A.; López-Gómez, J. & Vargas, H. (2002). Propuesta de correlación entre los sedimentos Pérmicos y Triásicos de la Cordillera Ibérica Este y de las Islas Baleares. *Geogaceta*, 32: 275–278.
- Arche, A.; López-Gómez, J.; Marzo, M. & Vargas, H. (2004). The siliciclastic Permian-Triassic deposits in Central and Northeastern Iberian Peninsula (Iberian, Ebro and Catalan Basins): A proposal for correlation. *Geologica Acta*, 2(4): 306–320.
- Balme, B.E. (1995). Fossil in situ spores and pollen grains: an annotated catalogue. *Review of Palaeobotany and Palynology*, 87(2–4): 81–323.
- Banda, E.; Parés, J.M. & Freeman, R. (1986). La técnica del paleomagnetismo. Estudio piloto en los bordes de la cuenca balear. *Estudios Geológicos*, 42: 147–165.
- Baranyi, V.; Rostási, Á.; Raucsik, B. & Kürschner, W.M. (2019). Palynological and X-ray fluorescence (XRF) data of Carnian (Late Triassic) formations from western Hungary. *Data in Brief*, 23: 103858.
- Barnolas, A. (1991a). *Mapa Geológico de España. Escala 1:50.000. Andraitx*. Segunda serie, primera edición. Instituto Tecnológico GeoMinero de España, Madrid. 56 pp. + 1 map + 5 stratigraphic logs.
- Barnolas, A. (1991b). *Mapa Geológico de España. Escala 1:50.000. Sóller*. Segunda serie, primera edición. Instituto Tecnológico GeoMinero de España, Madrid. 62 pp. + 1 map + 8 stratigraphic logs.
- Baucon, A.; Ronchi, A.; Felletti, F. & Neto de Carvalho, C. (2014). Evolution of Crustaceans at the edge of the end-Permian crisis: Ichnonetwork analysis of the fluvial succession of Nurra (Permian–Triassic, Sardinia, Italy). *Palaeogeography, Palaeoclimatology, Palaeoecology*, 410: 74–103.
- Baudrick, C.A. & Grant, G.E. (2001). Transport and deposition of large woody debris in streams: a flume experiment. *Geomorphology*, 41: 263–283.
- Bek, J.; Drábková, J.; Dašková, J. & Libertín, M. (2008). The sub-arborescent lycopsid genus *Polysporia* Newberry and its spores from the Pennsylvanian (Bolsovian–Stephanian B) continental basins of the Czech Republic. *Review of Palaeobotany and Palynology*, 152(3–4): 176–199.
- Benson, R.B. & Upchurch, P. (2013). Diversity trends in the establishment of terrestrial vertebrate ecosystems: interactions between spatial and temporal sampling biases. *Geology*, 41: 43–46.
- Benton, M.J. (2008). *When life nearly died. The greatest mass extinction of all time*. Thames & Hudson, London. 336 pp.
- Benton, M.J. & Twitchett, R.J. (2003). How to kill (almost) all life: the end-Permian extinction event. *TRENDS in Ecology and Evolution*, 18(7): 358–365.

- Bercovici, A.; Diez, J.B.; Broutin, J.; Bourquin, S.; Linol, B.; Villanueva-Amadoz, U.; López-Gómez, J. & Durand, M. (2009). A palaeoenvironmental analysis of Permian sediments in Minorca (Balearic Islands, Spain) with new palynological and megafloral data. *Review of Palaeobotany and Palynology*, 158: 14–28.
- Bernardi, M.; Petti, F.M.; Kustatscher, E.; Franz, M.; Hartkopf-Fröder, C.; Labandeira, C.C.; Wappler, T.; van Konijnenburg-van Cittert, J.H.A.; Peacock, B.R. & Angielczyk, K.D. (2017). Late Permian (Lopingian) terrestrial ecosystems: A global comparison with new data from the low-latitude Bletterbach Biota. *Earth-Science Reviews*, 175: 18–43.
- Billings, E. (1861–1865). *Palaeozoic fossils. Volume I. Containing descriptions and figures of new or little known species of organic remains from the Silurian rocks*. Geological Survey of Canada, Dawson Brothers & Baillière, Montreal, London, New York, Paris. 426 pp.
- Borruel-Abadía, V.; López-Gómez, J.; De la Horra, R.; Galán-Abellán, B.; Barrenechea, J.F.; Arche, A.; Ronchi, A.; Gretter, N. & Marzo, M. (2015). Climate changes during the Early–Middle Triassic transition in the E. Iberian plate and their palaeogeographic significance in the western Tethys continental domain. *Palaeogeography, Palaeoclimatology, Palaeoecology*, 440: 671–689.
- Bourquin, S.; Durand, M.; Diez, J.B.; Broutin, J. & Fluteau, F. (2007). The Permian-Triassic boundary and Early Triassic sedimentation in Western European Basins: an overview. *Journal of Iberian Geology*, 33(2): 221–236.
- Bourquin, S.; Bercovici, A.; López-Gómez, J.; Diez, J.B.; Broutin, J.; Ronchi, A.; Durand, M.; Arché, A.; Linol, B. & Amour, F. (2011). The Permian–Triassic transition and the onset of Mesozoic sedimentation at the northwestern peri-Tethyan domain scale: Palaeogeographic maps and geodynamic implications. *Palaeogeography, Palaeoclimatology, Palaeoecology*, 299: 265–280.
- Bourrouilh, R. (1983). Estratigrafía, sedimentología y tectónica de la isla de Menorca y del noreste de Mallorca. *Memorias del Instituto Geológico y Minero de España*, 99: 672 pp. + 95 pl. + 3 maps.
- Boutet, C.; Rangheard, Y.; Rosenthal, P.; Visscher, H. & Durand-Delga, M. (1982). Découverte d’une microflore d’âge Norien dans la Sierra Norte de Majorque (Baléares, Espagne). *Comptes Rendus de l’Académie des Sciences de Paris, Série 2*, 294: 1267–1270.
- Boyd, C. & McIlroy, D. (2017). Three-dimensional morphology of *Beaconites capronus* from northeast England. *Ichnos*, 24(4): 250–258.
- Bradshaw, M.A. (1981). Paleoenvironmental interpretations and systematics of Devonian trace fossils from the Taylor Group (lower Beacon Supergroup), Antarctica. *New Zealand Journal of Geology and Geophysics*, 24: 615–652.

- Brocklehurst, N. (2020). Olson's Gap or Olson's Extinction? A Bayesian tip-dating approach to resolving stratigraphic uncertainty. *Proceedings of the Royal Society B*, 287: 20200154.
- Brocklehurst, N.; Kammerer, C.F. & Fröbisch, J. (2013). The early evolution of synapsids, and the influence of sampling on their fossil record. *Paleobiology*, 39: 470–490.
- Brocklehurst, N.; Day, M.O.; Rubidge, B.S. & Fröbisch, J. (2017). Olson's Extinction and the latitudinal biodiversity gradient of tetrapods in the Permian. *Proceedings of the Royal Society B*, 284: 20170231.
- Broutin, J. & Kerp, H. (1994). Aspects of Permian palaeobotany and palynology. XIV. A new form-genus of broad-leaved late carboniferous and early Permian Northern hemisphere conifers. *Review of Palaeobotany and Palynology*, 83(1–3): 241–251.
- Buatois, L.A. & Mángano, M.G. (1998). Trace fossil analysis of lacustrine facies and basins. *Palaeogeography, Palaeoclimatology, Palaeoecology*, 140: 367–382.
- Buchwitz, M. & Voigt, S. (2018). On the morphological variability of *Ichniotherium* tracks and evolution of locomotion in the sistergroup of amniotes. *PeerJ*, 6:e4346.
- Calafat, F. (1986). Estratigrafía y sedimentología de la litofacies Buntsandstein de Mallorca. In: Cabrera, L. (Ed.). *Resúmenes del XI Congreso Español de Sedimentología*. Grupo Español de Sedimentología, Barcelona: p. 39.
- Calafat, F. (1987). Paleoambients de les facies Buntsandstein de Mallorca. In: *Llibre de resums de les I Jornades del Medi Ambient de les Illes Balears*. Societat d'Història Natural de les Balears, Palma: 16–17.
- Calafat, F. (1988). *Estratigrafía y sedimentología de la litofacies Buntsandstein de Mallorca*. Bachelor's Thesis. Universitat de Barcelona, Barcelona. 127 pp. + 31 annexed figs.
- Calafat, F.; Fornós, J.J.; Marzo, M.; Ramos, E. & Rodríguez-Perea, A. (1986). Icnología de vertebrados de las facies Buntsandstein de Mallorca. In: Cabrera, L. (Ed.). *Resúmenes del XI Congreso Español de Sedimentología*. Grupo Español de Sedimentología, Barcelona: p. 40.
- Calafat, F.; Fornós, J.J.; Marzo, M.; Ramos-Guerrero, E. & Rodríguez-Perea, A. (1986–1987). Icnología de vertebrados de las facies Buntsandstein de Mallorca. *Acta Geològica Hispànica*, 21–22: 515–520.
- Cassinis, G. & Ronchi, A. (2002). The (late-) Post-Variscan continental succession of Sardinia. *Rendiconti della Società Paleontologica Italiana*, 1: 77–92.
- Cassinis, G.; Durand, M. & Ronchi, A. (2003). Permian-Triassic continental sequences of Northwest Sardinia and South Provence: stratigraphic correlations and palaeogeographical implications. *Bollettino della Società Geologica Italiana*, volume speciale 2: 119–129.

- Cassinis, G.; Perotti, C.R. & Ronchi, A. (2012). Permian continental basins in the Southern Alps (Italy) and peri-mediterranean correlations. *International Journal of Earth Sciences/GR Geologische Rundschau*, 101: 129–157.
- Clement-Westerhof, J.A. (1984). Aspects of Permian palaeobotany and palynology. IV. The conifer *Ortiseia* Florin from the Val Gardena Formation of the Dolomites and the Vicentinian Alps (Italy) with special reference to a revised concept of the Walchiaceae (Göppert) Schimper. *Review of Palaeobotany and Palynology*, 41(1): 51–166.
- Clement-Westerhof, J.A. (1987). Aspects of Permian palaeobotany and palynology. VII. The Majonicaceae, a new family of Late Permian conifers. *Review of Palaeobotany and Palynology*, 52(4): 375–402.
- Colombo, F. (2010a). Abanicos aluviales: procesos de transporte y acumulación de materiales detríticos. In: Arche, A. (Ed.). *Sedimentología. Del proceso físico a la cuenca sedimentaria*. Consejo Superior de Investigaciones Científicas, Madrid: 85–130.
- Colombo, F. (2010b). Abanicos aluviales: secuencias y modelos de sedimentación. In: Arche, A. (Ed.). *Sedimentología. Del proceso físico a la cuenca sedimentaria*. Consejo Superior de Investigaciones Científicas, Madrid: 131–224.
- Couper, R.A. (1953). Upper Mesozoic and Cainozoic spores and pollen grains from New Zealand. *New Zealand Geological Survey paleontological bulletin*, 22: 1–77.
- Cuevas-López, F. (1958a). *Informe geológico y minero de los yacimientos de cobre de Banyalbufar y Estallenchs, Mallorca*. Barcelona. 37 pp. + 8 figs.
- Cuevas-López, F. (1958b). *Informe geológico y minero de los yacimientos de cobre de Banyalbufar y Valldemosa, Mallorca*. Barcelona. 23 pp. + 7 figs.
- d'Orbigny, A. (1842). *Voyage dans l'Amérique méridionale (le Brésil, la République Orientale de l'Uruguay, la République Argentine, la Patagonie, la République du Chili, la République de Bolivia, la République du Pérou) exécuté pendant les années 1826, 1827, 1828, 1829, 1830, 1831, 1832 et 1833*. Pitois-Levrault, Paris, Levrault, Strasbourg, 3(4) (Paléontologie). 188 pp.
- Davies, N.S. & Gibling, M.R. (2010). Paleozoic vegetation and the Siluro-Devonian rise of fluvial lateral accretion sets. *Geology*, 38(1): 51–54.
- Day, M.O.; Ramezani, J.; Bowring, S.A.; Sadler, P.M.; Erwin, D.H.; Abdala, F. & Rubidge, B.S. (2015). When and how did the terrestrial mid-Permian mass extinction occur? Evidence from the tetrapod record of the Karoo Basin, South Africa. *Proceedings of the Royal Society B*, 282: 20150834.
- De la Horra, R.; Galán-Abellán, A.B.; López-Gómez, J.; Barrenechea, J.F.; Luque, F.J.; Arche, A. & Benito, M.I. (2012). Paleoecological and paleoenvironmental changes during the

- continental Middle–Late Permian transition at the SE Iberian Ranges, Spain. *Global and Planetary Change*, 94–95: 46–61.
- Diez, J.B. (2000). *Geología y Paleobotánica de la Facies Buntsandstein en la Rama Aragonesa de la Cordillera Ibérica. Implicaciones paleogeográficas en el Peritethys Occidental*. Ph.D. dissertation. Universidad de Zaragoza–Université Pierre & Marie Curie, Paris VI, Zaragoza, Paris. 424 pp.
- Díez-Canseco, D.; Buatois, L.A.; Mángano, M.G.; Díaz-Molina, M. & Benito, M.I. (2016). Ichnofauna from coastal meandering channel systems (Upper Cretaceous Tresp Formation, South-Central Pyrenees, Spain): delineating the fluvial-tidal transition. *Journal of Paleontology*, 90(2): 250–268.
- Dudgeon, P. (1878). Note on a new fossil footprint from the Permian sandstone of Dumfriesshire. *Proceedings of the Royal Society of Edinburgh*, 9: 154–155.
- Durand, M. (2006). The problem of the transition from the Permian to the Triassic Series in southeastern France: comparison with other Peritethyan regions. *Geological Society, London, Special Publications*, 265: 281–296.
- Durand, M. (2008). Permian to Triassic continental successions in southern Provence (France): an overview. *Bollettino della Società Geologica Italiana*, 127(3): 697–716.
- Ebisemiju, F.S. (1994). The sinuosity of alluvial river channels in the seasonally wet tropical environment: Case study of river Elemi, southwestern Nigeria. *Catena*, 21: 13–25.
- Ellenberger, P. (1983). Sur l'intérêt paléontologique de la dalle à pistes de la Lieude (commune de Mérifons, Hérault, France). *Société de la Protection de la Nature du Languedoc Roussillon*, 1: 11–20.
- Erwin, D.H. (1994). The Permo–Triassic extinction. *Nature*, 367: 231–236.
- Escudero-Mozo, M.J.; Martín-Chivelet, J.; Goy, A. and López-Gómez, J. (2014). Middle-Upper Triassic carbonate platforms in Minorca (Balearic islands): Implications for Western Tethys correlations. *Sedimentary Geology*, 310: 41–48.
- Florin, R. (1927). Preliminary descriptions of some Palaeozoic genera of Coniferae. *Arkiv För Botanik*, 21A(13): 1–7.
- Florin, R. (1934). Notes on the nomenclature of Palaeozoic conifers. *Svensk Botanisk Tidskrift*, 26(4): 468–469.
- Forte, G.; Kustatscher, E.; Roghi, G. & Preto, N. (2018). The Permian (Kungurian, Cisuralian) palaeoenvironment and palaeoclimate of the Tregiovo Basin, Italy: Palaeobotanical, palynological and geochemical investigations. *Palaeogeography, Palaeoclimatology, Palaeoecology*, 495: 186–204.
- Francischini, H.; Lucas, S.G.; Voigt, S.; Marchetti, L.; Santucci, V.L.; Knight, C.L.; Wood, J.R.; Dentzien-Dias, P. & Schultz, C.L. (2020). On the presence of *Ichniotherium* in the

- Coconino Sandstone (Cisuralian) of the Grand Canyon and remarks on the occupation of deserts by non-amniote tetrapods. *Paläontologische Zeitschrift*: 94, 207–225.
- Franzel, M.; Jones, S.J.; Meadows, N.; Allen, M.B.; McCaffrey, K. & Morgan, T. (2021). Basin-scale fluvial correlation and response to the Tethyan marine transgression: An example from the Triassic of central Spain. *Basin Research*, 33(1): 1–25.
- Freeman, T. & Obrador, A. (1979). Paleosoils and coal in the distal part of the Spanish Buntsandstein (Menorca and Mallorca, Balearic Islands). *Boletín de la Sociedad de Historia Natural de Baleares*, 23: 47–50.
- Gand, G. (1988). *Les traces de vertébrés tétrapodes du Permien français: paléontologie, stratigraphie, paléoenvironnements*. Ph.D. dissertation. Université de Bourgogne, Dijon. 368 pp.
- Gand, G. & Durand, M. (2006). Tetrapod footprint ichno-associations from French Permian basins. Comparisons with other Euramerican ichnofaunas. *Geological Society, London, Special Publications*, 265: 157–177.
- Gand, G.; Kerp, H.; Parsons, C. & Martínez-García, E. (1997). Palaeoenvironmental and stratigraphic aspects of animal traces and plant remains in Spanish Permian red beds (Peña Sagra, Cantabrian Mountains, Spain). *Geobios*, 30(2): 295–318.
- Gand, G.; Garric, J.; Schneider, J.; Walter, H.; Lapeyrie, J.; Martin, C. & Thiery, A. (2008). Notostraca trackways in Permian playa environments of the Lodève basin (France). *Journal of Iberian Geology*, 34(1): 73–108.
- Geinitz, H.B. (1863). Beiträge zur Kenntnis der organischen Überreste in der Dyas. *Neues Jahrbuch für Mineralogie, Geologie und Paläontologie*, 1863: 385–398.
- Gilmore, C.W. (1927). Fossil footprints of the Grand Canyon: second contribution. *Smithsonian Miscellaneous Collections*, 80(3): 1–78 + 21 pls.
- Gómez-Gras, D.M. (1987). *Estratigrafía física y petrología sedimentaria del Pérmico y Buntsandstein de la isla de Menorca*. Bachelor's Thesis. Universitat Autònoma de Barcelona, Barcelona. XIV + 117 pp.
- Gómez-Gras, D.M. (1992). *El Permotrías de las Baleares, de la Cordillera Costero Catalana y de la vertiente mediterránea de la Cordillera Ibérica: Facies y Petrología Sedimentaria*. Ph.D. dissertation. Universitat Autònoma de Barcelona, Barcelona. XIX + 242 pp. + 55 figs. + 7 tabs.
- Gómez-Gras, D. (1993). El Permotrías de las Baleares y de la vertiente mediterránea de la Cordillera Ibérica y del Maestrat: Facies y Petrología Sedimentaria (Parte II). *Boletín Geológico y Minero*, 104: 467–515.

- Gómez-Gras, D. & Alonso-Zarza, A.M. (2003). Reworked calcretes: their significance in the reconstruction of alluvial sequences (Permian and Triassic, Minorca, Balearic Islands, Spain). *Sedimentary Geology*, 158: 299–319.
- Good, C.W. (1979). *Botryopteris* pinnules with abaxial sporangia. *American Journal of Botany*, 66(1): 19.
- Gould, R.E. & Delevoryas, T. (1977). The biology of *Glossopteris*: evidence from petrified seed-bearing and pollen-bearing organs. *Alcheringa: An Australasian Journal of Palaeontology*, 1(4): 387–399.
- Goy, A. (1995). Ammonoideos del Triásico Medio de España: Bioestratigrafía y correlaciones. *Cuadernos de Geología Ibérica*, 19: 21–60.
- Grauvogel-Stamm, L. (1969). Nouveaux types d'organes reproducteurs mâles de Conifères du Grès à Voltzia (Trias inférieur) des Vosges. *Bulletin du Service de la carte géologique d'Alsace et de Lorraine*, 22(2): 93–120.
- Grauvogel-Stamm, L. (1978). La flore du Grès à Voltzia (Buntsandstein supérieur) des Vosges du Nord (France). Morphologie, anatomie, interpretations phylogénique et paléogéographique. *Sciences Géologiques, bulletins et mémoires*, 50: 1–225 + 54 pl.
- Gretter, N.; Ronchi, A.; López-Gómez, J.; Arche, A.; De la Horra, R.; Barrenechea, J. & Lago, M. (2015). The Late Palaeozoic-Early Mesozoic from the Catalan Pyrenees (Spain): 60 Myr of environmental evolution in the frame of the western peri-Tethyan palaeogeography. *Earth-Science Reviews*, 150: 679–708.
- Gulbranson, E.L.; Cornamusini, G.; Ryberg, P.E. & Corti, V. (2020). When does large woody debris influence ancient rivers? Dendrochronology applications in the Permian and Triassic, Antarctica. *Palaeogeography, Palaeoclimatology, Palaeoecology*, 541: 109544.
- Hall, J. (1847). *Palaeontology of New York. Volume I. Containing descriptions of the organic remains of the Lower Division of the New York System (Equivalent to the Lower Silurian rocks of Europe)*. C. van Benthuyssen, Albany, New York. 338 pp.
- Hasiotis, S.T.; Platt, B.F.; Hembree, D.I. & Everhart, M.J. (2007). The Trace-Fossil Record of Vertebrates. In: William Miller, III (Ed.). *Trace Fossils: Concepts, Problems, Prospects*. Elsevier Science, Amsterdam, Oxford: 196–218.
- Haubold, H. (1970). Versuch der Revision der Amphibien-Fährten des Karbon und Perm. *Freiberger Forschungshefte C*, 260: 83–117.
- Haubold, H. (1971). Ichnia Amphibiourum et Reptiliorum fossilium. In: Kuhn, O. (Ed.). *Handbuch der Paläoherpetologie*. Gustav Fischer Verlag, Stuttgart. 124 pp.
- Haubold, H. (2000). Tetrapodenfährten aus dem Perm – Kenntnisstand und Progress 2000. *Hallesches Jahrbuch für Geowissenschaften, B*, 22: 1–16.

- Heer, O. (1876–1877). *Flora fossilis Helvetiae. Die vorweltliche Flora der Schweiz*. Verlag J. Wurster & Co., Zürich. 182 pp. [Parts 1, 2 (1876):1–90; Parts 3, 4 (1877): 91–182]
- Heinberg, C. (1974). A dynamic model for the meniscus filled tunnel (*Anchorichnus* n. ichnogen) from the Jurassic Pecten Sandstone of Milne Land, East Greenland. *Grønlands Geologiske Undersøgelse*, 62: 1–20.
- Henderson, C.M.; Shen, S.Z.; Gradstein, F.M. & Agterberg, F.P. (2020). Chapter 24 - The Permian Period. In: Gradstein, F.M.; Ogg, J.G.; Schmitz, M.D. & Ogg, G.M. (Eds.). *Geologic Time Scale 2020*. Elsevier: 875–902.
- Hernández-Castillo, G.R.; Rothwell, G.W. & Mapes, G. (2001). Thucydiaeae Fam. Nov., with a review and reevaluation of Paleozoic walchian conifers. *International Journal of Plant Sciences*, 162(5): 1155–1185.
- Hitchcock, E. (1858). *Ichnology of New England. A report on the sandstone of the Connecticut Valley, especially its fossil footmarks*. W. White, Boston. 220 pp.
- Homar, Ll. (1985). *Toponímia del litoral de la costa d'Estellencs, Banyalbufar i Valldemossa: de na Foradada a sa Foradada*. 7 aerial photographs.
- Hounslow, M.W. & Balabanov, Y.P. (2018). A geomagnetic polarity timescale for the Permian, calibrated to stage boundaries. *Geological Society, London, Special Publications*, 450(1): 61–103.
- Huisink, M. (2000). Changing river styles in response to Weichselian climate changes in the Vecht valley, eastern Netherlands. *Sedimentary Geology*, 133: 115–134.
- Hunt, A.P. & Lucas, S.G. (2006). Permian tetrapod ichnofacies. *Geological Society, London, Special Publications*, 265: 137–156.
- IDEIB (2019). *Infraestructura de dades espacials de les Illes Balears*. Conselleria d'Agricultura, Medi Ambient i Territori. Govern de les Illes Balears. <http://www.ideib.cat> (last accessed on 26/07/2019).
- Juncal, M.A. (2019). *Nuevas aportaciones a la palinoestratigrafía pérmica del dominio peritético occidental*. Ph.D. dissertation. Universidade de Vigo, Vigo. 361 pp.
- Juncal, M.A.; Bourquin, S.; Beccaletto, L. & Diez, J.B. (2018). New sedimentological and palynological data from the Permian and Triassic series of the Sancerre-Couy core, Paris Basin, France. *Geobios*, 51: 517–535.
- Juncal, M.A.; Diez, J.B.; Lloret, J.; de la Horra, R.; Gretter, N.; Ronchi, A.; Barrenechea, J.F.; Borruel-Abadía, V. & López-Gómez, J. (2020). Re-calibrating the Late Palaeozoic palynostratigraphy in the basins of the southern domain of the Variscan Belt (southwestern Europe). In: *EGU General Assembly 2020, Online, 4–8 May 2020*: EGU2020-19788.

- Kerp, J.H.F. (1988). Aspects of Permian palaeobotany and palynology. X. The West- and Central European species of the genus *Autunia* Krasser emend. Kerp (Peltaspermaceae) and the form-genus *Rhachiphyllum* Kerp (Callipterid Foliage). *Review of Palaeobotany and Palynology*, 54(3–4): 249–360.
- Kirschvink, J.L. (1980). The least-squares line and plane and the analysis of palaeomagnetic data. *Geophysical Journal International*, 62(3): 699–718.
- Klaus, W. (1963). Sporen aus dem südalpinen Perm: Vergleichsstudie für die Gliederung nordalpiner Salzserien. *Jahrbuch der Geologischen Bundesanstalt Wien*, 106: 229–363.
- Klein, H. & Niedźwiedzki, G. (2012). Revision of the Lower Triassic tetrapod ichnofauna from Wióry, Holy Cross Mountains, Poland. *New Mexico Museum of Natural History and Science Bulletin*, 56: 1–62.
- Klembara, J.; Berman, D.S.; Henrici, A.C.; Čerňanský, A.; Werneburg, R. & Martens, T. (2007). First description of skull of lower Permian *Seymouria sanjuanensis* (Seymouriamorpha: Seymouriidae) at an early juvenile growth stage. *Annals of Carnegie Museum*, 76(1): 53–72.
- Koymans, M.R.; Langereis, C.G.; Pastor-Galán, D. & van Hinsbergen, D.J.J. (2016). Paleomagnetism.org: An online multi-platform open source environment for paleomagnetic data analysis. *Computers & Geosciences*, 93: 127–137.
- Koymans, M.R.; van Hinsbergen, D.J.J.; Pastor-Galán, D.; Vaes, B. & Langereis, C.G. (2020). Towards FAIR Paleomagnetic Data Management Through Paleomagnetism.org 2.0. *Geochemistry, Geophysics, Geosystems*, 21(2): e2019GC008838.
- Krapovickas, V.; Mángano, M.G.; Mancuso, A.; Marsicano, C.A. & Volkheimer, W. (2008). Icnofaunas triásicas en abanicos aluviales distales: evidencias de la Formación Cerro Puntudo, cuenca cuyana, Argentina. *Ameghiniana*, 45(2): 463–472.
- Kustatscher, E.; van Konijnenburg-van Cittert, J.H.A. & Roghi, G. (2010). Macrofloras and palynomorphs as possible proxies for palaeoclimatic and palaeoecological studies: A case study from the Pelsonian (Middle Triassic) of Kühwiesenkopf/Monte Prà della Vacca (Olang Dolomites, N-Italy). *Palaeogeography, Palaeoclimatology, Palaeoecology*, 290(1–4): 71–80.
- Kustatscher, E.; Nowak, H.; Forte, G. & Roghi, G. (2019). Triassic macro- and microfloras of the Eastern Southern Alps. *Geo.Alp*, 16: 5–43.
- Lagnaoui, A.; Voigt, S.; Belahmira, A.; Saber, H.; Klein, H.; Hminna, A. & Schneider, J.W. (2018). Late Carboniferous Tetrapod Footprints from the Souss Basin, Western High Atlas Mountains, Morocco. *Ichnos*, 25(2–3): 81–93.

- Legler, B. & Schneider, J.W. (2013). High-frequency cyclicity preserved in nonmarine and marine deposits (Permian, Germany and North Sea). *New Mexico Museum of Natural History and Science Bulletin*, 60: 200–211.
- Leonardi, G. (1987). *Glossary and Manual of Tetrapod Footprint Palaeoichnology*. Departamento Nacional de Produção Mineral, Brasília. 117 pp.
- Leonardi, P.; Conti, M.A.; Leonardi, G.; Mariotti, N. & Nicosia, U. (1975). *Pachypes dolomiticus* n. gen. n. sp.; Pareiasaur footprint from the “Arenaria di Val Gardena” (Middle Permian) in the Western Dolomites (N. Italy). *Accademia Nazionale dei Lincei, Rendiconti, Classe Scienze matematiche fisiche e naturali*, 8th series, 57(3–4): 221–232.
- Li, Y.-X. & Kodama, K.P. (2016). Detecting and correcting for paleomagnetic inclination shallowing of sedimentary rocks: a review. *Frontiers in Earth Science*, 4:7.
- Liebrecht, T.; Fortuny, J.; Galobart, A.; Müller, J. & Sander, P.M. (2017). A large, multiple-tooth-rowed captorhinid reptile (Amniota: Eureptilia) from the Upper Permian of Mallorca (Balearic Islands, Western Mediterranean). *Journal of Vertebrate Paleontology*, 37(1): e1251936.
- Lindström, S.; McLoughlin, S. & Drinnan, A.N. (1997). Intraspecific variation of taeniate bisaccate pollen within Permian glossopterid sporangia, from the Prince Charles Mountains, Antarctica. *International Journal of Plant Sciences*, 158(5): 673–684.
- Linol, B.; Bercovici, A.; Bourquin, S.; Diez, J.B.; López-Gómez, J.; Broutin, J.; Durand, M. & Villanueva-Amadoz, U. (2009). Late Permian to Middle Triassic correlations and palaeogeographical reconstructions in south-western European basins: New sedimentological data from Minorca (Balearic Islands, Spain). *Sedimentary Geology*, 220: 77–94.
- Litwin, R.J. (1985). Fertile organs and in situ spores of ferns from the late Triassic Chinle Formation of Arizona and New Mexico, with discussion of the associated dispersed spores. *Review of Palaeobotany and Palynology*, 44(1): 101–146.
- Logghe, A.; Muijal, E.; Marchetti, L.; Nel, A.; Pouillon, J.-M.; Giner, S.; Garrouste, R. & Steyer, J.-S. (2021). *Hyloidichnus* trackways with digit and tail drag traces from the Permian of Gonfaron (Var, France): New insights on the locomotion of captorhinomorph eureptiles. *Palaeogeography, Palaeoclimatology, Palaeoecology*, 573: 110436.
- Looy, C.V. & Hotton, C.L. (2014). Spatiotemporal relationships among Late Pennsylvanian plant assemblages: Palynological evidence from the Markley Formation, West Texas, U.S.A. *Review of Palaeobotany and Palynology*, 211: 10–27.
- Lopez, M.; Gand, G.; Körner, F. & Schneider, J. (2008). The playa environments of the Lodève Permian basin (Languedoc-France). *Journal of Iberian Geology*, 34(1): 29–56.

- López-Gómez, J.; Arche, A. & Pérez-López, A. (2002). Permian and Triassic. *In*: Gibbons, W. & Moreno, M.T. (Eds.). *The Geology of Spain*. Geological Society, London: 185–212.
- López-Gómez, J.; Alonso-Azcárate, J.; Arche, A.; Arribas, J.; Fernández-Barrenechea, J.; Borruel-Abadía, V.; Bourquin, S.; Cadenas, P.; Cuevas, J.; De la Horra, R.; Díez, J.B.; Escudero-Mozo, M.J.; Fernández-Viejo, G.; Galán-Abellán, B.; Galé, C.; Gaspar-Escribano, J.; Gisbert-Aguilar, J.; Gómez-Gras, D.; Goy, A.; Gretter, N.; Heredia-Carballo, N.; Lago, M.; Lloret, J.; Luque, J.; Márquez, L.; Márquez-Aliaga, A.; Martín-Algarra, A.; Martín-Chivelet, J.; Martín-González, F.; Marzo, M.; Mercedes-Martín, R.; Ortí, F.; Pérez-López, A.; Pérez-Valera, F.; Pérez-Valera, J.A.; Plasencia, P.; Ramos, E.; Rodríguez-Méndez, L.; Ronchi, A.; Salas, R.; Sánchez-Fernández, D.; Sánchez-Moya, Y.; Sopeña, A.; Suárez-Rodríguez, Á.; Tubía, J.M.; Ubide, T.; Valero-Garcés, B.; Vargas, H. & Viseras, C. (2019a). Permian-Triassic rifting stage. *In*: Vergés, J. & Kullberg, J.C. (Coord.). *The Geology of Iberia: A Geodynamic Approach. Volume 3: The Alpine Cycle*. Springer, Cham: 29–112.
- López-Gómez, J.; Martín-González, F.; Heredia, N.; De la Horra, R.; Barrenechea, J.F.; Cadenas, P.; Juncal, M.; Díez, J.B.; Borruel-Abadía, V.; Pedreira, D.; García-Sansegundo, J.; Farias, P.; Galé, C.; Lago, M.; Ubide, T.; Fernández-Viejo, G. & Gand, G. (2019b). New lithostratigraphy for the Cantabrian Mountains: a common tectono-stratigraphic evolution for the onset of the Alpine cycle in the W Pyrenean realm, N Spain. *Earth-Science Reviews*, 188: 249–271.
- López-Gómez, J.; De la Horra, R.; Barrenechea, J.F.; Borruel-Abadía, V.; Martín-Chivelet, J.; Juncal, M.; Martín-González, F.; Heredia, N.; Díez, B. & Buatois, L.A. (2021). Early Permian during the Variscan orogen collapse in the equatorial realm: insights from the Cantabrian Mountains (N Iberia) into climatic and environmental changes. *International Journal of Earth Sciences*, 110: 1355–1387.
- Lucas, S.G. (2009). Timing and magnitude of tetrapod extinctions across the Permo–Triassic boundary. *Journal of Asian Earth Sciences*, 36: 491–502.
- Lucas, S.G. (2017). Permian tetrapod extinction events. *Earth-Science Reviews*, 170: 31–60.
- Lucas, S.G. (2019). An ichnological perspective on some major events of Paleozoic tetrapod evolution. *Bollettino della Società Paleontologica Italiana*, 58(3): 223–266.
- Lucas, S.G.; Lozovsky, V.R. & Shishkin, M.A. (1999). Tetrapod footprints from early Permian redbeds of the northern Caucasus, Russia. *Ichnos*, 6(4): 277–281.
- Lucas, S.G.; Lerner, A.J. & Haubold, H. (2001). First record of *Amphisauropus* and *Varanopus* in the Lower Permian Abo Formation, central New Mexico. *Hallesches Jahrbuch für Geowissenschaften, B*, 23: 69–78.

- Lucas, S.G.; Krainer, K.; Chaney, D.S.; DiMichele, W.A.; Voigt, S.; Berman, D.S. & Henrici, A.C. (2013). The Lower Permian Abo Formation in central New Mexico. *New Mexico Museum of Natural History and Science Bulletin*, 59: 161–180.
- Lucas, S.G.; Kollar, A.D.; Berman, D.S. & Henrici, A.C. (2016). Pelycosaurian-grade (Amniota: Synapsida) footprints from the Lower Permian Dunkard Group of Pennsylvania and West Virginia. *Annals of Carnegie Museum*, 83(4): 287–294.
- Mack, G.H.; James, W.C. & Monger, H.C. (1993). Classification of paleosols. *Geological Society of America Bulletin*, 105: 129–136.
- MacLeod, K.G.; Quinton, P.C. & Bassett, D.J. (2017). Warming and increased aridity during the earliest Triassic in the Karoo Basin, South Africa. *Geology*, 45(6): 483–486.
- Mädler, K. (1964). Die geologische Verbreitung von Sporen und Pollen - in der deutschen Trias. *Beihefte zum Geologischen Jahrbuch*, 65: 1–145.
- Marchetti, L. (2016). New occurrences of tetrapod ichnotaxa from the Permian Orobic Basin (Northern Italy) and critical discussion of the age of the ichnoassociation. *Papers in Palaeontology*, 2(3): 363–386.
- Marchetti, L.; Avanzini, M. & Conti, M.A. (2013). *Hyloidichnus bifurcatus* Gilmore, 1927 and *Limnopus heterodactylus* (King, 1845) from the Early Permian of Southern Alps (N Italy): A new equilibrium in the ichnofauna. *Ichnos*, 20: 202–217.
- Marchetti, L.; Forte, G.; Bernardi, M.; Wappler, T.; Hartkopf-Fröder, C.; Krainer, K. & Kustatscher, E. (2015a). Reconstruction of a Late Cisuralian (Early Permian) floodplain lake environment: Palaeontology and sedimentology of the Tregiovo Basin (Trentino-Alto Adige, Northern Italy). *Palaeogeography, Palaeoclimatology, Palaeoecology*, 440: 180–200.
- Marchetti, L.; Ronchi, A.; Santi, G.; Schirolli, P.; Conti, M.A. (2015b). Revision of a classic site for Permian tetrapod ichnology (Collio Formation, Trompia and Caffaro valleys, N. Italy), new evidences for the radiation of captorhinomorph footprints. *Palaeogeography, Palaeoclimatology, Palaeoecology*, 433: 140–155.
- Marchetti, L.; Ronchi, A.; Santi, G. & Voigt, S. (2015c). The Gerola Valley site (Orobic Basin, Northern Italy): A key for understanding late Early Permian tetrapod ichnofaunas. *Palaeogeography, Palaeoclimatology, Palaeoecology*, 439: 97–116.
- Marchetti, L.; Tessarollo, A.; Felletti, F. & Ronchi, A. (2017a). Tetrapod footprint palaeoecology: behavior, taphonomy and ichnofauna disentangled. A case study from the Lower Permian of the Southern Alps (Italy). *Palaios*, 32: 506–527.
- Marchetti, L.; Voigt, S. & Klein, H. (2017b). Revision of Late Permian tetrapod tracks from the Dolomites (Trentino–Alto Adige, Italy). *Historical Biology*, 31(6), 2019: 748–783.

- Marchetti, L.; Mujal, E. & Bernardi, M. (2017c). An unusual *Amphisauropus* trackway and its implication for understanding seymouriamorph locomotion. *Lethaia*, 50: 162–174.
- Marchetti, L.; Voigt, S. & Santi, G. (2018). A rare occurrence of Permian tetrapod footprints: *Ichniotherium cotta* and *Ichniotherium sphaerodactylum* on the same stratigraphic surface. *Ichnos*, 25(2–3): 106–118.
- Marchetti, L.; Belvedere, M.; Voigt, S.; Klein, H.; Castanera, D.; Díaz-Martínez, I.; Marty, D.; Xing, L.; Feola, S.; Melchor, R.N. & Farlow, J.O. (2019a). Defining the morphological quality of fossil footprints. Problems and principles of preservation in tetrapod ichnology with examples from the Palaeozoic to the present. *Earth-Science Reviews*, 193: 109–145.
- Marchetti, L.; Voigt, S. & Lucas, S.G. (2019b). An anatomy-consistent study of the Lopingian eolian tracks of Germany and Scotland reveals the first evidence of the end-Guadalupian mass extinction at low paleolatitudes of Pangea. *Gondwana Research*, 73: 32–53.
- Marchetti, L.; Klein, H.; Buchwitz, M.; Ronchi, A.; Smith, R.M.H.; De Klerk, W.J.; Sciscio, L. & Groenewald, G.H. (2019c). Permian-Triassic vertebrate footprints from South Africa: Ichnotaxonomy, producers and biostratigraphy through two major faunal crises. *Gondwana Research*, 72: 139–168.
- Marchetti, L.; Voigt, S.; Lucas, S.G.; Francischini, H.; Dentzien-Dias, P.; Sacchi, R.; Mangiacotti, M.; Scali, S.; Gazzola, A.; Ronchi, A. & Millhouse, A. (2019d). Tetrapod ichnotaxonomy in eolian paleoenvironments (Coconino and De Chelly formations, Arizona) and late Cisuralian (Permian) sauropsid radiation. *Earth-Science Reviews*, 190: 148–170.
- Marchetti, L.; Voigt, S.; Lucas, S.G.; Stimson, M.R.; King, O.A. & Calder, J.H. (2020). Footprints of the earliest reptiles: *Notalacerta missouriensis* – Ichnotaxonomy, potential trackmakers, biostratigraphy, palaeobiogeography and palaeoecology. *Annales Societatis Geologorum Poloniae*, 90: 271–290.
- Marchetti, L.; Voigt, S.; Buchwitz, M.; MacDougall, M.J.; Lucas, S.G.; Fillmore, D.L.; Stimson, M.R.; King, O.A.; Calder, J.H. & Fröbisch, J. (2021a). Tracking the origin and early evolution of reptiles. *Frontiers in Ecology and Evolution*, 9:696511.
- Marchetti, L.; Voigt, S.; Mujal, E.; Lucas, S.G.; Francischini, H.; Fortuny, J. & Santucci, V.L. (2021b). Extending the footprint record of Pareiasauromorpha to the Cisuralian: earlier appearance and wider palaeobiogeography of the group. *Papers in Palaeontology*, 7(3): 1297–1319.
- Marchetti, L.; Forte, G.; Kustatscher, E.; DiMichele, W.A.; Lucas, S.G.; Roghi, G.; Juncal, M.A.; Hartkopf-Fröder, C.; Krainer, K.; Morelli, C. & Ronchi, A. (2022). The Artinskian Warming Event: an Euramerican change in climate and the terrestrial biota during the early Permian. *Earth-Science Reviews*, in press: 103922.

- Marsh, O.C. (1894). Footprints of vertebrates in the Coal Measures of Kansas. *American Journal of Science*, 48: 81–84.
- Martí, J.; Paniello, X.; Pomar, L.; Ramos, E. & Rodríguez-Perea, A. (1985). El Triásico de las Balears. In: Mateu Ibars, F. & Marzo, M. (Eds.). *Resúmenes del II Coloquio de Estratigrafía y Paleogeografía del Pérmico y Triásico de España*. Institut d'Estudis Ilerdencs and Grupo Español del Mesozoico, La Seu d'Urgell: 84–85.
- Matamales-Andreu, R.; Fortuny, J.; Muijal, E. & Galobart, À. (2019). Tetrapod tracks from the Permian of Mallorca (western Mediterranean): preliminary data, biostratigraphic and biogeographic inferences. In: *The Palaeontological Association, 63rd annual meeting, 15th–21st December 2019*. The Palaeontological Association, València: p. 107.
- Matamales-Andreu, R.; Oms, O. & Fortuny, J. (2021a). Paleoeosistemes del Permià i Triàsic continental de Mallorca (Illes Balears, Mediterrània occidental): síntesi i perspectives futures. In: Gómez-Pujol, Ll.; Roig-Munar, F.X.; Gelabert, B. & Martín, J.A. (Eds.). *De la terra a la mar i de la mar a la terra. Homenatge a Antonio Rodríguez-Perea. Monografies de la Societat d'Història Natural de Balears*, 34. Societat d'Història Natural de les Balears, Palma: 17–39.
- Matamales-Andreu, R.; Peñalver, E.; Muijal, E.; Oms, O.; Scholze, F.; Juárez, J.; Galobart, À. & Fortuny, J. (2021b). Early–Middle Triassic fluvial ecosystems of Mallorca (Balearic Islands): biotic communities and environmental evolution in the equatorial western peri-Tethys. *Earth-Science Reviews*, 222: 103783.
- Matamales-Andreu, R.; Roig-Munar, F.X.; Oms, O.; Galobart, À. & Fortuny, J. (2021c). A captorhinid-dominated assemblage from the palaeoequatorial Permian of Menorca (Balearic Islands, western Mediterranean). *Earth and Environmental Science Transactions of the Royal Society of Edinburgh*, 112(2): 125–145.
- Matamales-Andreu, R.; Muijal, E.; Galobart, À. & Fortuny, J. (2021d). Insights on the evolution of synapsid locomotion based on tetrapod tracks from the lower Permian of Mallorca (Balearic Islands, western Mediterranean). *Palaeogeography, Palaeoclimatology, Palaeoecology*, 579: 110589.
- Matamales-Andreu, R.; Galobart, À. & Fortuny, J. (2021e). New occurrences of small moradisaurine captorhinid eureptiles from the Permian of Mallorca (western Mediterranean). In: Belvedere, M.; Díez Díaz, V.; Mecozzi, B. & Sardella, R. (Eds.). *Abstract book of the XVIII annual conference of the European Association of Vertebrate Palaeontologists, online, 5th–9th July 2021*. *Palaeovertebrata*, 44: p. 115.
- Matamales-Andreu, R.; Oms, O.; Galobart, À. & Fortuny, J. (2021f). Middle–Upper Triassic marine vertebrates of Mallorca (Balearic Islands, western Mediterranean). *Historical Biology*, 33(10): 2520–2533.

- 1 Maxbauer, D.P.; Feinberg, J.M. & Fox, D.L. (2016). MAX UnMix: A web application for
2 unmixing magnetic coercivity distributions. *Computers & Geosciences*, 95: 140–145.
- 3 McCann, T.; Pascal, C.; Timmerman, M.J.; Krzywiec, P.; López-Gómez, J.; Wetzel, A.;
4 Krawczyk, C.M.; Rieke, H. & Lamarche, J. (2006). Post-Variscan (end Carboniferous–
5 Early Permian) basin evolution in Western and Central Europe. *Geological Society,
6 London, Memoirs*, 32: 355–388.
- 7 McFadden, P.L. & McElhinny, M.W. (1988). The combined analysis of remagnetization circles
8 and direct observations in palaeomagnetism. *Earth and Planetary Science Letters*, 87(1),
9 161–172.
- 10 Meade, L.E.; Jones, A.S. & Butler, R.J. (2016). A revision of tetrapod footprints from the late
11 Carboniferous of the West Midlands, UK. *PeerJ*, 4: e2718.
- 12 Melchor, R.N. & Sarjeant, W.A.S. (2004). Small amphibian and reptile footprints from the
13 Permian Carapacha Basin, Argentina. *Ichnos*, 11: 57–78.
- 14 Meyen, S.V. (1987). *Fundamentals of palaeobotany*. Chapman and Hall, London. 432 pp.
- 15 Miall, A.D. (1977). A review of the braided-river depositional environment. *Earth-Science
16 Reviews*, 13: 1–62.
- 17 Miall, A.D. (1985). Architectural-Element Analysis: a new method of facies analysis applied to
18 fluvial deposits. *Earth-Science Reviews*, 22: 261–308.
- 19 Miall, A.D. (2006). *The Geology of Fluvial Deposits: Sedimentary Facies, Basin Analysis, and
20 Petroleum Geology*. 4th ed. Springer, Berlin, Heidelberg, New York. 582 pp.
- 21 Michel, L.A.; Tabor, N.J.; Montañez, I.P.; Schmitz, M.D. & Davydov, V.I. (2015).
22 Chronostratigraphy and Paleoclimatology of the Lodève Basin, France: Evidence for a
23 pan-tropical aridification event across the Carboniferous–Permian boundary.
24 *Palaeogeography, Palaeoclimatology, Palaeoecology*, 430: 118–131.
- 25 Minter, N.J.; Krainer, K.; Lucas, S.G.; Braddy, S.J. & Hunt, A.P. (2007). Palaeoecology of an
26 Early Permian playa lake trace fossil assemblage from Castle Peak, Texas, USA.
27 *Palaeogeography, Palaeoclimatology, Palaeoecology*, 246: 390–423.
- 28 Mishra, S.; Jha, N. & Gahalain, S.S. (2017). Taphonomic and palaeovegetational studies in lower
29 Permian (Asselian-Sakmarian) deposits of Chintalapudi Area, Godavari Graben, South
30 India. *Revue de Micropaléontologie*, 60(2): 193–211.
- 31 Montañez, I.P. & Poulsen, C.J. (2013). The late Paleozoic ice age: an evolving paradigm. *Annual
32 Review of Earth and Planetary Sciences*, 41: 629–656.
- 33 Montañez, I.P.; Tabor, N.J.; Niemeier, D.; DiMichele, W.A.; Frank, T.D.; Fielding, C.R.; Isbell,
34 J.L.; Birgenheier, L.T. & Rygel, M. (2007). CO₂-forced climate and vegetation instability
35 during Late Paleozoic glaciation. *Science*, 315: 87–91.

- Moodie, R.L. (1929). Vertebrate footprints from the Red Beds of Texas. *American Journal of Science*, 97: 352–368.
- Mujal, E. & Marchetti, L. (2020). *Ichniotherium* tracks from the Permian of France, and their implications for understanding the locomotion and palaeobiogeography of large diadectomorphs. *Palaeogeography, Palaeoclimatology, Palaeoecology*, 547: 109698.
- Mujal, E. & Schoch, R.R. (2020). Middle Triassic (Ladinian) amphibian tracks from the Lower Keuper succession of southern Germany: Implications for temnospondyl locomotion and track preservation. *Palaeogeography, Palaeoclimatology, Palaeoecology*, 543: 109625.
- Mujal, E.; Fortuny, J.; Oms, O.; Bolet, A.; Galobart, À. & Anadón, P. (2016). Palaeoenvironmental reconstruction and early Permian ichnoassemblage from the NE Iberian Basin (Pyrenean Basin). *Geological Magazine*, 153(4): 578–600.
- Mujal, E.; Fortuny, J.; Pérez-Cano, J.; Dinarès-Turell, J. Ibáñez-Insa, J.; Oms, O.; Vila, I.; Bolet, A. & Anadón, P. (2017a). Integrated multi-stratigraphic study of the Coll de Terrers late Permian–Early Triassic continental succession from the Catalan Pyrenees (NE Iberian Peninsula): A geologic reference record for equatorial Pangaea. *Global and Planetary Change*, 159: 46–60.
- Mujal, E.; Fortuny, J.; Bolet, A.; Oms, O. & López, J.A. (2017b). An archosauromorph dominated ichnoassemblage in fluvial settings from the late Early Triassic of the Catalan Pyrenees (NE Iberian Peninsula). *PLoS ONE*, 12(4): e0174693.
- Mujal, E.; Fortuny, J.; Marmi, J.; Dinarès-Turell, J.; Bolet, A. & Oms, O. (2018). Aridification across the Carboniferous–Permian transition in central equatorial Pangea: the Catalan Pyrenean succession (NE Iberian Peninsula). *Sedimentary Geology*, 363: 48–68.
- Mujal, E.; Marchetti, L.; Schoch, R.R. & Fortuny, J. (2020). Upper Paleozoic to lower Mesozoic tetrapod ichnology revisited: photogrammetry and relative depth pattern inferences on functional prevalence of autopodia. *Frontiers in Earth Science*, 8:248.
- Nicholson, H.A. (1873). Contributions to the study of the errant annelides of the older Palaeozoic rocks. *Proceedings of the Royal Society of London*, 21: 288–290.
- Obrador, A. (1983). El Pérmico de las Baleares. In: Martínez-Díaz, C. (Ed.). *Carbonífero y Pérmico de España, X Congreso Internacional de Estratigrafía y Geología del Carbonífero*. Ministerio de Industria y Energía, Instituto Geológico y Minero de España, Madrid: 463–470.
- Olroyd, S.L. & Sidor, C.A. (2017). A review of the Guadalupian (middle Permian) global tetrapod fossil record. *Earth-Science Reviews*, 171: 583–597.
- Özdemir, Ö. & Dunlop, D.J. (2014). Hysteresis and coercivity of hematite. *Journal of Geophysical Research: Solid Earth*, 119(4): 2582–2594.

- Pant, D.D. & Nautiyal, D.D. (1960). Some seeds and sporangia of *Glossopteris* flora from Raniganj Coalfield, India. *Palaeontographica Abteilung B*, 107(1–3): 41–64.
- Parés, J.M.; Freeman, R. & Sàbat, F. (1989). Síntesis de los resultados paleomagnéticos de los bordes de la Cuenca Catalano-Balear. *Cuadernos de Geología Ibérica*, 12: 59–74.
- Parés, J.M.; Freeman, R. & Roca, E. (1992a). Neogene structural development in the Valencia trough margins from palaeomagnetic data. *Tectonophysics*, 203: 111–124.
- Parés, J.M.; Roca, E. & Freeman, R. (1992b). Datos paleomagnéticos de los márgenes del surco de Valencia. Papel de las rotaciones en la estructuración neógena. *Física de la Tierra*, 4: 231–246.
- Parrish, J.T. (1993). Climate of the supercontinent Pangea. *Journal of Geology*, 101: 215–233.
- Pemberton, S.G. & Frey, R.W. (1982). Trace fossil nomenclature and the *Planolites-Palaeophycus* dilemma. *Journal of Paleontology*, 56(4): 843–881.
- Pérez-Valera, J.A. (2015). *Ammonoideos y bioestratigrafía del Triásico Medio (Ladiniense) del sector oriental de la Cordillera Bética*. Ph.D. Dissertation. Universidad Complutense de Madrid, Madrid. 489 pp.
- Pérez-Valera, J.A.; Escudero-Mozo, M.J.; Arche, A.; Goy, A.; López-Gómez, J.; Pérez-López, A. & Pérez-Valera, F. (2016). Los ammonioideos del Triásico Medio de España. Implicaciones bioestratigráficas y paleobiogeográficas. In: Meléndez, G.; Núñez, A. and Tomás, M. (Eds.). *Actas de las XXXII Jornadas de la Sociedad Española de Paleontología. Cuadernos del Museo Geominero*, 20: 471–478.
- Pohlig, H. (1892). Altpermische Saurierfährten, Fische und Medusen der Gegend von Friedrichroda i. Thüringen. In: *Festschrift zum 70. Geburtstag von Rudolf Leuckardt*. Engelmann, Leipzig: 59–64.
- Pomar-Gomà, L. (1979). *The Triassic of the Balearic Islands*. Geology Department, Palma de Mallorca University, Palma. 49 pp. + 7 Petrologic Logs.
- Poort, R.J.; Clement-Westerhof, J.A.; Looy, C.V. & Visscher, H. (1997). Aspects of Permian palaeobotany and palynology. XVII. Conifer extinction in Europe at the Permian-Triassic junction: Morphology, ultrastructure and geographic/stratigraphic distribution of *Nuskoisporites dulhuntyi* (prepollen of *Ortiseia*, Walchiaceae). *Review of Palaeobotany and Palynology*, 97(1–2): 9–39.
- Postma, G. (1990). Depositional architecture and facies of river and fan deltas: a synthesis. *Special Publications of the International Association of Sedimentologists*, 10: 13–27.
- Potonié, R. (1962). Synopsis der Sporae in situ. Die Sporen der fossilen Fruktifikationen (thallophyta bis Gymnospermophyta) im natürlichen System und im Vergleich mit den Sporae dispersae. Hannover. *Beihefte zum Geologischen Jahrbuch*, 52: 91–93.

- Potonié, R. & Kremp, G. (1956). Die Sporae Dispersae des Ruhrkarbons, ihre Morphographie und Stratigraphie mit Ausblicken auf Arten anderer Gebiete und Zeitabschnitte. Teil II. *Palaeontographica Abteilung B*, 99(4–6): 85–191.
- Raine, J.I.; Mildenhall, D.C. & Kennedy, E.M. (2011). New Zealand fossil spores and pollen: an illustrated catalogue. In: *GNS Science Miscellaneous Series*. GNS Science, Lower Hutt, New Zealand: https://www.gns.cri.nz/what/earthhist/fossils/spore_pollen/catalog/index.htm.
- Ramos, A. (1995). Transition from alluvial to coastal deposits (Permian–Triassic) on the Island of Mallorca, western Mediterranean. *Geological Magazine*, 132(4): 435–447.
- Ramos, A. & Doubinger, J. (1989). Premières datations palynologiques dans le facies Buntsandstein de l'île de Majorque (Baléares, Espagne). *Comptes Rendus de l'Académie des Sciences de Paris, Série 2*, 309: 1089–1094.
- Ramos, A. & García-Ramos, S. (1992). Niveles de bioturbación en las facies tipo Buntsandstein del Pérmico-Triásico de Mallorca. In: García-Ramos, J.C. (Ed.). *Reunión Monográfica sobre Biosedimentación*, Servicio de Publicaciones de la Universidad de Oviedo, Oviedo: 41–43.
- Ramos, A.; Olmo, P. del & Alvaro, M. (1985). El Buntsandstein de la isla de Mallorca. In: Mateu Ibars, F. & Marzo, M. (Eds.). *Resúmenes del II Coloquio de Estratigrafía y Paleogeografía del Pérmico y Triásico de España*. Institut d'Estudis Ilerdencs and Grupo Español del Mesozoico, La Seu d'Urgell: 103–104.
- Ramos, E. & Rodríguez-Perea, A. (1985). Découverte d'un affleurement de terrains paléozoïques dans l'île de Majorque (Baléares, Espagne). *Comptes Rendus de l'Académie des Sciences de Paris, Série 2*, 301: 1205–1207.
- Rangheard, Y. (1971). Étude géologique des îles d'Ibiza et de Formentera (Baléares). *Memorias del Instituto Geológico y Minero de España*, 82: 2–340 + 23 pl.
- Retallack, G.J. (1997). Earliest Triassic origin of *Isoetes* and quillwort evolutionary radiation. *Journal of Paleontology*, 71(3): 500–521.
- Retallack, G.J.; Metzger, C.A.; Greaver, T.; Jahren, A.H.; Smith, R.M.H. & Sheldon, N.D. (2006). Middle-Late Permian mass extinction on land. *GSA Bulletin*, 118(11/12): 1398–1411.
- Rodríguez-Perea, A. & Ramos, E. (1984). Presencia de Paleozoico en la Sierra de Tramuntana (Mallorca). *Bolletí de la Societat d'Història Natural de Balears*, 28: 145–148.
- Rodríguez-Perea, A.; Ramos-Guerrero, E.; Pomar, L.; Paniello, X.; Obrador, A. & Martí, J. (1987). El Triásico de las Baleares. *Cuadernos de Geología Ibérica*, 11: 295–321.
- Romano, M.; Citton, P. & Nicosia, U. (2016). Corroborating trackmaker identification through footprint functional analysis: the case study of *Ichniotherium* and *Dimetropus*. *Lethaia*, 49: 102–116.

- Romano, M.; Citton, P.; Maganuco, S.; Sacchi, E.; Caratelli, M.; Ronchi, A. & Nicosia, U. (2019). New basal synapsid discovery at the Permian outcrop of Torre del Porticciolo (Alghero, Italy). *Geological Journal*, 54(3): 1554–1566.
- Romano, M.; Bernardi, M.; Petti, F.M.; Rubidge, B.; Hancox, J. & Benton, M.J. (2020). Early Triassic terrestrial tetrapod fauna: a review. *Earth-Science Reviews*, 210: 103331.
- Romer, A.S. & Price, L.I. (1940). Review of the Pelycosauria. *Geological Society of America Special Papers*, 28: 1–538.
- Roscher, M. & Schneider, J.W. (2006). Permo-Carboniferous climate: Early Pennsylvanian to Late Permian climate development of central Europe in a regional and global context. *Geological Society, London, Special Publications*, 265: 95–136.
- Roscher, M.; Berner, U. & Schneider, J.W. (2008). A Tool for the Assessment of the Paleodistribution of Source and Reservoir Rocks. *OIL GAS European Magazine*, 3: 131–137.
- Rosell, J.; Arribas, J.; Elizaga, E. & Gómez, D. (1988). Caracterización sedimentológica y petrográfica de la serie roja permo-triásica de la isla de Menorca. *Boletín Geológico y Minero*, 99(1): 71–82.
- Rosell, J.; Gómez-Gras, D. & Elízaga, E. (1989). *Mapa Geológico de España. Escala 1:25.000. Isla de Menorca. Cap Menorca y Ciutadella*. Segunda serie, primera edición. Instituto Tecnológico GeoMinero de España, Madrid. 51 pp. + 3 maps.
- Rothwell, G.W.; Mapes, G. & Hernández-Castillo, G.R. (2005). *Hanskerpia* gen. nov. and phylogenetic relationships among the most ancient conifers (Voltziales). *Taxon*, 54(3): 733–750.
- Rowntree, K.M. & Dollar, E.S.J. (1999). Vegetation controls on channel stability in the Bell River, Eastern Cape, South Africa. *Earth Surface Processes and Landforms*, 24: 127–134.
- Ruta, M. & Benton, M.J. (2008). Calibrated diversity, tree topology and the mother of mass extinctions: the lesson of temnospondyls. *Palaeontology*, 51: 1261–1288.
- Sacchi, E.; Cifelli, R.; Citton, P.; Nicosia, U. & Romano, M. (2014). *Dimetropus osageorum* n. isp. from the Early Permian of Oklahoma (USA): A Trace and its Trackmaker. *Ichnos*, 21: 175–192.
- Sahney, S. & Benton, M.J. (2008). Recovery from the most profound mass extinction of all time. *Proceedings of the Royal Society B*, 275: 759–765.
- Salter, J.W. (1857). On annelide-burrows and surface-markings from the Cambrian rocks of the Longmynd. No. 2. *Quarterly Journal of the Geological Society*, 13: 199–206.
- Santi, G.; Marchetti, L.; Schirolli, P. & Ronchi, A. (2020). The Cisuralian tetrapod ichnoassociation from Italy: from historical findings to a standard reference status. *Journal of Mediterranean Earth Sciences*, 12: 39–59.

- Schaarschmidt, F. & Maubeuge, P.L. (1969). Eine männliche Gymnospermen-Fruktifikation aus dem Voltziensandstein (Untere Trias) der Vogesen. *Senckenbergiana lethaea*, 50(5–6): 377–397.
- Schneider, J.W.; Kömer, F.; Roscher, M. & Kroner, U. (2006). Permian climate development in the northern peri-Tethys area — The Lodève basin, French Massif Central, compared in a European and global context. *Palaeogeography, Palaeoclimatology, Palaeoecology*, 240: 161–183.
- Schneider, J.W.; Lucas, S.G.; Scholze, F.; Voigt, S.; Marchetti, L.; Klein, H.; Opluštil, S.; Werneburg, R.; Golubev, V.K.; Barrick, J.E.; Nemyrovska, Y.; Ronchil, A.; Day, M.O.; Silantiev, V.V.; Rößler, R.; Saber, H.; Linnemann, U.; Zharinova, V. & Shen, S.-Z. (2020). Late Paleozoic–early Mesozoic continental biostratigraphy — Links to the Standard Global Chronostratigraphic Scale. *Palaeoworld*, 29(2): 186–238.
- Schoch, R.R. (2014). *Amphibian Evolution: The Life of Early Land vertebrates*. Wiley Blackwell. 264 pp.
- Schweitzer, H.J. (1962). Die Makroflora des niederrheinischen Zechsteins. *Fortschritte der Geologie des Rheinlande und Westfalen*, 6: 331–376.
- Scotese, C.R. (2014a). Atlas of Permo-Carboniferous Paleogeographic Maps, maps 53 – 64 from Volume 4 of the PALEOMAP Atlas for ArcGIS (Late Paleozoic), Mollweide Projection, PALEOMAP Project, Evanston, Illinois.
- Scotese, C.R. (2014b). Atlas of Middle & Late Permian and Triassic Paleogeographic Maps, maps 43 – 48 from Volume 3 of the PALEOMAP Atlas for ArcGIS (Jurassic and Triassic) and maps 49 – 52 from Volume 4 of the PALEOMAP Atlas for ArcGIS (Late Paleozoic), Mollweide Projection, PALEOMAP Project, Evanston, Illinois.
- Sevillano, A. & Barnolas, A. (2018). Mapa Geológico Digital Continuo E. 1:50.000, Zona Mallorca (Zona-2210). In: GEODE. Mapa Geológico Digital continuo de España. Available online at: <http://info.igme.es/visorweb/> (last visited: 06/06/2018)
- Seyfullah, L.J.; Kustatscher, E. & Taylor, W.A. (2013). The first discovery of *in situ* *Verrucosisporites applanatus* spores from the Middle Triassic flora from Bromsgrove (Worcestershire, UK). *Review of Palaeobotany and Palynology*, 197: 15–25.
- Sidor, C.A.; O’Keefe, F.R.; Damiani, R.; Steyer, J.S.; Smith, R.M.H.; Larsson, H.C.E.; Sereno, P.C.; Ide, O. & Maga, A. (2005). Permian tetrapods from the Sahara show climate-controlled endemism in Pangaea. *Nature*, 434: 886–889.
- Smith, R.M.H. (1993). Vertebrate taphonomy of late Permian floodplain deposits in the southwestern Karoo Basin of South Africa. *Palaios*, 8: 45–67.

- Smith, R.M.H.; Sidor, C.A.; Tabor, N.J. & Steyer, J.S. (2015). Sedimentology and vertebrate taphonomy of the Moradi Formation of northern Niger: A Permian wet desert in the tropics of Pangaea. *Palaeogeography, Palaeoclimatology, Palaeoecology*, 440: 128–141.
- Sopeña, A.; Virgili, C.; Hernando, S. & Ramos, A. (1977). Pérmico continental en España. *Cuadernos de Geología Ibérica*, 4: 11–34.
- Speksnijder, A. (1985). Anatomy of a strike-slip fault controlled sedimentary basin, Permian of the southern Pyrenees, Spain. *Sedimentary Geology*, 44: 179–223.
- Stampfli, G.M.; Hochard, C.; Vérard, C.; Wilhem, C. & vonRaumer, J. (2013). The formation of Pangea. *Tectonophysics*, 593: 1–19.
- Steiner, M.B. (2006). The magnetic polarity time scale across the Permian-Triassic boundary. *Geological Society, London, Special Publications*, 265(1): 15–38.
- Steyer, J.S.; Damiani, R.; Sidor, C.A.; O’Keefe, F.R.; Larsson, H.C.E.; Magal, A. & Ide, O. (2006). The vertebrate fauna of the Upper Permian of Niger. IV. *Nigerpeton ricqlesi* (Temnospondyli: Cochleosauridae), and the edopoid colonization of Gondwana. *Journal of Vertebrate Paleontology*, 26(1): 18–28.
- Sun, Y.; Joachimski, M.M.; Wignall, P.B.; Yan, C.; Chen, Y.; Jiang, H.; Wang, L. & Lai, X. (2012). Lethally hot temperatures during the Early Triassic greenhouse. *Science*, 338(6105): 366–370.
- Tabor, N.J. & Poulsen, C.J. (2008). Palaeoclimate across the Late Pennsylvanian–Early Permian tropical palaeolatitudes: a review of climate indicators, their distribution, and relation to palaeophysiographic climate factors. *Palaeogeography, Palaeoclimatology, Palaeoecology*, 268: 293–310.
- Taylor, T.N. & Taylor, E.L. (1987). The ultrastructure of fossil gymnosperm pollen. *Bulletin de la Société Botanique de France. Actualités Botaniques*, 134(2): 121–140.
- Taylor, T.N.; Taylor, E.L. & Krings, M. (2009). *Paleobotany: the biology and evolution of fossil plants*. Elsevier Academic Press, Amsterdam. 1252 pp.
- Traverse, A.T. (2007). Paleopalynology. *Topics in Geobiology*, 28: 1–832.
- Uchman, A.; Pika-Biolzi, M. & Hochuli, P.A. (2004). Oligocene trace fossils from temporary fluvial plain ponds: An example from the Freshwater Molasse of Switzerland. *Eclogae Geologicae Helvetiae*: 97, 133–148.
- Valentini, M.; Nicosia, U. & Conti, M.A. (2009). A re-evaluation of *Pachypes*, a pareiasaurian track from the Late Permian. *Neues Jahrbuch für Geologie und Paläontologie*, 251: 71–94.
- Van Allen, H.E.K.; Calder, J.H. & Hunt, A.P. (2005). The trackway record of a tetrapod community in a walthian conifer forest from the Permo-Carboniferous of Nova Scotia. *New Mexico Museum of Natural History and Science Bulletin*, 30: 322–332.

- Vázquez, M.S. & Césari, S.N. (2017). The Permian palynological *Lueckisporites-Weylandites* Biozone in the San Rafael Block and its correlation in Western Gondwana. *Journal of South American Earth Sciences*, 76: 165–181.
- Vera, J.-A.; Alonso-Chaves, F.M.; Andreo, B.; Arias, C.; Azañón, J.M.; Balanyá, J.C.; Barón, A.; Booth-Rea, G.; Castro, J.M.; Chacón, B.; Company, M.; Crespo-Blanc, A.; Delgado, F.; Díaz de Federico, A.; Esteras, M.; Estévez, A.; Fernández, J.; Fornós, J.J.; Galindo-Zaldívar, J.; García-Casco, A.; García-Dueñas, V.; García-Hernández, M.; Garrido, C.J.; Gea, G.A. de; Gelabert, B.; Gervilla, F.; González-Lodeiro, F.; Jabaloy, A.; López-Garrido, A.C.; Luján, M.; Martín-Algarra, A.; Martín-Chivelet, J.; Martín-Martín, M.; Molina, J.M.; Morata, D.; Nieto, J.M.; Obrador, A.; O'Dogherty, L.; Orozco, M.; Pérez-López, A.; Pomar, L.; Puga, E.; Ramos, E.; Rey, J.; Rivas, P.; Rodríguez-Cañero, R.; Ruiz-Cruz, M.D.; Ruiz-Ortiz, P.A.; Sàbat, F.; Sánchez-Gómez, M.; Sánchez-Navas, A.; Sandoval, J.; Sanz de Galdeano, C.; Soto, J.I.; Torres-Roldán, R.L. & Villas, L. (2004). Capítulo 4. Cordillera Bética y Baleares. In: Vera, J.-A. (Ed.). *Geología de España*. Instituto Geológico y Minero de España, Madrid: 346–464.
- Virgili, C. (1952). Hallazgo de nuevos *Ceratites* en el Triásico mallorquín. *Memorias y Comunicaciones del Instituto Geológico de la Diputación Provincial de Barcelona*, 9: 19–39.
- Visscher, H. (1967). Permian and Triassic palynology and the concept of “Tethys twist”. *Palaeogeography, Palaeoclimatology, Palaeoecology*, 3: 151–166.
- Visscher, H. (1968). On the Thuringian age of the upper Palaeozoic sedimentary and volcanic deposits of the Estérel (Southern France). *Review of Palaeobotany and Palynology*, 6: 71–83.
- Visscher, H.; Kerp, J.H.F.; Clement–Westerhof, J.A. (1986). Aspects of Permian Palaeobotany and palynology. VI. Towards a flexible system of naming Paleozoic conifers. *Acta Botanica Neerlandica*, 35: 87–100.
- Voigt, S. (2005). *Die Tetrapodenichnofauna des kontinentalen Oberkarbon und Perm im Thüringer Wald - Ichnotaxonomie, Paläoökologie und Biostratigraphie*. Cuvillier Verlag, Göttingen. 308 pp.
- Voigt, S. & Ganzelewski, M. (2010). Toward the origin of amniotes: Diadectomorph and synapsid footprints from the early Late Carboniferous of Germany. *Acta Palaeontologica Polonica*, 55(1): 57–72.
- Voigt, S. & Lucas, S.G. (2015). Permian tetrapod ichnodiversity of the Prehistoric Trackways National Monument (south-central New Mexico, USA). *New Mexico Museum of Natural History and Science Bulletin*, 65: 153–167.

- Voigt, S.; Berman, D.S. & Henrici, A.C. (2007). First well-established track-trackmaker association of Paleozoic tetrapods based on *Ichniotherium* trackways and diadectid skeletons from the lower Permian of Germany. *Journal of Vertebrate Paleontology*, 27(3): 553–570.
- Voigt, S.; Hminna, A.; Saber, H.; Schneider, J.W. & Klein, H. (2010). Tetrapod footprints from the uppermost level of the Permian Ikakern Formation (Argana Basin, Western High Atlas, Morocco). *Journal of African Earth Sciences*, 57: 470–478.
- Voigt, S.; Lagnaoui, A.; Hminna, A.; Saber, H. & Schneider, J.W. (2011). Revisional notes on the Permian tetrapod ichnofauna from the Tiddas Basin, central Morocco. *Palaeogeography, Palaeoclimatology, Palaeoecology*, 302: 474–483.
- Voigt, S.; Niedźwiedzki, G.; Raczynski, P.; Mastalerz, K & Ptaszyński, T. (2012). Early Permian tetrapod ichnofauna from the Intra-Sudetic Basin, SW Poland. *Palaeogeography, Palaeoclimatology, Palaeoecology*, 313–314: 173–180.
- Whyte, M.A. & Romano, M. (2001). A dinosaur ichnocoenosis from the Middle Jurassic of Yorkshire, UK. *Ichnos*, 8: 223–234.
- Zavialova, N. & van Konijnenburg-van Cittert, J.H.A. (2011). Exine ultrastructure of in situ peltasperm pollen from the Rhaetian of Germany and its implications. *Review of Palaeobotany and Palynology*, 168(1): 7–20.
- Zavialova, N.; Kustatscher, E. & van Konijnenburg-van Cittert, J.H.A. (2010). Spore ultrastructure of *Selaginellites leonardii* and diversity of Selaginellalean spores. *Geo.Alp*, 7: 1–17.
- Zijderveld, J.D.A. (2013). A. C. Demagnetization of Rocks: Analysis of Results. *Developments in Solid Earth Geophysics*, 3: 254–286.
- Zouicha, A.; Voigt, S.; Saber, H.; Marchetti, L.; Hminna, A.; El Attari, A.; Ronchi, A. & Schneider, J.W. (2021). First record of permian continental trace fossils in the jebilet massif, Morocco. *Journal of African Earth Sciences*, 173: 104015.

Figures

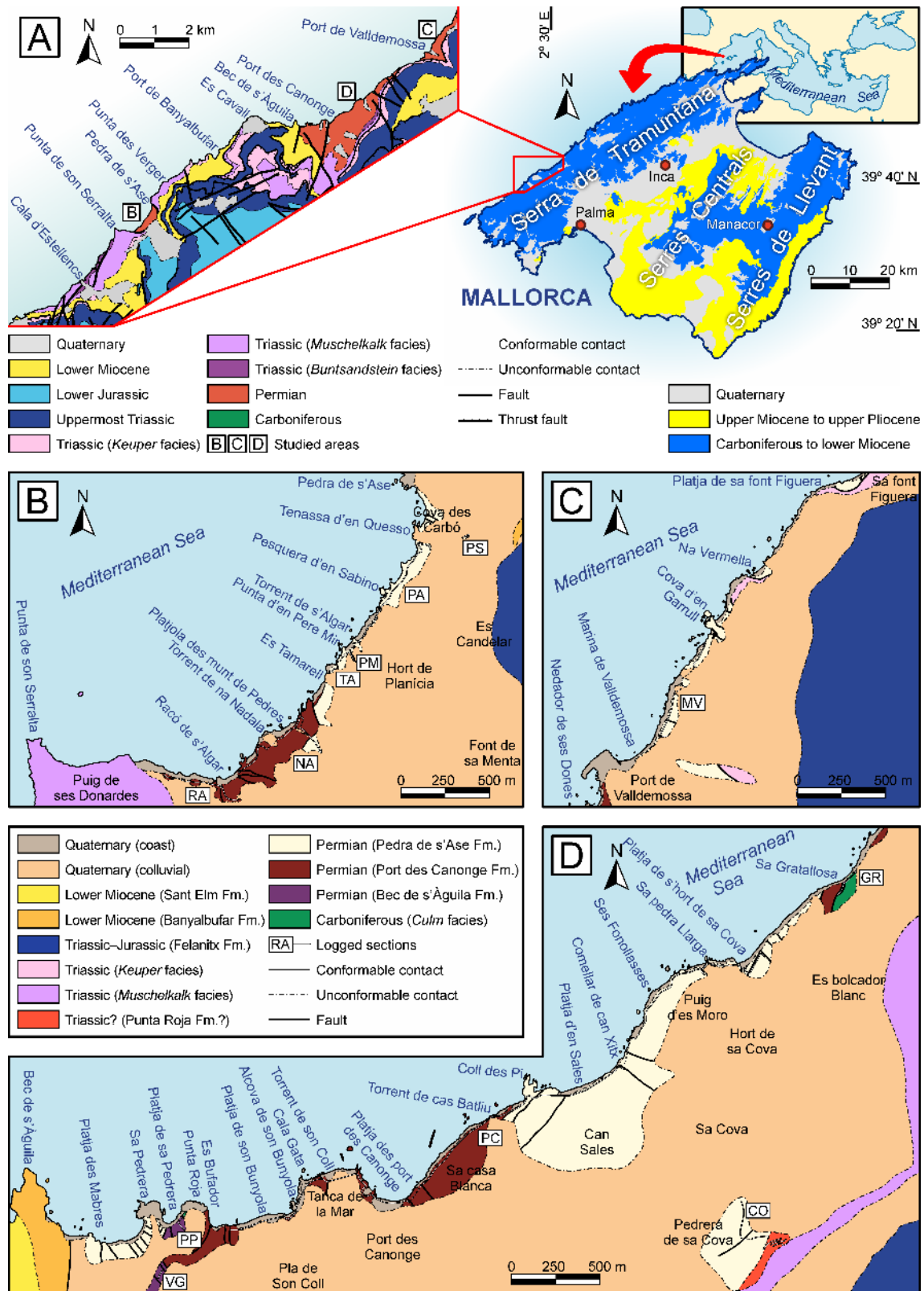


Figure 1. A: Synthetic geological map of the island of Mallorca (Balearic Islands), with a close-up of the study zone, indicating the location of subfigures B, C and D. Simplified from Sevillaño & Barnolas (2018). **B:** Detailed geological map of the outcrops between Punta de son Serralta and Pedra de s'Ase (Banyalbufar, Mallorca), with indication of the location of the six logged

1 sections (RA: Racó de s'Algar; NA: Torrent de na Nadala; TA: Es Tamarell; PM: Punta d'en Pere
2 Mir; PA: Pedra de s'Ase; PS: Pedra de s'Ase - Summit). **C:** Detailed geological map of the
3 outcrops in the surroundings of Port de Valldemossa (Valldemossa, Mallorca), with indication of
4 the location of the logged section (MV: Marina de Valldemossa). **D:** Detailed geological map of
5 the outcrops between Bec de s'Àguila and Sa Gratallosa (Valldemossa, Mallorca), with indication
6 of the location of the four logged sections (PP: Platja de sa Pedrera; VG: Volta des General; PC:
7 Port des Canonge–Hort de sa Cova; GR: Sa Gratallosa; CO: Pedrera de sa Cova). Toponyms of
8 all the maps after Homar (1985) and IDEIB (2019).

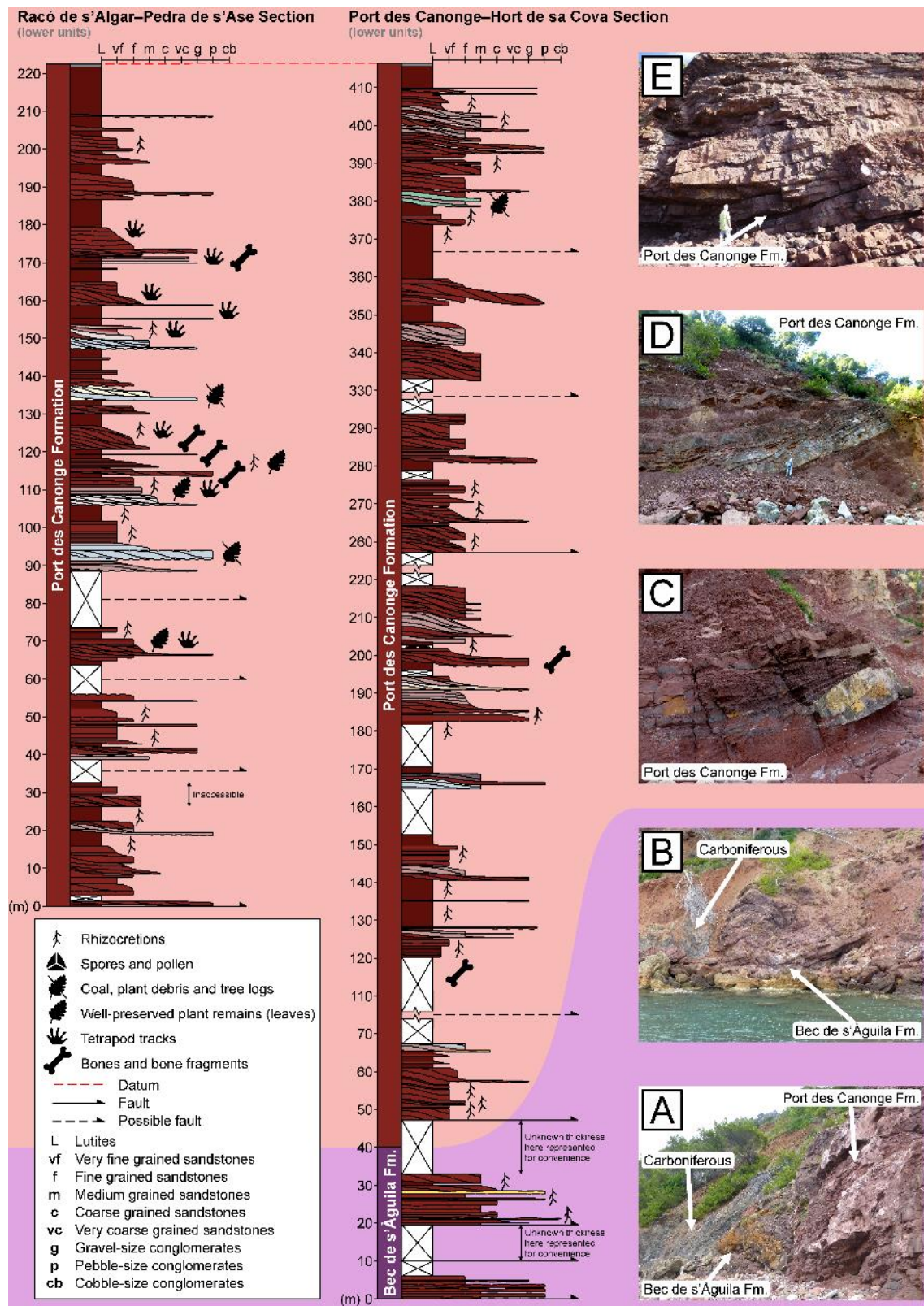


Figure 2. Synthetic logs of the Bec de s'Àguila and Port des Canonge formations at the Racó de s'Algar–Pedra de s'Ase section and at the Port des Canonge–Hort de sa Cova section. See also Supplementary Logs and Supplementary Correlations. **A–E:** Field pictures of some representative points in those two logs. **A:** Faulted contact between the Carboniferous deposits, the Bec de

1 s'Àguila Formation and the Port des Canonge Formation at Sa Gratallosa. **B:** Contact between
2 the Carboniferous deposits and the Bec de s'Àguila Formation at Platja de sa Pedrera. **C:** Infill
3 deposits of a small channel with lateral accretion and associated crevasse splay and floodplain
4 deposits, Port des Canonge Formation at Racó de s'Algar. **D:** General aspect of the Port des
5 Canonge Formation at Platjola des munt de Pedres, note alternation of main channels (sandstones)
6 and floodplain (lutites) deposits. **E:** General aspect of the Port des Canonge Formation near
7 Torrent de cas Batliu, note the lateral accretion sets. Changes in background colour represent
8 boundaries between formations.
9

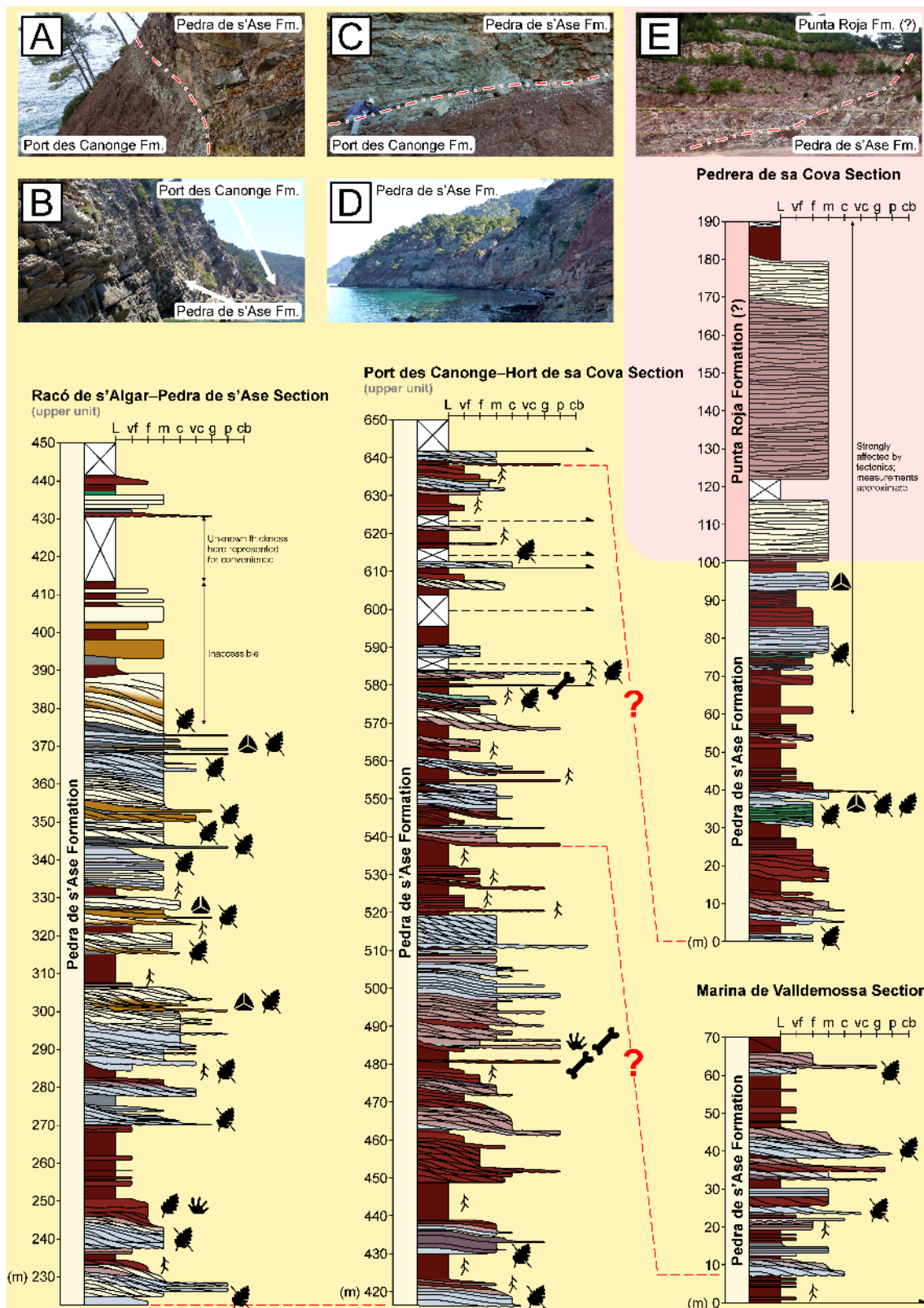


Figure 3. Synthetic logs of the Pedra de s'Ase Formation and the Punta Roja Formation(?) at the Racó de s'Algar-Pedra de s'Ase section, at the Port des Canonge-Hort de sa Cova section, at the Pedrera de sa Cova section and at the Marina de Valldemossa section. Symbols of fossils, lithology and other structures as in Figure 2. See also Supplementary Logs and Supplementary

Correlations. **A–E:** Field pictures of some representative points in some of those logs. **A:** Boundary between the Port des Canonge Formation and the Pedra de s’Ase Formation at Platjola des munt de Pedres. **B:** General aspect of the Pedra de s’Ase Formation at Pedra de s’Ase, note the outcrops of the Port des Canonge Formation in the distance. **C:** Boundary between the Port des Canonge Formation and the Pedra de s’Ase Formation near Torrent de cas Batliu. **D:** General aspect of the Pedra de s’Ase Formation at Platja d’en Sales, note the higher abundance of interbedded red lutites compared to the type section. **E:** Boundary between the Pedra de s’Ase Formation and the Punta Roja Formation(?) at Pedrera de sa Cova (upper quarry). Changes in background colour represent boundaries between formations.

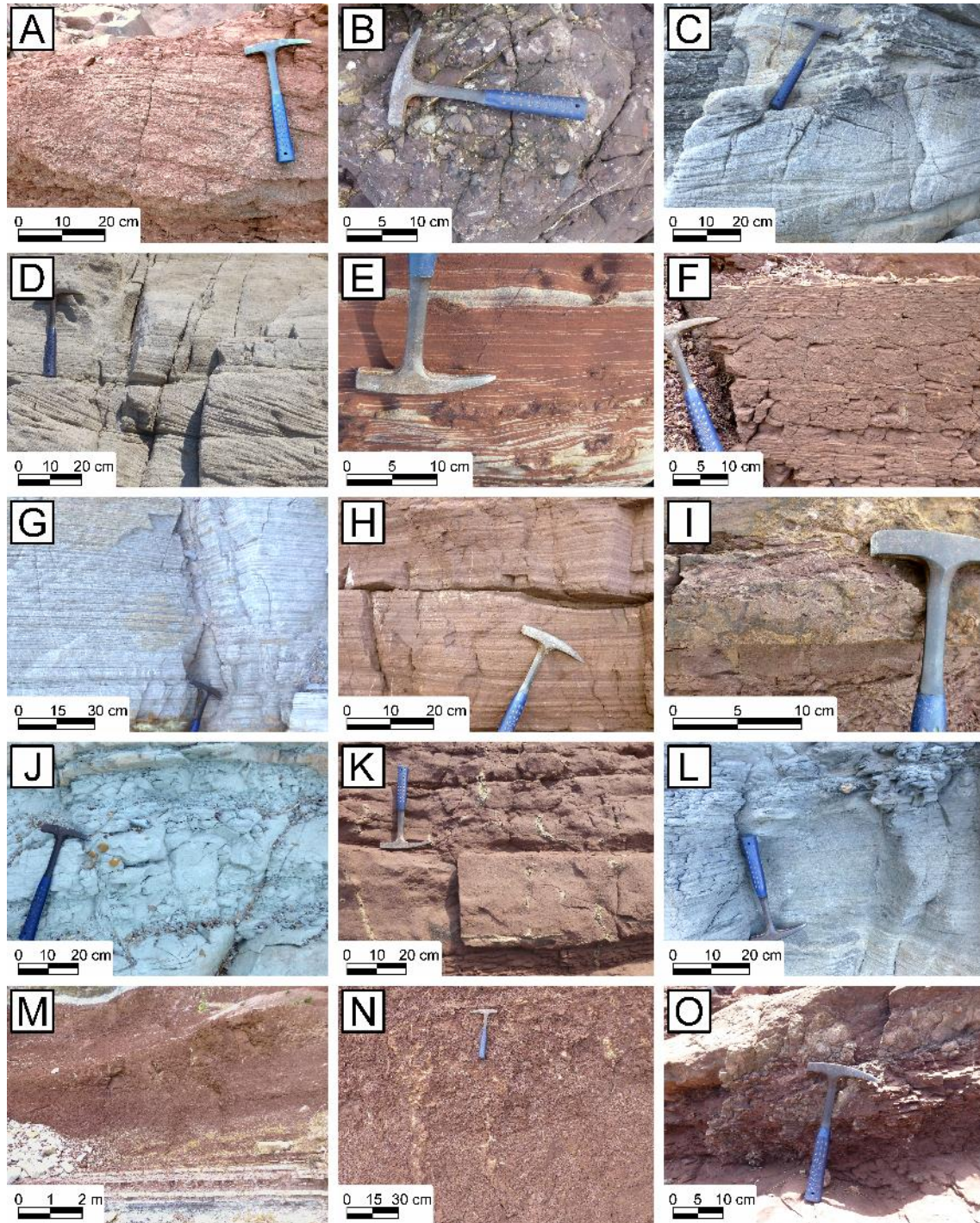
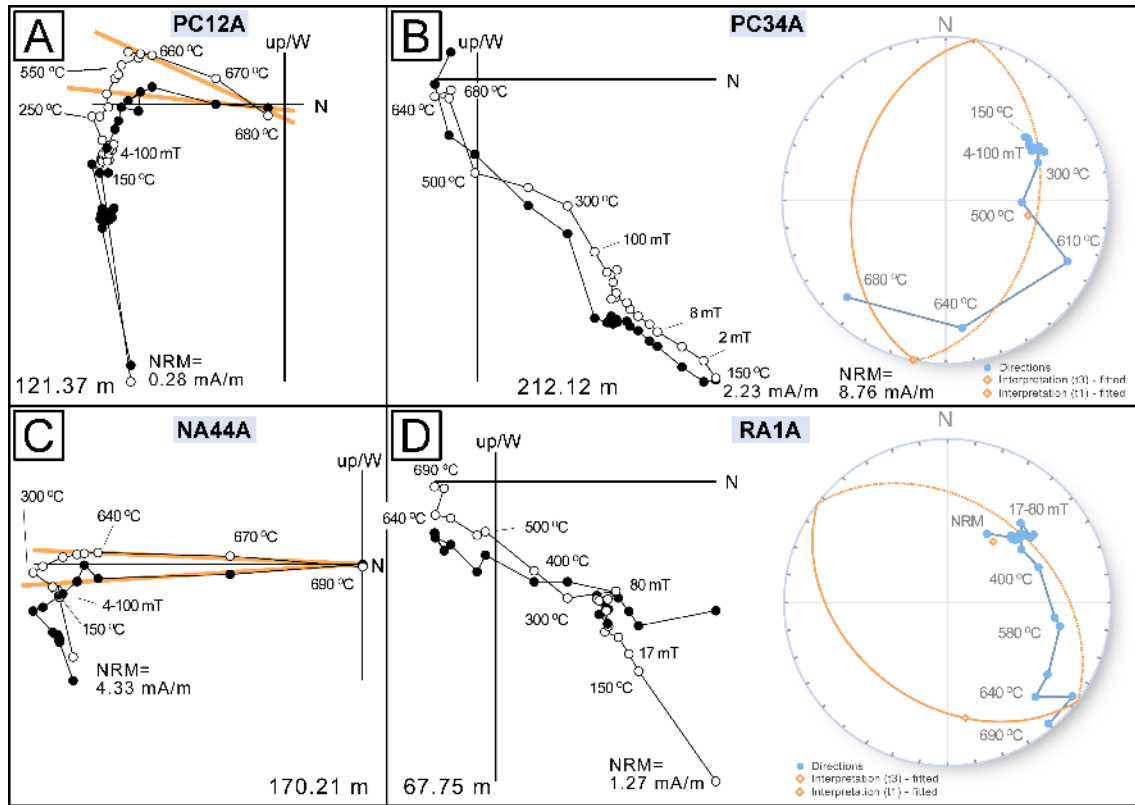


Figure 4. Photographic examples of most of the lithofacies mentioned in the present work (see also Table 1). **A:** Intraformational breccias with trough cross-bedding (*Gt*), Port des Canonge Formation. **B:** Extraformational conglomerates (*GmP*), Bec de s'Àguila Formation. **C:** Sandstones with trough cross-bedding (*St*), Pedra de s'Ase Formation. **D:** Sandstones with planar cross-bedding (*Sp*), Pedra de s'Ase Formation. **E:** Sandstones with ripple lamination (*Sr*), Pedra de s'Ase Formation. **F:** Silty sandstones with ripple lamination, heavily affected by fluid-scape structures (*Sr?*), Port des Canonge Formation. **G:** Sandstones with horizontal bedding (*Sh*), Pedra de s'Ase Formation. **H:** Sandstones with low-angle cross-bedding (*Sl*), Port des Canonge

1 Formation. **I:** Sandstones filling a scour, with soft pebbles and without visible bedding (*Ss*), Port
2 des Canonge Formation. **J:** Massive sandstones (*Sm*) with nodules, Pedra de s'Ase Formation. **K:**
3 Bioturbated sandstones (*Sb*) with rhizocretions, Port des Canonge Formation. **L:** Laminated
4 lutites (*Fl*), in this case with horizontal lamination, Pedra de s'Ase Formation. **M:** Massive lutites
5 (*Fm*), Pedra de s'Ase Formation. **N:** Lutites with rhizocretions (*Fr*), Port des Canonge Formation.
6 **O:** Palaeosols (*P*), in this case a Calcisol, Port des Canonge Formation.

7



8

9 **Figure 5. A–D:** Representative orthogonal demagnetisation diagrams with bedding corrected
10 coordinates (tectonic). The natural remanent magnetisation (NRM) intensity, the stratigraphic
11 position and some demagnetisation steps are indicated. Open and closed symbols represent
12 inclination and declination, respectively. A coloured thick line shows the linear fitted reverse
13 ChRM direction (samples PC12A and NA44A). For samples PC34A and RA1A, demagnetisation
14 data are also plotted on respective equal-area stereogram showing a fitted great circle and
15 interpreted directions.

16

depicted. Statistical information is given (Ns, number of total samples; N, number of samples for the mean; Dec., declination; Inc., inclination; k, Fisher's precision parameter; \square_{95} , radius of the 95% confidence cone). The upper-right stereogram is the VGP distribution in tectonic coordinates where red dots represent discarded directions after applying a 45° cut-off angle. The lower-right stereogram plots both all linear (L) fitted directions and the ones derived from great circles (GC). See Supplementary Table 2 and Supplementary Table 3 for all sample and mean directional data respectively.

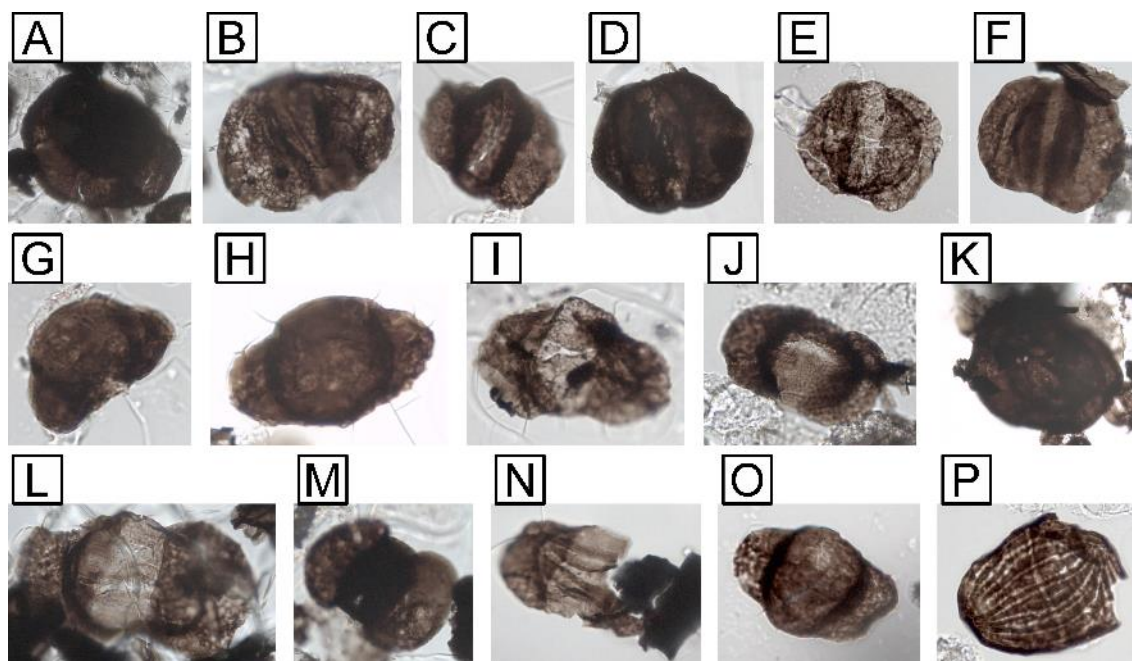


Figure 7. Best-preserved spores and pollen from the Roadian–Wordian (middle Permian) middle part of the Pedra de s’Ase Formation of Mallorca. **A:** *Playfordiaspora cancellosa*, P-PA-05/IV, N16/4, diameter = 125 μ m. **B:** *Alisporites splendens*, P-PA-05/III, J47/3, width = 73 μ m. **C:** *Alisporites splendens*, P-PA-05/IV, N49/4, width = 60 μ m. **D:** *Gigantosporites aletoides*, P-PA-05/III, C42/2, diameter = 125 μ m. **E:** *Illinites* sp., P-PA-05/IV, R46/4, diameter = 50 μ m. **F:** *Jugasporites delasaucei*, P-PA-12/II, U38/3, width = 64 μ m. **G:** *Klausipollenites schaubergeri*, P-PA-05/II, K45, width = 43 μ m, height = 31 μ m. **H:** *Klausipollenites* sp., P-PA-05/I, H42, diameter = 80 μ m. **I:** *Limitisporites rectus*, P-PA-05/IV, C39, width = 55 μ m. **J:** *Lueckisporites virkkiae*, P-PA-09/I, E38, width = 52 μ m, height = 32 μ m. **K:** *Nuskoisporites dulhuntyi*, P-PA-05/III, Y52, diameter = 162 μ m. **L:** *Strotersporites* sp., P-PA-05/III, Y30/3, width = 107 μ m. **M:** *Platysaccus leschikii*, P-PA-05/III, C45, width = 56 μ m. **N:** *Protohaploxypinus limpidus*, P-PA-05/IV, X47/2, width = 62 μ m. **O:** *?Triadispora* sp., P-PA-05/III, L47/1, width = 56 μ m. **P:** *Vittatina* sp., P-PA-09/II, J37/4, width = 53 μ m.

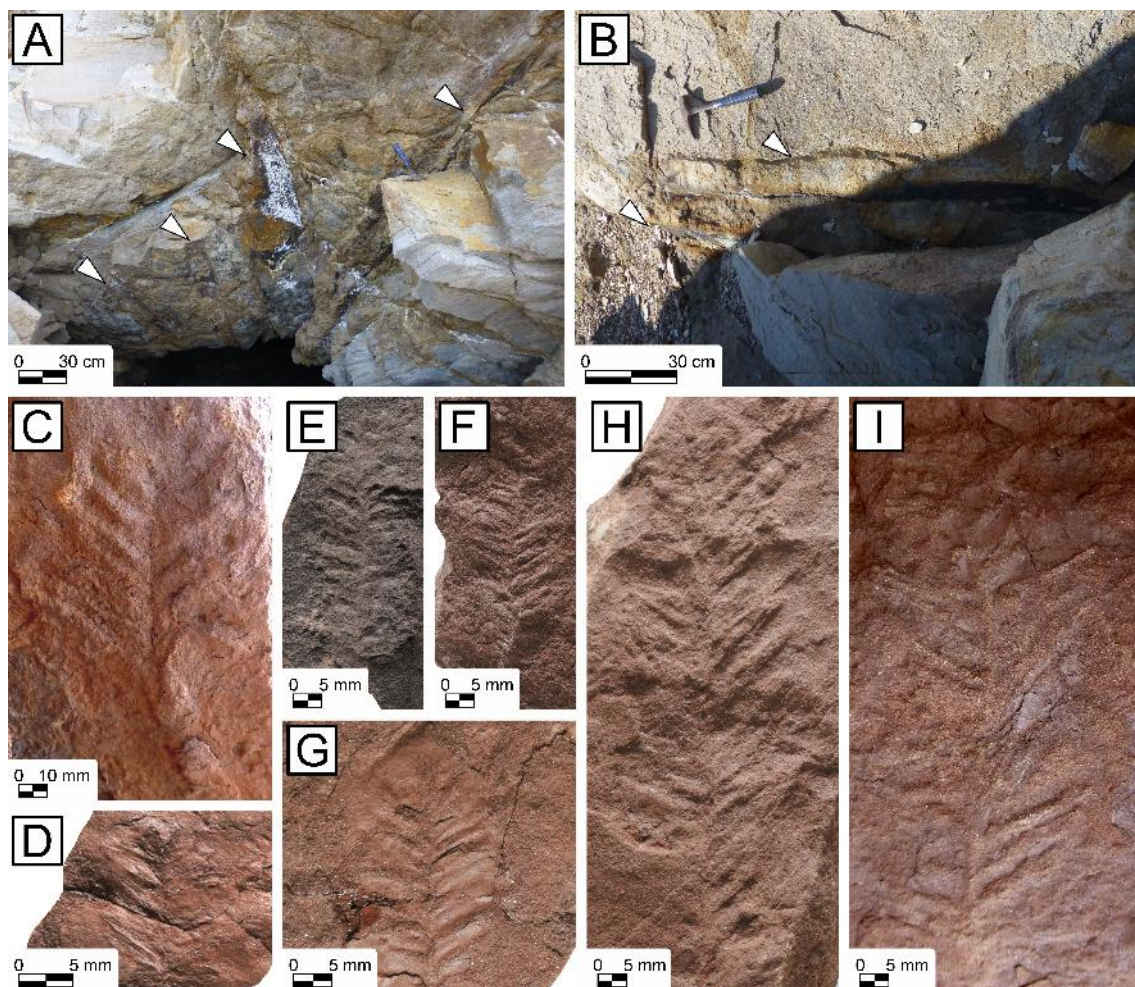


Figure 8. Macroplant remains from the Permian of Mallorca. **A:** Large carbonised woody debris in the base of a fluvial channel deposit and oriented towards the main palaeocurrent trend, middle part of the Pedra de s'Asse Formation, Roadian–Wordian, Cova des Carbó. **B:** Sphenophyta indet., middle part of the Pedra de s'Asse Formation, Roadian–Wordian, between Tenassa d'en Quesso and Pesquera d'en Sabino. **C–D:** *Hermitia* sp.; **C:** DA/21-15-05-01, upper part of the Port des Canonge Formation, Artinskian–Kungurian, Racó de s'Algar; **D:** DA/21-15-05-05, from an *ex situ* rock in the upper part of the Port des Canonge Formation, Artinskian–Kungurian, Racó de s'Algar. **E–I:** *?Feysia* sp.; **E:** DA/21-15-03-03, from the middle part of the Port des Canonge Formation, Artinskian–Kungurian, Racó de s'Algar; **F:** DA21/15-04-02, from an *ex situ* rock in the middle–upper part of the Port des Canonge Formation, Artinskian–Kungurian, Racó de s'Algar; **G:** DA/21-15-05-06, from an *ex situ* rock in the upper part of the Port des Canonge Formation, Artinskian–Kungurian, Racó de s'Algar. **H:** DA/21-15-08-07, from an *ex situ* rock in the upper part of the Port des Canonge Formation, Artinskian–Kungurian, Platjola des Munt de Pedres; **I:** Specimen not collected, from an *ex situ* rock in the lower part of the Pedra de s'Asse Formation, Roadian–Wordian?, Es Tamarell.

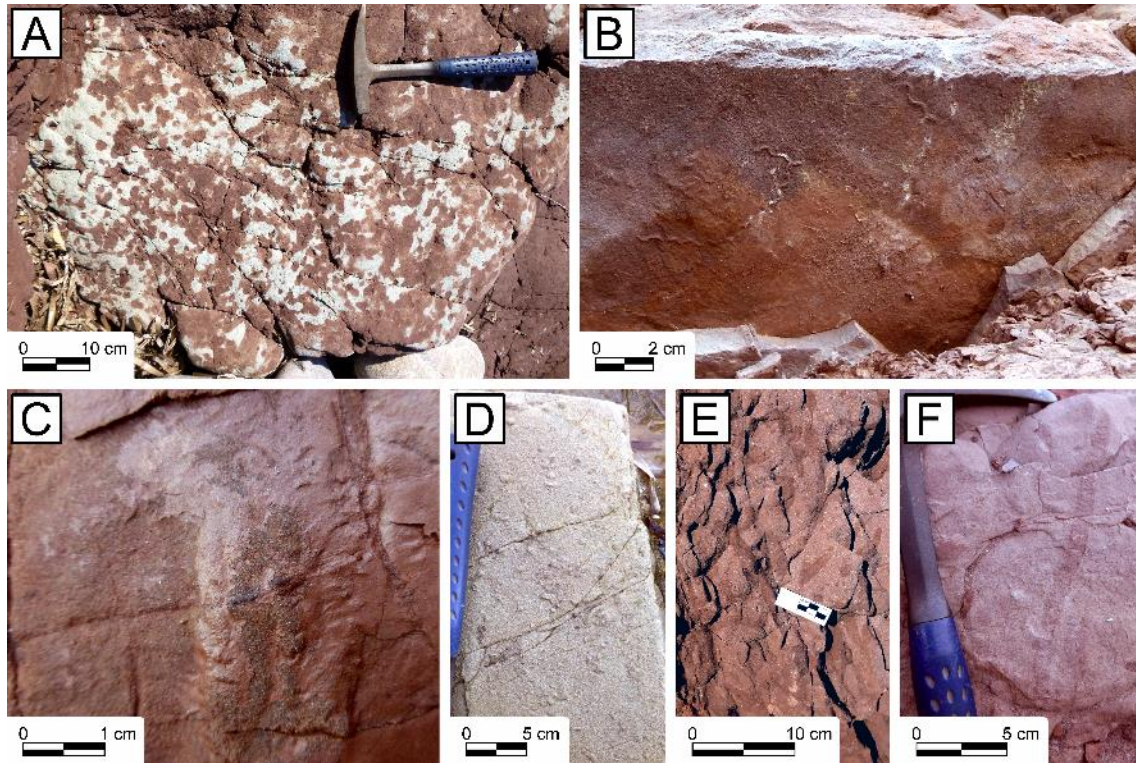


Figure 9. Invertebrate trace fossils identified in the Permian sequences of Mallorca. **A:** *Arenicolites* isp., middle part of the Pedra de s'Ase Formation, Roadian–Wordian, Puig des Moro. **B:** *Cochlichnus anguineus*, upper part of the Port des Canonge Formation, Artinskian–Kungurian, Racó de s'Algar. **C:** *Cruziana* isp., lower part of the Port des Canonge Formation, Sakmarian–Kungurian?, Alcova de son Bunyola. **D:** *Palaeophycus tubularis*, upper part of the Pedra de s'Ase Formation, Roadian–Wordian, Platja de s'hort de sa Cova. **E:** *Planolites beverleyensis*, lower part of the Pedra de s'Ase Formation, Roadian–Wordian, Punta d'en Pere Mir. **F:** *Taenidium barretti*, middle part of the Pedra de s'Ase Formation, Roadian–Wordian, Pesquera d'en Sabino.

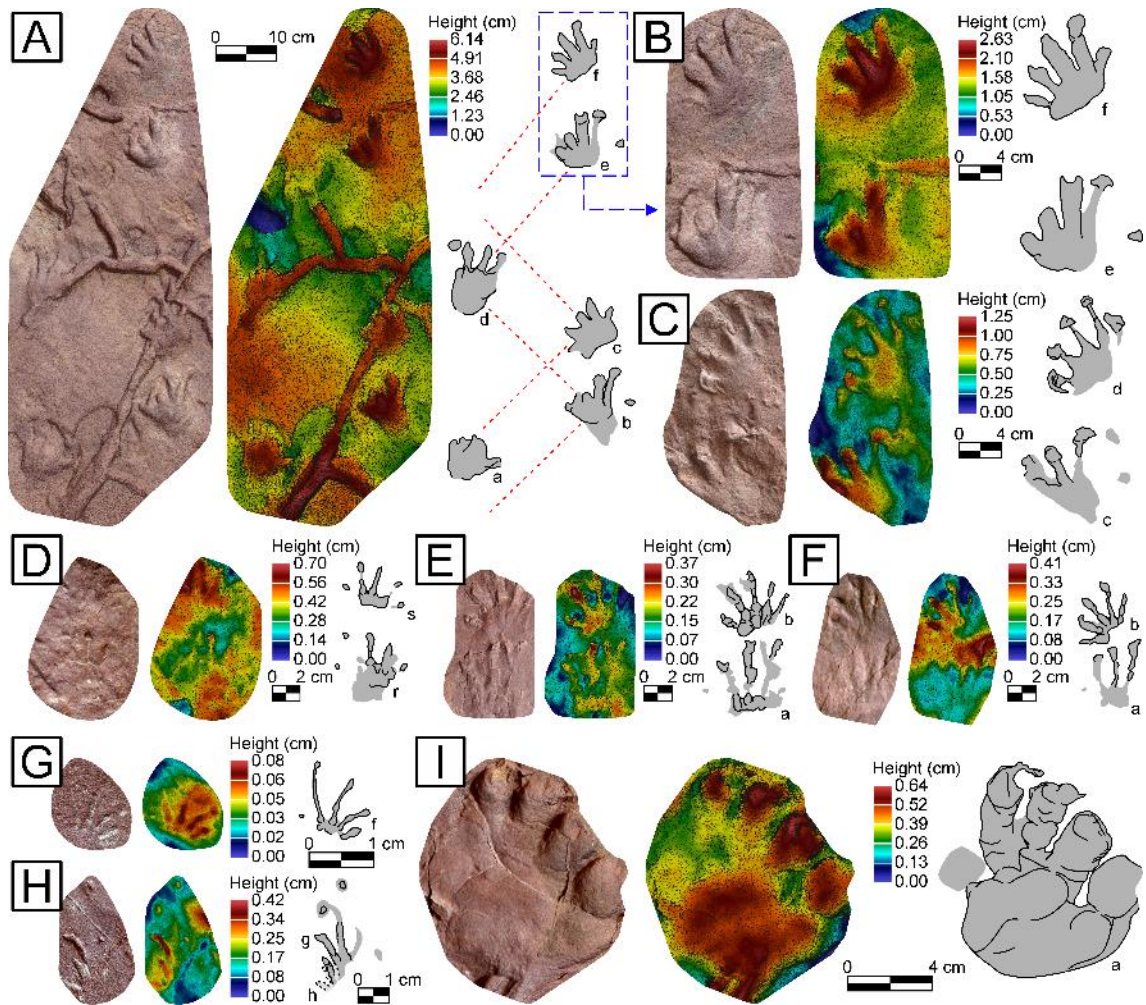


Figure 10. Tetrapod ichnites attributed to eureptile and parareptile trackmakers studied herein, all as textured 3D models, false colour-coded 3D models and interpretative drawings. **A–C:** *Hyloidichnus bifurcatus*, large morphotype; **A–B:** NA-25.6-01; **C:** NA-26.0-02. **D–F:** *Hyloidichnus bifurcatus*, small morphotype; **D:** NA-26.0-09; **E:** NA-66.4-02; **F:** NA-66.4-04. **G–H:** *Dromopus* isp., NA-77.5-01. **I:** cf. *Pachypes olieri*, NA-66.6-01. All from the Torrent de na Nadala section (Mallorca, Balearic Islands, western Mediterranean), Port des Canonge Formation, Artinskian–Kungurian, Permian.

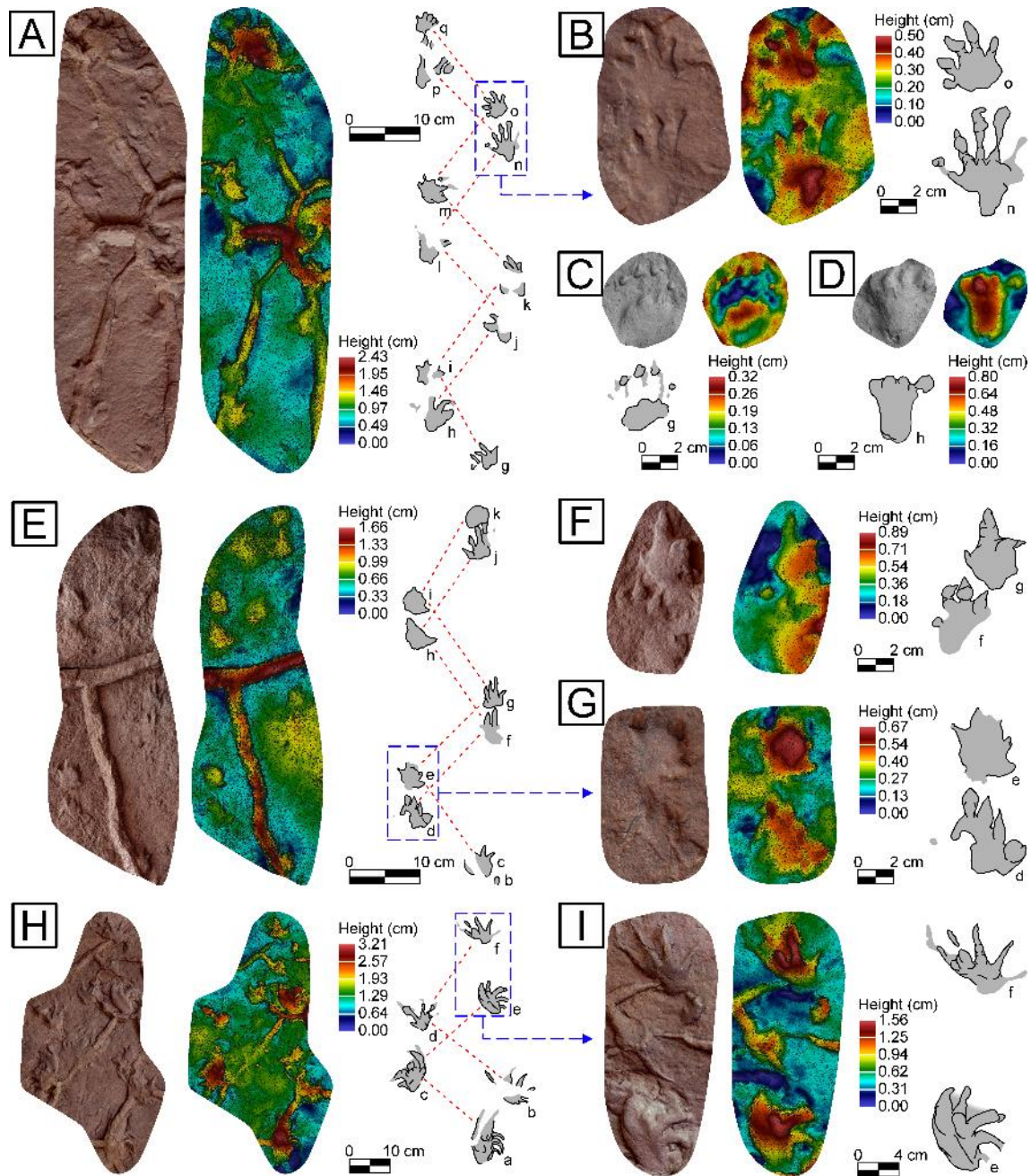


Figure 11. Tetrapod ichnites herein studied attributed “pelycosaur”-grade synapsid trackmakers studied herein, all as textured 3D models, false colour-coded 3D models and interpretative drawings. **A–H:** *Dimetropus leisnerianus*; **A–B:** NA-26.0-09; **C–D:** NA-25.6-01; **E, G:** NA-26.0-03; **F:** NA-26.0-02. **H–I:** cf. *Dimetropus* isp., NA-26.0-09 (taken from Matamalas-Andreu *et al.*, 2021c). All from the Torrent de na Nadala section (Mallorca, Balearic Islands, western Mediterranean), Port des Canonge Formation, Artinskian–Kungurian, Permian.

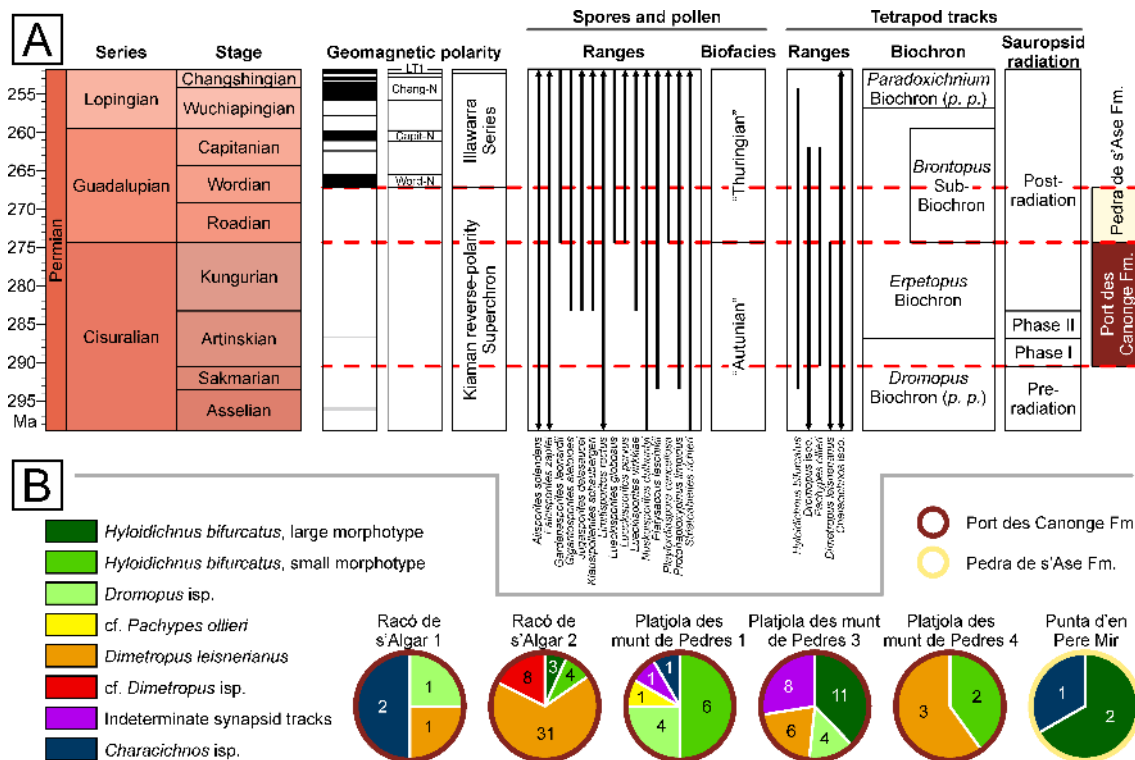


Figure 12. A: Magneto- and biostratigraphic data of the Permian of Mallorca. The geomagnetic polarity reference scales are taken from Henderson *et al.* (2020) (the whole Permian sequence of Mallorca belongs to the Kiaman reverse-polarity Superchron). The biostratigraphic ranges of the spores and pollen found in the present work in the Pedra de s'Ase Formation are taken from Supplementary Table 4 and references therein. The biostratigraphic ranges of the ichnotaxa recognised in the Port des Canonge Formation are based on Schneider *et al.* (2020) and Marchetti *et al.* (2021b). **B:** Pie charts showing the relative proportions of the recognised ichnotaxa in the six main ichnite-bearing beds (Racó de s'Algar 1: lower part of log NA; Racó de s'Algar 2: m 25.6–26 of log NA; Platjola des munt de Pedres 1: m 66.5 of log NA; Platjola des munt de Pedres 2: m 72.5 of log NA; Platjola des munt de Pedres 3: m 77.5 of log NA; Platjola des munt de Pedres 4: m 90 of log NA; Punta d'en Pere Mir: m 15.7 of log PM). For the stratigraphic position of sites see Figure 13.

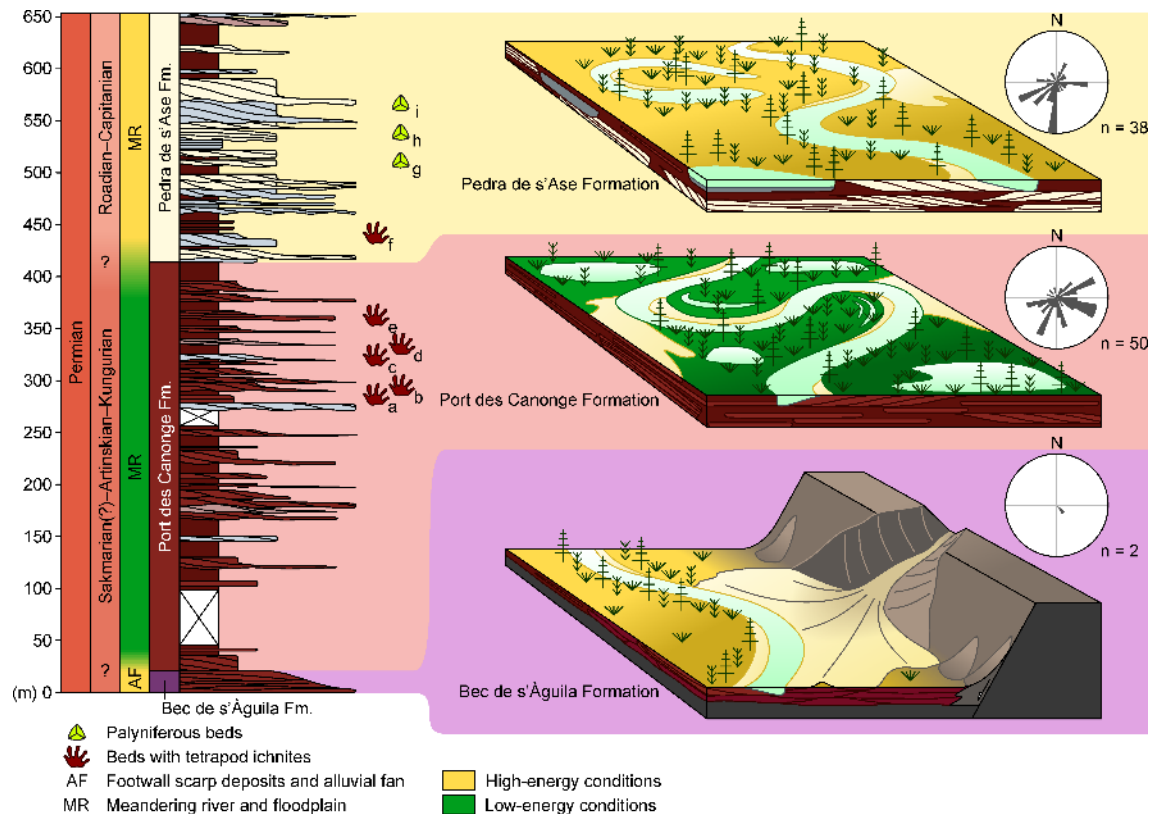


Figure 13. Synthetic stratigraphic log for the three formations of the Permian of Mallorca defined here and their respective palaeoenvironmental interpretations, showing the beds that contain tetrapod tracks (some dated as lower Permian) and palynomorphs (some dated as middle Permian). Letters a–f correspond to tracksites and letter g–i, to palynological samples. a: Racó de s'Algar 1, b: Racó de s'Algar 2, c: Platjola des munt de Pedres 1, d: Platjola des munt de Pedres 3, e: Platjola des munt de Pedres 4, f: Punta d'en Pere Mir, g: sample P-PA-05, h: sample P-PA-09, i: sample P-PA-12 of the present work and sample “Pedra de s'Ase” of Diez (2000) and Juncal (2019). Uppermost part of the Pedra de s'Ase Formation (Pedrera de sa Cova section) not shown because correlations can only be made tentatively at present.

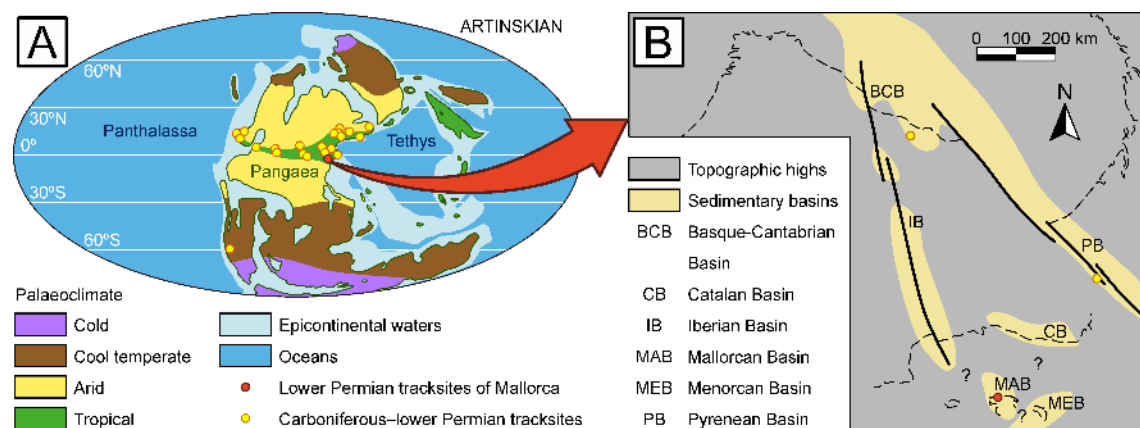


Figure 14. Palaeogeographical position of the tracksites of Mallorca. **A:** Distribution of the

known Carboniferous–Permian and lower Permian tracksites (data from Marchetti *et al.*, 2019c and references therein). Note that almost all of them are in the equatorial latitudes and under tropical climates. Artinskian world map modified after Scotese (2014a), with palaeoclimate data after Tabor & Poulsen (2008). **B**: Detail of the Iberian area (dashed lines represent present-day coastline) with its main sedimentary basins and location of the known tracksites (Mujal *et al.*, 2016; López-Gómez *et al.*, 2021; the present work). Map based on Sopena *et al.* (1977), Gretter *et al.* (2015) and López-Gómez *et al.* (2021).

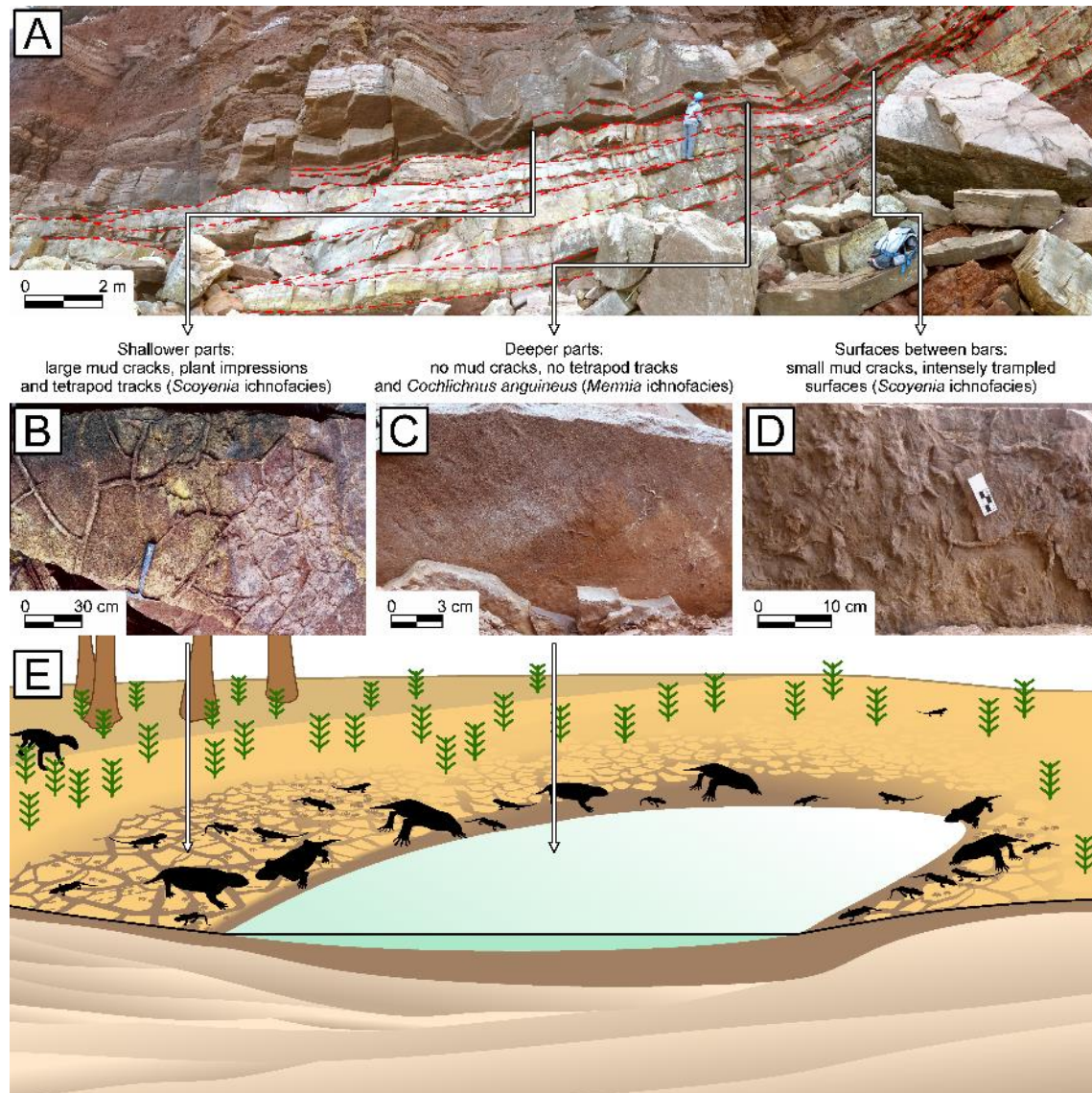


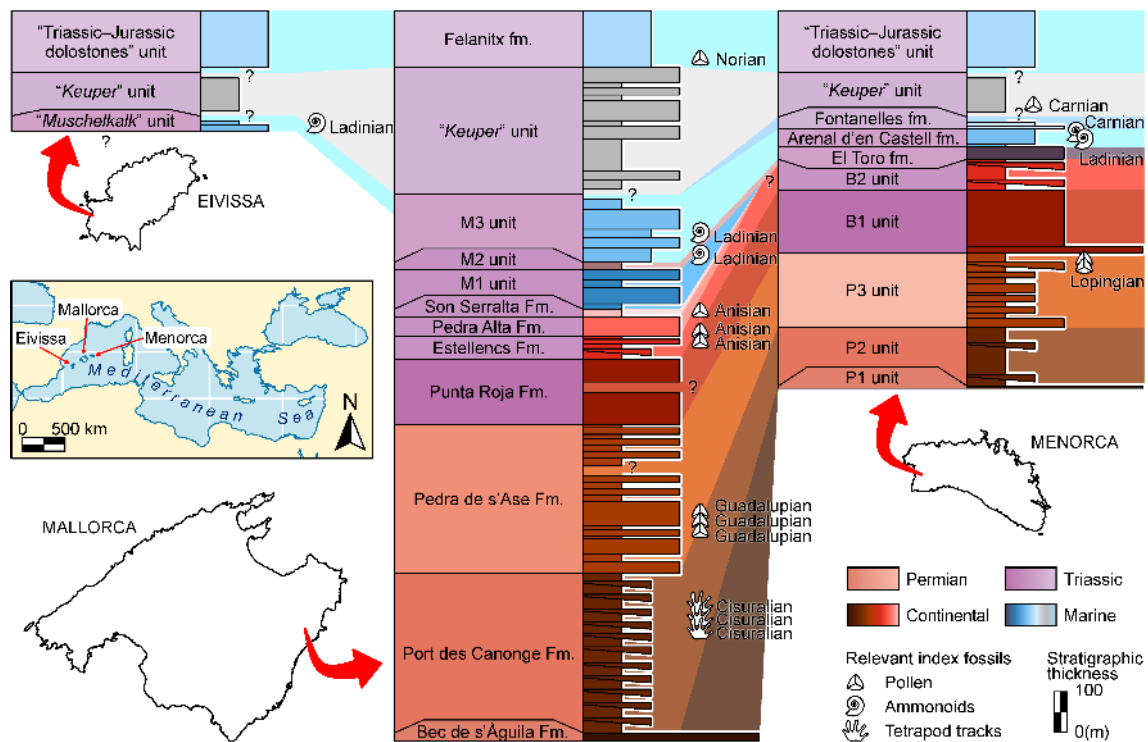
Figure 15. Interpretation of the Racó de s'Algar 1 tracksite as a waterhole. **A**: Field view of the tracksite. **B**: Surface (UIB174620) with natural casts of large mud cracks and tetrapod ichnites (*Hyloidichnus*, *Dimetropus*), with a thin bed of lutites/very fine-grained sandstones below. Photograph courtesy of J.J. Fornós, taken in the 1980s. **C**: Surface without mud cracks and with natural casts of ichnofossils of the *Mermia* ichnofacies (*Cochlichnus anguineus*), with a thick bed

of lutites/very fine-grained sandstones below. It is a lateral variation of the same surface depicted in B. **D:** Densely trampled (*Hyloidichnus*, *Dimetropus*) surface with natural casts of narrow mud cracks. It is located above a fine lutite drape between two sandstone bars. **E:** Schematic representation of the palaeoenvironment represented by the Racó de s'Algar 1 tracksite as a waterhole developed in a swale or an abandoned chute channel in the near-channel environment, indicating the inferred position for the sub-environments depicted in B and C. Plants and tetrapods represented only schematically.



Figure 16. Reconstruction of the palaeoecosystem of the Artinskian–Kungurian (Cisuralian, lower Permian) Port des Canonge Formation of Mallorca. In the foreground, there is a small captorhinid eureptile (Matamales-Andreu *et al.*, 2021d, purported trackmaker of the small form of *Hyloidichnus bifurcatus*) walking on the mud, where desiccation cracks are starting to develop. Imprinted in it there are the ichnotaxa *Hyloidichnus bifurcatus* (small and large morphotypes), *Dromopus* isp. and *Dimetropus leisnerianus*. In the background, two indeterminate “pelycosaur”-grade synapsids (purported trackmakers of *Dimetropus leisnerianus*) approach a large moradisaurine captorhinid eureptile (Liebrecht *et al.*, 2017; purported trackmaker of the large form of *Hyloidichnus bifurcatus*). On the water surface there are several *?Feysia* conifer shoots, and a tree log uprooted in a previous flood. Created by Henry Sutherland Sharpe. © 2021 Henry Sutherland Sharpe. Used under license.

1





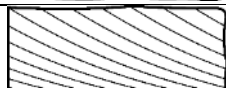
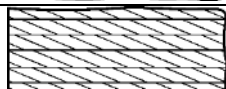
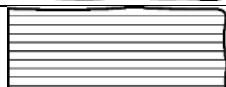







2

Figure 17. Correlation proposal of the Permian and Triassic sequences of the Balearic Islands, with continental units represented by brown-red-pink colours, lagoonal units in grey and marine units in blue. Biostratigraphically relevant fossils are indicated, together with their age attribution. Changes in background colours represent boundaries between similar lithosomes, but do not imply isochrony. Thicknesses based on: Rangheard (1971) [“Keuper” and “Triassic–Jurassic dolostones” units of Eivissa, approximate]; Bourrouilh (1983) [“Keuper” and “Triassic–Jurassic dolostones” units of Menorca, approximate]; Gómez-Gras (1987) [B1 and B2 units]; Rodríguez-Perea *et al.* (1987) [“Muschelkalk” unit of Eivissa]; Barnolas (1991a, 1991b) [Felanitx fm., approximate]; Escudero-Mozo *et al.* (2014) [El Toro, Arenal d’en Castell and Fontanelles formations]; Matamales-Andreu *et al.* (2021a) [Estellencs Formation, Pedra Alta Formation, Son Serralta Formation and upper part of the Punta Roja Formation]; Matamales-Andreu *et al.* (2021b) [P1, P2 and P3 units]; Matamales-Andreu *et al.* (2021e) [M1, M2, M3 and “Keuper” units of Mallorca, approximate]; the present work [Bec de s’Àguila Formation, Port des Canonge Formation, Pedra de s’Ase Formation and lower part of the Punta Roja Formation]. Age attributions based on: Rangheard (1971) [upper Ladinian *Protrachyceras* sp. from Eivissa]; Boutet *et al.* (1982) [upper Norian spores/pollen from Mallorca]; Rosell *et al.* (1989) [lower Carnian spores/pollen from Menorca]; Bercovici *et al.* (2009) [Lopingian spores/pollen from Menorca]; Diez *et al.* (2010) [lower Anisian spores/pollen from Mallorca]; Escudero-Mozo *et al.* (2014) [lower Ladinian *Eoprotrachyceras vilanovai*, upper Ladinian *Protrachyceras* spp. and lower Carnian *Daxatina canadensis* from Menorca]; Matamales-Andreu *et al.* (2021e) [lower

- 1 Ladinian *Gevanites* spp. and upper Ladinian *Protrachyceras* sp. from Mallorca]; the present work
- 2 [Cisuralian *Dimetropus* ispp. and Guadalupian spores/pollen from Mallorca].
- 3
- 4 **Tables**

Table 1. Sedimentary lithofacies recognised in the outcrops of the Permian of Mallorca, mostly based on the table 1 of Matamales-Andreu *et al.* (2021a).

Code	Lithofacies	Sedimentary structures, processes and fossil content	Diagrams
<i>Gt</i>	Stratified, matrix to clast-supported, gravel to pebble-sized breccia of reworked mudstone, sandstone or calcrete (intraformational) clasts.	Distinct to crude trough stratification. Positive granoselection has rarely been observed in some beds. It corresponds to 3D megaripples that rework the floodplains, or scour fills of major channels (Miall, 1977; Gómez-Gras & Alonso-Zarza, 2003). In some cases, it contains tetrapod bones and bone fragments.	
<i>Gm</i>	Massive, matrix to clast-supported, gravel to pebble-sized breccia of reworked mudstone, sandstone or calcrete (intraformational) clasts.	Massive. It corresponds to 3D megaripples that rework the floodplains, or scour fills of major channels (Miall, 1977; Gómez-Gras & Alonso-Zarza, 2003). In some cases, it contains tetrapod bones and bone fragments.	
<i>GmP</i>	Massive, matrix to clast-supported, gravel to cobble-sized sub-rounded polygenic breccias and conglomerates of extraformational clasts.	Massive to very crude planar, irregular stratification. Positive or negative granoselection has been observed, although the clasts are usually randomly sorted. It corresponds to alluvial-fan debris-flows and water-laid deposits, somewhat unconfined, similarly to the P1 unit of Menorca (Gómez-Gras & Alonso-Zarza, 2003). Large rhizocretions sometimes present.	
<i>St</i>	Stratified, very fine- to very coarse-grained sandstone.	Trough cross stratification. It corresponds to sinuous or linguoid 3D megaripples of lower flow regime (Miall, 1985, 2006). In some cases, it contains rhizocretions.	
<i>Sp</i>	Stratified, very fine- to coarse-grained sandstone.	Planar cross stratification. It corresponds to transverse or linguoid 2D bars of lower flow regime (Miall, 1977, 1985, 2006). In some cases, it contains rhizocretions.	
<i>Sr</i>	Stratified, very fine- to medium-grained sandstone.	Ripple-marks, mostly climbing ripples; current ripples and wave ripples are less frequent. Sometimes convolute lamination. It corresponds to low regime and waning flows, at the top of channel sequences or at crevasse splays (Miall, 1985). Rhizocretions or invertebrate traces sometimes present. Mud-cracks, tetrapod tracks and plant impressions may appear on the base.	
<i>Sh</i>	Stratified, very fine- to medium-grained sandstone.	Horizontal stratification and lamination, sometimes alternating finer-grained layers with coarser ones. It corresponds to planar bed flow of lower flow regime or traction carpets in upper flow regime (Miall, 1977, 1985, Postma, 1990).	
<i>Sl</i>	Stratified, very fine- to coarse-grained sandstone.	Low-angle cross stratification. Sometimes convolute lamination. It corresponds to scour fills, crevasse splays, antidunes (Miall, 1985, 2006). Rhizocretions or invertebrate traces sometimes present. Mud-cracks, tetrapod tracks and leaf impressions may appear on the base.	
<i>Ss</i>	Stratified to massive, fine- to coarse-grained sandstone.	Clear to crude trough cross stratification. Usually with soft pebbles. It corresponds to scour fills (Miall, 2006).	
<i>Sm</i>	Massive, very fine- to coarse-grained sandstone.	Massive (in macroscopic view). It corresponds to sediment gravity flows (Miall, 2006) or to beds with lamination obliterated by bioturbation. It may be affected by mud-cracks. Rarely, articulated to semi-articulated tetrapod skeletons may appear.	
<i>Sb</i>	Massive, very fine- to medium-grained sandstone.	Abundant invertebrate burrows and/or root traces. It corresponds to the biotic reworking of overbank deposits (Miall, 1985).	
<i>Fl</i>	Laminated lutites.	Fine lamination, consisting of small ripples, low-angle cross lamination or horizontal lamination. It corresponds to overbank, abandoned channel (including oxbow lakes) or waning flood deposits (Miall, 2006).	





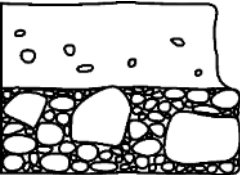
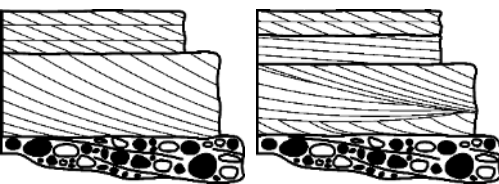
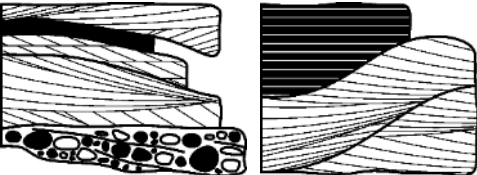
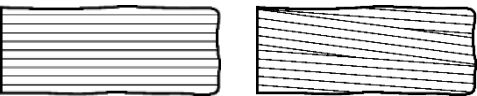
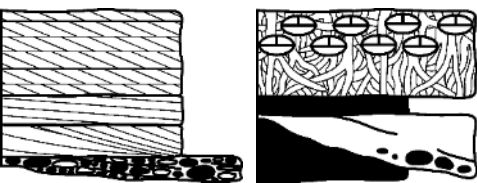
<i>Fm</i>	Massive lutites.	Massive. It corresponds to overbank, abandoned channel or drape deposits (Postma, 1990; Miall, 2006). Mud-cracks, leaf impressions and tetrapod tracks often present. Rarely, thin coal seams may appear.	
<i>Fr</i>	Lutites with roots.	Lamination usually obliterated by root bioturbation. Carbonate nodules sometimes present, indicating the formation of an incipient soil. It corresponds to the biotic (plant) reworking of other lutitic lithofacies.	
<i>Fb</i>	Lutites with burrows.	Lamination usually obliterated by horizontal and/or vertical burrows of invertebrates. Mud-cracks often present. It corresponds to the biotic reworking of other lutitic lithofacies.	
<i>P</i>	Lutites or sandstones with carbonate nodules and, generally, root traces.	Massive or crudely laminated because of the bioturbation (root traces or invertebrate burrows). Carbonate nodules are always very abundant, sometimes forming continuous crusts or even thick calcretes. Gleyed patches, sometimes surrounding coalified plant remains, are also common. It corresponds to either calcic Vertisols, vertic Calcisols or Calcisols (Mack <i>et al.</i> , 1993).	

Table 2. Architectural elements recognised in the outcrops of the Permian of Mallorca, mostly based on table 2 of Matamalas-Andreu *et al.* (2021a). Arrows (→) indicate the usual succession. Lithofacies in brackets are often missing in the “ideal” succession. Formations in brackets only present that architectural element rarely.

Code	Element	Principal lithofacies assemblages	Interpretation	Diagrams	Formation
<i>GB</i> + <i>SG</i>	Gravel bars and bedforms and Sediment gravity flows	<i>GmP</i> → <i>Sm</i>	Water-laid deposits by tractive currents and interbedded debris flows sedimented in alluvial fans (Colombo, 2010a, 2010b).		Bec de s'Àguila Formation
<i>SB</i>	Sandy bedforms	(<i>Gt/Gm</i>)→ <i>Sp</i> →(<i>Sr</i>) (<i>Gt/Gm</i>)→ <i>St</i> → <i>Sl</i> → <i>Sr</i>	Shallow channel-fill assemblages and channel-floor dune fields, respectively (both in the sense of Miall, 2006).		Pedra de s'Ase Formation
<i>LA</i>	Lateral accretion deposits	<i>Gt/Gm</i> → <i>St/Sl</i> → <i>Sr/Sl</i> →(<i>Fl</i>)→ <i>Fm</i> <i>St</i> → <i>Fl</i>	Point bars of meandering rivers (Miall, 2006). Rarely, oxbow lakes with abundant plant remains.		Pedra de s'Ase Formation Port des Canonge Formation Bec de s'Àguila Formation
<i>LS</i>	Laminated sand sheets	<i>Sh</i> <i>Sl</i>	Flash flood deposits under upper flow-regime plane bed conditions (Miall, 2006).		Pedra de s'Ase Formation
<i>LV</i> + <i>CR</i> + <i>CS</i>	Levees and Crevasse channels and Crevasse splays	(<i>St</i>)→ <i>Sl</i> → <i>Sr</i> →(<i>Sm/Sb/P</i>) <i>Gt/Gm/Ss</i> →(<i>Sl/Sr</i>)→(<i>Sm/Sb/P</i>)	Overbank flooding (Miall, 2006), including the sand wedges bordering the channels (levees), the crevasse channels and the sheetflood deposits of crevasse splays. May be affected by pedogenesis. Given the limited lateral extension of the studied deposits, it has usually not been possible to precisely differentiate the three architectural elements.		Pedra de s'Ase Formation Port des Canonge Formation
<i>FF</i>	Floodplain fines	<i>Fl</i> → <i>Fm</i> → <i>Fr/Fb</i> → <i>P</i>	Deposits of overbank low-energy flows or sedimentation in pools and playa-lakes (Miall,		Pedra de s'Ase Formation Port des Canonge Formation (Bec de s'Àguila Formation)


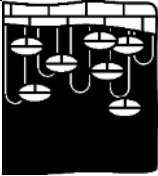
			<p>2006). Carbonate or gleyed palaeosols usually appear towards the top of the sequences.</p>			
--	--	--	---	--	--	--

Table 3. Botanical affinities of the various spores and pollen (see also Supplementary Table 4). The consideration of botanical affinities is based on in situ evidence from the Permian and closely related time periods. Several spore/pollen taxa have a higher putative botanical range than indicated here but for time periods outside the investigated time range and with plant groups that did not exist during the Permian.

Sporomorphs	Plant affinities	References
<i>Alisporites</i>	Seed ferns, Corystospermales (<i>Pteruchus</i>), Peltaspermales (e.g., <i>Amphorispermum</i> , <i>Autunia conferta</i>); Conifers, Voltziales, Ullmanniaceae (<i>Ullmannia</i>), Voltziales (<i>Willsiostrobus</i>)	Grauvogel-Stamm (1978), Balme (1995), Looy & Hotton (2014), Marchetti <i>et al.</i> (2015a)
<i>Bascanisporites</i>	Unknown affinity	-
<i>Calamospora</i>	Sphenophytes, Sphenophyllales, Equisetales, Calamitaceae	Balme (1995), Taylor <i>et al.</i> (2009), Looy & Hotton (2014)
<i>Chordasporites</i>	Conifers, unknown affinity	Kustatscher <i>et al.</i> (2010)
<i>Cordaitina</i>	Coniferales, Rufloriaceae, Vojnovskyaceae, Emporiaceae (<i>Kungurodendro</i>); Cordaitales	Meyen (1987), Balme (1995)
<i>Crucisaccites</i>	Unknown affinity	-
<i>Crustasporites</i>	Seed ferns, Glossopteridales, perhaps aberrant forms	Lindström <i>et al.</i> (1997)
<i>Deltoidospora</i>	Ferns	Looy & Hotton (2014)
<i>Densoisporites</i>	Lycophytes, Selaginellales (<i>Bisporangiostrabus</i>)	Zavialova <i>et al.</i> (2010)
<i>Endosporites</i>	Lycophytes, Chalonieriaceae	Balme (1995), Bek <i>et al.</i> (2008), Marchetti <i>et al.</i> (2015a)
<i>Falcisporites</i>	Seed ferns, Corystospermales (<i>Nidistrobus</i> , <i>Pteruchus</i>), Peltaspermales (<i>Cardiolepis</i> , <i>Permotheca</i>); Conifers, Ullmanniaceae, Voltziaceae	Balme (1995), Potonié & Kremp (1956), Looy & Hotton (2014), Marchetti <i>et al.</i> (2015a)
<i>Gardenasporites</i>	Unknown affinity	-
<i>Gigantosporites</i>	Conifers, Coniferales	Marchetti <i>et al.</i> (2015a)
<i>Granulatisporites</i>	Ferns, Botryopteridales, Lyginopteridales	Potonié (1962), Balme (1995), Looy & Hotton (2014)
<i>Illinites</i>	Conifers, Voltziales, <i>in situ</i> in <i>Willsiostrobus</i>	Grauvogel-Stamm (1978), Kustatscher <i>et al.</i> (2010), Looy & Hotton (2014)
<i>Jugasporites</i>	Conifers, Ullmanniaceae <i>in situ</i> , Voltziaceae	Balme (1995), Kustatscher <i>et al.</i> (2010)
<i>Klausipollenites</i>	Seed ferns, Peltaspermales or conifers	Raine <i>et al.</i> (2011), Mishra <i>et al.</i> (2017)
<i>Kraeuselisporites</i>	Lycophytes, Lycopodiales, Selaginellales.	Kustatscher <i>et al.</i> (2010), Raine <i>et al.</i> (2011)
<i>Leiotriletes</i>	Seed ferns, Zygopteridales; Ferns, Botryopteridaceae	Good (1979), Balme (1995)
<i>Limitisporites</i>	Conifers, Ullmanniaceae	Balme (1995)
<i>Lueckisporites</i>	Conifers, Ullmanniaceae (<i>Majonica alpina</i>) but also associated with other conifers	Clement-Westerhof (1974, 1987), Meyen (1987)
<i>Lunatisporites</i>	Conifers	Alvin <i>et al.</i> (1994), Balme (1995), Traverse (2007), Clement-Westerhof (1974)
<i>Lundbladispora</i>	Lycophytes, Isoetales, Selaginellales	Balme (1995), Retallack (1997)
<i>Lycospora</i>	Lycophytes, Lepidodendrales (<i>Lepidostrobus binneyanus</i>)	Meyen (1987)
<i>Maculatasporites</i>	Algae	-
<i>Marsupipollenites</i>	Seed ferns, Glossopteridales (<i>Polytheca elongata</i>)	Pant & Nautiyal (1960), Balme (1995).
<i>Minutosaccus</i>	Conifers, Voltziales	Baranyi <i>et al.</i> (2019)
<i>Nuskosporites</i>	Conifers, Voltziales (<i>Ortiseia</i>); Utrechtiaceae	Clement-Westerhof (1987), Balme (1995), Poort <i>et al.</i> (1997), Looy & Hotton (2014)
<i>Osmundacidites</i>	Osmundales	Couper (1953), Litwin (1985), Balme (1995)
<i>Palaeospongisporis</i>	Unknown affinity	-
<i>Paravesicaspora</i>	Seed ferns, ?Callistophytaceae, ?Peltaspermaceae	Looy & Hotton (2014)
<i>Platysaccus</i>	Seed ferns, Peltaspermales	Mishra <i>et al.</i> (2017)
<i>Playfordispora</i>	Unknown affinity	-

<i>Potonieisporites</i>	Voltziales, Ullmanniaceae (<i>Otovicia hypnoides</i>); Rufloriaceae, Emporiaceae, Utrechtiaceae	Balme (1995), Hernández-Castillo <i>et al.</i> (2001), Rothwell <i>et al.</i> (2005)
<i>Protohaploxypinus</i>	Seed ferns, Glossopteridales (<i>Arberiella</i> , <i>Pterygospermum</i>), Peltaspermales (<i>Permotheca</i> , <i>Salpingocarpus</i> , <i>Tatarina</i>)	Gould & Delevoryas (1977), Balme (1995), Lindström <i>et al.</i> (1997), Traverse (2007), Looy & Hotton (2014), Marchetti <i>et al.</i> (2015a)
<i>Reticulatisporites</i>	Bryophytes	Balme (1995)
<i>Sahnisporites</i>	Conifers, Voltziales	Looy & Hotton (2014)
<i>Striatoabieites</i>	Unknown gymnosperms	-
<i>Strotersporites</i>	Seed ferns, Glossopteridales; Conifers	Mishra <i>et al.</i> (2017)
<i>Taeniasporites</i>	Seed ferns, Corystospermales	Traverse (2007)
<i>Tiwariasporis</i>	Unknown affinity	-
<i>Triadispora</i>	Conifers, Voltziales (<i>Darneya</i> , <i>Sertostrobus</i>)	Grauvogel-Stamm (1969, 1978), Schaarschmidt & Mauberge (1969), Taylor & Taylor (1987)
<i>Uvaesporites</i>	Lycophytes, Selaginellales (<i>Selaginellites leonardii</i>)	Balme (1995), Kustatscher <i>et al.</i> (2019)
<i>Verrucosisporites</i>	Ferns, Marattiales (<i>Eoangiopteris goodii</i>); Sphenophytes, Equisetales (<i>Bromsgrovia willsii</i>); Seed ferns, Zygopteridales (<i>Corynepteris</i>)	Taylor <i>et al.</i> (2009), Seyfullah <i>et al.</i> (2013)
<i>Vesicaspora</i>	Seed ferns, Callistophytales (<i>Callospermation</i> , <i>Idanothekion</i>), Peltaspermales	Kerp (1988), Balme (1995), Zavialova & van Konijnenburg-van Cittert (2011), Looy & Hotton (2014)
<i>Vitreisporites</i>	Seed ferns, Corystospermales, Caytoniales	Meyen (1987), Traverse (2007)
<i>Vittatina</i>	Seed ferns, Peltaspermales	Balme (1995), Looy & Hotton (2014)